LIGHTWEIGHT OPTIMIZATION OF ELECTRIC BUS BODY STRUCTURE

E076491

DITTAPOOM SHINABUTH

เลขหมู่.....
เลขทะเบียน.....76491
วัน,เดือน,ปี.....25 ส.ค. 2557

.b.....
.i.....

A THESIS SUBMITTED IN PARTIAL FULFILLMENT

OF THE REQUIREMENT FOR THE DEGREE OF

MASTER OF ENGINEERING IN AUTOMOTIVE ENGINEERING

(INTERNATIONAL PROGRAM)

INTERNATIONAL COLLEGE

KING MONGKUT'S INSTITUTE OF TECHNOLOGY LADKRABANG

2013

KMITL-2013-IC-M-004-024

This material is reserved for educational use only, not allowed for commercial use.
Forbidden to modify the content, and cite the document when use.

COPYRIGHT 2013

INTERNATIONAL COLLEGE

KING MONGKUT'S INSTITUTE OF TECHNOLOGY LADKRABANG

NATIONAL SCIENCE AND TECHNOLOGY DEVELOPMENT AGENCY

This material is reserved for educational use only, not allowed for commercial use.

Forbidden to modify the content, and cite the document when use.

Thesis title	Lightweight Optimization of Electric Bus Body Structure
Student	Mr. Dittapoom Shinabuth
Student ID	52600903
Degree	Master of Engineering in Automotive Engineering (International Program)
Year	2013
Thesis advisors	Asst. Prof. Dr. Monsak Pimsarn
	Dr. Chi-na Benyajati
	Prof. Dr. Masaaki Okuma

ABSTRACT

In this work, strength of an electric bus structure was examined using finite element analysis (FEA) and experimental measurement. In experimental part, dynamic responses of the bus structure during actual driving conditions were measured by strain gages and accelerometer. Three different conditions of braking, cornering, and lane changing were investigated on no-load and fully-loaded electric bus. In analytical part, dynamic behaviours of the structure were simulated via commercial FEA code. The obtained analysis solutions were then compared with the experimental results for finite element (FE) model validation before structural optimization of the existing bus model was carried out.

The novel approach of creating an appropriate FE bus model was proposed by including linear spring elements representing bus suspensions. The proposed FE model generated a maximum deviation of 19% for stresses between analysis and experiment. In contrast, the FE model of the bus structure excluding the spring suspensions displayed a much higher deviation or reversed stress direction compared to those calculated from the model including the spring suspensions. Furthermore, the proposed FE model has clearly shown a computational advantage over the conventional approach. From a structural optimization, the maximum reduction of wall thickness was 43.75% at the central tubular body resulting in a decrease in the structural stiffness by 31.36%. The optimized structure was then analyzed under severe driving conditions to determine the corresponding structural strengths. As a result, safety factors of 6.86, 4.06, 4.16, and 3.6 were obtained from braking, cornering, bending, and torsion cases respectively. The optimized structure of an electric bus showed a satisfactory solution by significantly reducing structural mass by 13.15% or 258.1 kg while maintaining sufficient strength and torsional stiffness compared to those of the original model.

This material is reserved for educational use only, not allowed for commercial use.
Forbidden to modify the content, and cite the document when use.

ACKNOWLEDGEMENTS

The study was a scholarship in Automotive Engineering program under Thailand Advanced Institute of Science and Technology and Tokyo Institute of Technology (TAIST-Tokyo Tech) which is a collaboration of National Science and Technology Development Agency (NSTDA), Thailand, Tokyo Institute of Technology (Tokyo Tech), Japan, and King Mongkut's Institute of Technology Ladkrabang (KMITL), Thailand. This study has been conducted during the year 2009-2013 as a part of a research project in the Automotive Laboratory, National Metal and Materials Technology Center (MTEC), Thailand.

I would like to express my special gratefulness to Dr. Chi-na Benyajati, my major advisor and head of Automotive Laboratory, for his generous support, technical guidance, and encouragement all the time during the research work. I would like to direct my gratitude to my advisors, Assistant Professor Dr. Monsak Pimsarn, department of Mechanical Engineering, KMITL and Professor Dr. Masaaki Okuma, department of Mechanical and Aerospace Engineering, Tokyo Tech, for kind advice and suggestions. I am very grateful to Dr. Sittikorn Lapapong, Mr. Anek Phuchamnong and all members in Automotive Laboratory for their help and technical guidance in data acquisition and experimental measurement during field tests. I would like to extend my appreciation to Mr. Jenwit Soparat and Mr. Prasit Wattanawongsakun, senior TAIST-Tokyo Tech students, for their information and time for discussions.

Finally, I would like to give this success to my mother and my father who always stand by me, encourage me, and have infinite faith in my research work.

Dittapoom Shinabuth

June 2013

This material is reserved for educational use only, not allowed for commercial use.

Forbidden to modify the content, and cite the document when use.

TABLE OF CONTENTS

PAGE

ABSTRACT I

ACKNOWLEDGEMENTS II

TABLE OF CONTENTS III

LIST OF TABLES VII

LIST OF FIGURES VIII

CHAPTER 1 INTRODUCTION 1

1.1 Background 1

1.2 Problem Statement 2

1.3 Objectives 2

1.4 Scopes 2

1.5 Result Expectations 3

1.6 Research Methodology 3

1.7 Thesis Outlines 4

CHAPTER 2 BACKGROUND THEORY AND LITERATURE REVIEWS 7

2.1 Computational Modelling 7

2.2 Finite Element Analysis 8

2.2.1 One Dimensional Spring-Damper Element 10

2.2.2 Mixed-Dimensional Elements by Constraint Equations 11

2.2.3 Static Structural Analysis 13

2.2.4 Dynamic Structural Analysis 14

2.3 Strain Gage 15

2.4 Accelerometer 20

2.5 Data Acquisition 22

2.6 Structural Deformation of Vehicle 23

2.7 Vehicle Testing 24

2.7.1 Braking 24

2.7.2 Cornering 25

2.7.3 Double Lane Change 26

This material is reserved for educational use only, not allowed for commercial use.

Forbidden to modify the content, and cite the document when use.

TABLE OF CONTENTS (CONT.)

PAGE

CHAPTER 2 BACKGROUND THEORY AND LITERATURE REVIEWS (CONT.)

2.7.4 Structural Integrity 27

2.7.5 Torsional Stiffness 27

2.8 Structural Optimization 31

2.8.1 Design of Experiment (DOE) 32

2.8.2 Sensitivity Analysis 33

2.8.3 Multi-Objective Genetic Algorithm (MOGA) 33

2.9 Previous Studies on Bus Analysis and Structural Optimization 34

CHAPTER 3 EXPERIMENTAL PROCEDURES 42

3.1 Electric Bus Prototype 42

3.2 Experimental Setup 43

3.2.1 Strain Gage Attachment 45

3.2.2 Acceleration Measurement 46

3.2.3 Data Acquisition 47

3.2.4 Graphical LabVIEW Programming 47

3.3 Experimental Conditions 48

3.3.1 Braking Meneuver 48

3.3.2 Cornering Meneuver 49

3.3.3 Double Lane Change Meneuver 50

3.4 Conclusions 51

CHAPTER 4 FINITE ELEMENT ANALYSIS AND OPTIMIZATION 52

4.1 FE Model of Electric Bus Structure 52

4.1.1 Mixed Element Verification 54

4.1.2 Suspension Modelling 58

4.2 Assigned Material and Distributed Loads 64

4.3 Boundary Conditions 65

4.4 Lightweight Optimization 68

4.5 Conclusions 71

This material is reserved for educational use only, not allowed for commercial use.

Forbidden to modify the content, and cite the document when use.

TABLE OF CONTENTS (CONT.)

PAGE

CHAPTER 5 RESULTS 73

5.1 Experimental Investigation of Computational Bus Model 73

5.1.1 Braking Meneuver 73

5.1.2 Cornering Meneuver 77

5.1.3 Double Lane Change Meneuver 81

5.2 Bus Analysis under Severe Load Conditions 85

5.2.1 Braking Meneuver 86

5.2.2 Cornering Meneuver 86

5.2.3 Bending Case 87

5.2.4 Torsional Case (stress) 89

5.2.5 Torsional Case (stiffness) 89

5.3 Structural Strength of Original Bus Structure 90

5.4 Optimization Results 91

5.4.1 Optimization Sensitivity 92

5.4.2 Cross-Sectional Feature Modification 93

CHAPTER 6 DISCUSSIONS 95

6.1 Finite Element Model Validation 95

6.2 Comparison of Computational Efficiency between Static and Dynamic Analysis 99

6.3 Comparison of Structural Strength between Original Structure and Optimized Structure 101

6.4 Optimization Response 106

6.5 Conclusions 108

CHAPTER 7 CONCLUSIONS AND SUGGESTIONS 109

7.1 Conclusions 109

7.2 Suggestions for Further Research 110

7.2.1 Experimental Measurement 110

7.2.2 Finite Element Analysis 110

This material is reserved for educational use only, not allowed for commercial use.

Forbidden to modify the content, and cite the document when use.

TABLE OF CONTENTS (CONT.)

PAGE

CHAPTER 7 CONCLUSIONS AND SUGGESTIONS (CONT.)

7.2.3 Structural Optimization 111

REFERENCES 112

APPENDIX A: LABVIEW BLOCK DIAGRAM 116

APPENDIX B: STRAIN GAGE SPECIFICATIONS AND BONDING PROCEDURES 118

APPENDIX C: ACCELERATION SPECIFICATIONS 121

APPENDIX D: DATA ACQUISITION SPCIFICATIONS 123

APPENDIX E: PROCEEDINGS 127

BIOGRAPHY 150

This material is reserved for educational use only, not allowed for commercial use.

Forbidden to modify the content, and cite the document when use.

LIST OF TABLES

TABLE		PAGE
4.1	FE model summary	54
4.2	Element types for T-joint specimens	55
4.3	Deviation of simulation results in different element types respecting to shell element	57
4.4	Material properties of leaf springs	60
4.5	Parameters for leaf spring calculation	61
4.6	Investigation of leaf spring stiffness	62
4.7	Parameters of electric bus suspension calculated from 1/4 bus	64
4.8	Material properties of common steel	64
4.9	External loads for bus analysis	65
4.10	Boundary conditions for finite element analysis	66
4.11	Lightweight optimization of bus structure	69
5.1	Definition of lines for dynamic stress responses representation	74
5.2	Summary numerical simulation in bending and torsional cases	91
5.3	Comparison between initial and optimized design	93
6.1	Steps controls for static and dynamic analysis	99
6.2	Computer specifications used for FEA simulation	99
6.3	Structural strength and stiffness verification of the optimized structure	106

This material is reserved for educational use only, not allowed for commercial use.
Forbidden to modify the content, and cite the document when use.

LIST OF FIGURES

FIGURE		PAGE
1.1	Example of bus construction	1
1.2	Electric bus prototype by MTEC	1
1.3	Computational model of the electric bus	3
2.1	Example of truck chassis	7
2.2	Example of automobile model	8
2.3	Finite element procedures	8
2.4	Simple spring element	9
2.5	Spring-damper element	11
2.6	Definition of constrain equations	12
2.7	Mixed element applied to B-pillars on passenger car	13
2.8	Principle of strain gage in tension	15
2.9	Structure of foil strain gage	16
2.10	Strain gage bridge for 1 active gage in 2-wire system	17
2.11	Strain gage in 3-wire system	17
2.12	Strain gage attachment on the door frame of an airport bus	18
2.13	Dynamic load measurement using strain gages	19
2.14	Strain gage attachment on suspension lower control arm	19
2.15	Basic configuration of strain gage accelerometer	20
2.16	Multiple accelerometers mounted on 3-axis bracket	20
2.17	Drift vehicle performing a left-hand drift on the test track	21
2.18	Acceleration measurement on the vehicle chassis and the axle	21
2.19	Data acquisition system	22
2.20	Data acquisition in testing of vehicle dynamics	22
2.21	Deformation modes of vehicle frame	23
2.22	Longitudinal loading	24
2.23	Lateral loading	26
2.24	Right-hand approach of double lane change maneuver	27
2.25	Bus loaded to 2.5 times passenger weight	27

This material is reserved for educational use only, not allowed for commercial use.
Forbidden to modify the content, and cite the document when use.

LIST OF FIGURES (CONT.)

FIGURE		PAGE
2.26	Front view of vehicle body subjected to vertical loads in opposite directions	28
2.27	Applied loads and constraints for torsional analysis	29
2.28	Simplified bus structure subjected to torsional load	30
2.29	Torsion test	31
2.30	Portable twist fixture for torsional stiffness measurement	31
2.31	Central composite designs	33
2.32	Articulated bus structure	35
2.33	Rollover test	36
2.34	Structural optimization process	38
2.35	Roof door of mass transit bus	40
3.1	An electric bus prototype	42
3.2	Battery packs	42
3.3	Electric motor drive	42
3.4	Interior for 20 passengers	42
3.5	Experimental procedure flow chart	43
3.6	Experimental configuration of strain and acceleration measurement on the bus	44
3.7	Additional loads provided by sandbags	44
3.8	Strain gage attachment locations	45
3.9	Uniaxial strain gage	45
3.10	An example of strain gage attachment at location S7	45
3.11	Center of gravity determination	46
3.12	Data flow of strain and acceleration measurement using data acquisition tools	47
3.13	(a) LabVIEW programming codes (b) Front panel for DAQ devices interface	48
3.14	Braking configuration	49
3.15	Cornering configuration	49
3.16	Cornering maneuver	50
3.17	Double lane change configuration	50
3.18	Double lane change maneuver	51

This material is reserved for educational use only, not allowed for commercial use.
Forbidden to modify the content, and cite the document when use.

LIST OF FIGURES (CONT.)

FIGURE		PAGE
4.1	Electric bus prototype	52
4.2	FE model and local areas for stress monitoring	53
4.3	Mixed element of T-joint specimen by multipoint constraints (MPCs) approach	54
4.4	T-joint connection of square tubes subjected to 3 components of force	55
4.5	Comparison of X-deformation in different element types	56
4.6	Comparison of Y-deformation in different element types	56
4.7	Comparison of Z-deformation in different element types	56
4.8	Simply supported constraints for bus analysis	58
4.9	Suspensions of studied bus	59
4.10	(a) Configuration of front suspension and (b) Static equilibrium of front leaf	59
4.11	(a) Configuration of rear suspension and (b) Static equilibrium of rear leaf	60
4.12	Deflection of front leaf	61
4.13	Deflection of rear leaf	61
4.14	Spring stiffness of front leaf	62
4.15	Spring stiffness of rear leaf	62
4.16	Suspension model of the bus	63
4.17	Loads on the bus structure	64
4.18	Optimization formulation for an improvement of the bus structure	68
4.19	Specified four design variables	70
4.20	Design variables for lightweight optimization	70
4.21	Optimization procedures	72
5.1	Deceleration measured during a braking maneuver at test speed of 40 km/hr	73
5.2	Dynamic stress responses measured during a braking maneuver	73
5.3	Stress distributions in normal braking case using static analysis with suspension	76
5.4	Stress distributions in normal braking case using dynamic analysis with suspension	76
5.5	Stress distributions in normal braking case using static analysis without suspension	77
5.6	Lateral acceleration measured during a cornering maneuver at test speed of 30 km/hr	78
5.7	Dynamic stress response measured during a cornering maneuver	78

This material is reserved for educational use only, not allowed for commercial use.
Forbidden to modify the content, and cite the document when use.

LIST OF FIGURES (CONT.)

FIGURE		PAGE
5.8	Stress distributions in normal cornering case using static analysis with suspension	80
5.9	Stress distributions in normal cornering case using dynamic analysis with suspension	80
5.10	Stress distributions in normal cornering case using static analysis without suspension	81
5.11	Lateral acceleration measured during a double lane change maneuver at test speed of 30 km/hr	82
5.12	Dynamic strain response measured during a double lane change maneuver	82
5.13	Stress distributions in normal double lane change case using static analysis with suspension	84
5.14	Stress distributions in normal double lane change case using dynamic analysis with suspension	84
5.15	Stress distributions in normal double lane change case using static analysis without suspension	85
5.16	Stress distributions in severe braking case on original structure	86
5.17	Stress distributions in severe cornering case on original structure	86
5.18	Stress distributions in bending load	87
5.19	Vertical deflections along longitudinal members of left-side frame in bending case	88
5.20	Stress distributions under torsional load	89
5.21	Vertical deformation under torsional load	89
5.22	Comparison of torsional stiffness under different load cases	90
5.23	Stress comparison between normal and severe loads	91
5.24	Sensitivities of structural mass	92
5.25	Sensitivities of torsional stiffness	93
6.1	Comparison of deviations between computational models with and without spring suspension in braking case	95
6.2	Comparison of deviations between computational models with and without spring suspension in cornering case	96
6.3	Comparison of deviations between computational models with and without spring suspension in double lane change case	96

This material is reserved for educational use only, not allowed for commercial use.
Forbidden to modify the content, and cite the document when use.

LIST OF FIGURES (CONT.)

FIGURE PAGE

6.4 Deformed shape during deceleration with suspension with resulting deflection value at location S3 97

6.5 Deformed shape during deceleration without suspension with resulting deflection value at location S3 98

6.6 FLOPS comparison 100

6.7 CPU time comparison 100

6.8 Resulting stress comparison under severe braking case 101

6.9 Resulting stress comparison under severe cornering case 102

6.10 Resulting stress comparison under bending case 103

6.11 Resulting stress comparison under severe torsional case 105

6.12 Optimization history regarding structural mass and torsional stiffness 107

This material is reserved for educational use only, not allowed for commercial use.

Forbidden to modify the content, and cite the document when use.

CHAPTER 1

INTRODUCTION

1.1 Background

Due to an increasing demand for bus transport in Thailand, many buses have been constructed especially for tourism industries and public transportations. Most small or medium-sized bus structures were fabricated by local mechanic skills, as an example shown in Figure 1.1, with only a few being supervised by qualified engineers. These buses might be subjected to various problems such as tire wear, inadequate structural durability, and excessive structural weight. As a result, a lighter bus body structure is one of important strategies to optimize overall energy consumption in bus applications. On the other hand, one needs to ensure that in modifying existing bus structure, the resulting structure should still be strong enough to carry additional load such as battery packs and passengers. Furthermore, because of environmental issues, automotive industries and research centres have started concentrating their research on alternative energy applications such as Electric Vehicle (EV) and Fuel Cell Vehicle (FCV). An electric vehicle has become one of the solutions to reduce the usage of fossil fuel on land vehicles. In Thailand, while most buses are generally operated with an internal combustion engine (ICE), there are only few driven by an electric motor. Recently, Automotive Laboratory, National Metal and Materials Technology Centre (MTEC), has been working on a development of a fully-functioned electric bus prototype. This prototype is an 8-meter bus driven by an electric motor with high voltage electricity from battery packs as can be seen in Figure 1.2. Generally, it has been observed that the structural weight including the battery packs is relatively high compared to that of a conventional bus. Performance-wise, this could directly cause higher electricity consumption. Therefore, a subject of improving structural weight of an electric bus has become an interesting challenge for this study.

Figure 1.1 Example of bus construction

Figure 1.2 Electric bus prototype by MTEC

This material is reserved for educational use only, not allowed for commercial use.
Forbidden to modify the content, and cite the document when use.

1.2 Problem Statement

Nowadays, 80% of buses in Thailand are locally manufactured based on the skill and experience of local mechanics while another 20% are imported from other countries. Many buses that are now operating on the road are not fully inspected and approved by qualified engineers. Some problems that are associated with of these kind of models are susceptibility to damage, unbalance weight of structure which could affect tire wear, and also high fuel consumption due to excessive structural weight. Additionally, a deeper problem lies in a limited flexibility of local mechanics to modify existing models. Recently, as energy crisis and environmental problem becomes more evident, the trend of electric vehicles has rapidly increased in the last few years. Since public city buses or interstate coaches are a popular mode of travelling in Thailand, an electric bus is an attractive prospect in terms of environmental and economical aspects. As a result, a lighter bus body structure than existing one is important to optimize energy consumption on the bus. On the other hand, the structure should still be strong enough to carry additional loads such as batteries, electrical motor, and other electronic devices.

1.3 Objectives

1.3.1 To study structural strength and behaviour of an electric bus prototype in real driving conditions

1.3.2 To investigate the computational model via experimental data

1.3.3 To obtain the lightweight model which is acceptable by structural requirements and suitable for a medium-sized electric bus

1.4 Scopes

1.4.1 To examine structural strength and optimize the 8-metre electric bus prototype by computational and experimental stress-strain methods

1.4.2 To conduct structural analysis and parametric optimization by ANSYS software

1.4.3 To investigate the computational model via braking, cornering, and double lane change conditions

1.4.4 To employ wall thickness and torsional stiffness as design variable and constraint in optimization process respectively

This material is reserved for educational use only, not allowed for commercial use.
Forbidden to modify the content, and cite the document when use.

1.5 Result Expectations

1.5.1 Learning the commercial CAD/CAE software

1.5.2 Gaining Knowledge in a bus design and lightweight optimization

1.5.3 Possible cooperation with company for planning the new generation electric bus

1.6 Research Methodology

1.6.1 Evaluate the real dimensions from the MTEC EV bus prototype (actual electric bus)

1.6.2 Create CAD model according to the actual model

1.6.3 Run static/dynamic analysis

1.6.4 Install strain gages and accelerometer on the bus structure in order to measure structural characteristics under different driving conditions

1.6.5 Verify the experimental data

1.6.6 Compare the experimental and computational results

1.6.7 Execute structural optimization

1.6.8 Obtain lightweight electric bus structure

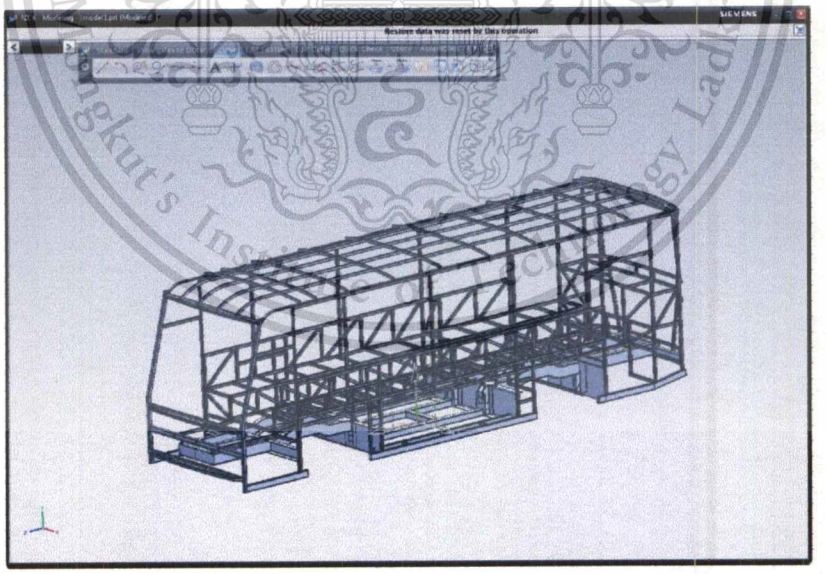

Figure 1.3 Computational model of the electric bus

This material is reserved for educational use only, not allowed for commercial use.
Forbidden to modify the content, and cite the document when use.

1.7 Thesis Outlines

The thesis is divided into 7 Chapters, the contents of which are summarized as followed:

Chapter 1 : Introduction

This chapter introduces the general background of an electric bus structure, the important of the lightweight bus structure, the objectives, the scopes, the result expectations, and the research methodology.

Chapter 2 : Background Theory and Literature Review

In this chapter, the basic equations related to finite element analysis of structural problems, vehicle testing, and structural optimization are provided. With these background theories, several applications from the published literature are also reviewed. At the end of the chapter, numerous studies involving the bus applications, i.e. structural analysis and optimization, are illustrated.

Chapter 3 : Experimental Procedures

This chapter presents the experimental setup of strain gages and accelerometer which are then connected to the data acquisition for a measurement of dynamic strain response and acceleration respectively. In addition, the driving maneuvers consisting of braking, cornering, and double lane change are explained.

Chapter 4 : Finite Element Analysis and Optimization

This chapter explains the process of finite element analysis and structural optimization. The computational processes are comprised of the mixed element validation, the suspension modeling, boundary conditions, and the optimization parameters.

Chapter 5 : Results

This chapter shows the comparison between experimental data and numerical solutions, the structural strength of the studied bus structure analyzed under severe loading conditions, and all optimal design parameters given by the structural optimization.

This material is reserved for educational use only, not allowed for commercial use.
Forbidden to modify the content, and cite the document when use.

Chapter 6 : Discussions

The obtained results from the previous chapter are discussed in this chapter. The discussions consist of the finite element model validation, the comparison of computation efficiency between static and dynamic analysis, the comparison of structural strength between original and optimized bus structure under severe loading conditions, and the optimization response.

Chapter 7 : Conclusions and Suggestions

This chapter illustrates a summary of the present study and provides suggestions for further research.

This material is reserved for educational use only, not allowed for commercial use.
Forbidden to modify the content, and cite the document when use.

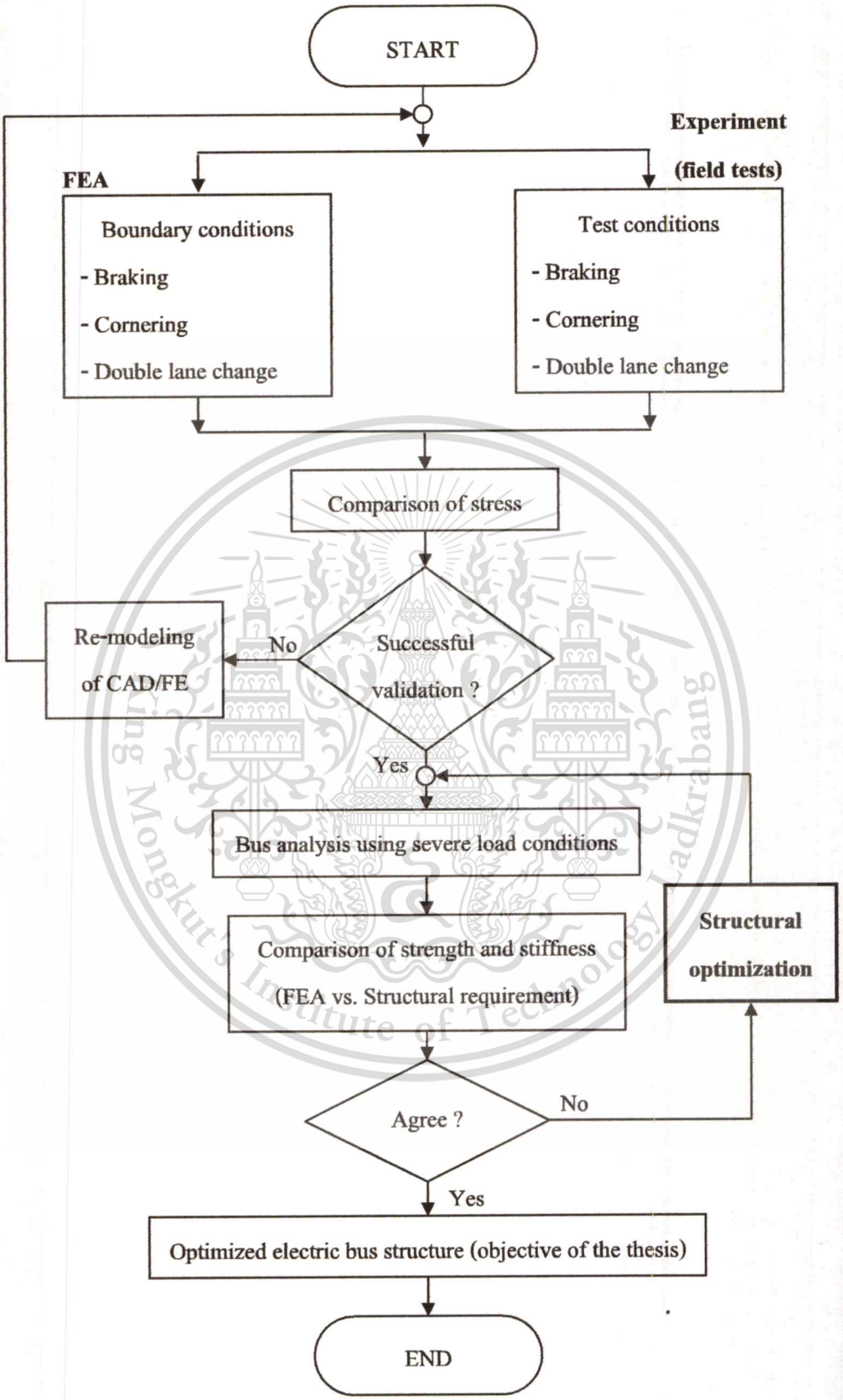

Figure 1.4 Research methodology flow chart

This material is reserved for educational use only, not allowed for commercial use.
Forbidden to modify the content, and cite the document when use.

CHAPTER 2

BACKGROUND THEORY AND LITERATURE REVIEWS

2.1 Computational Modelling

Computational modeling is a general work for the traditional engineering professions. The modeling has become an important technology with the scope of computer-aided technologies and a beneficial tool such as lower product development costs and a greatly shortened design cycle. This technology enables engineers and designers to layout and develops their work on screen resulting in saving time. Current engineering design software ranges from 2D vector-based drafting systems to 3D solid and surface modelers called Computer-Aided Design (CAD). Figure 2.1 (a) shows a heavy truck used for long distant application. The truck chassis shown in Figure 2.1 (b) was modeled using line bodies because several members had the same cross-sectional areas. The line bodies with the assigned cross sections were efficiently converted to finite element (FE) model as beam elements. This method of CAD modeling could save a computational time in finite element analysis (FEA).

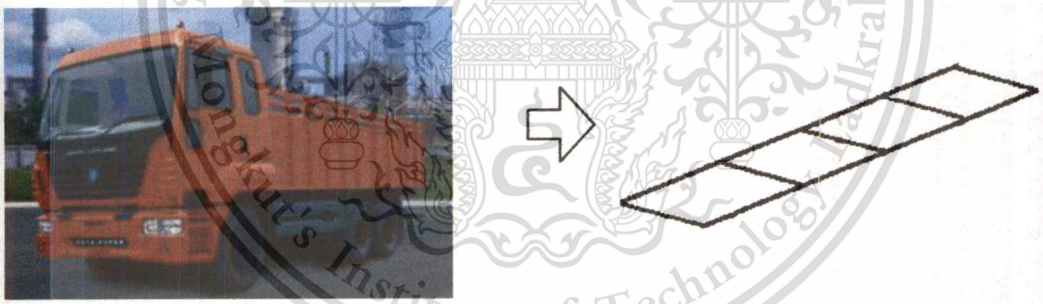

(a) (b)

Figure 2.1 Example of truck chassis: (a) heavy truck (b) CAD of truck chassis [1]

In general, a vehicle body consists of many components which are connected by welding and fasteners. Most surfaces of the vehicle body are steel sheets with small thickness, so that the actual automobile geometry represented by surface bodies is shown in Figure 2.2 (b). The generated surface bodies were then applied to crash analysis. The shell mesh was considered for creating an FE model. It was found that shell elements could accurately replicate the actual shape of the thin structure such as automobile body. Moreover, it could result in obtaining a precise solution in FEA system.

This material is reserved for educational use only, not allowed for commercial use.
Forbidden to modify the content, and cite the document when use.

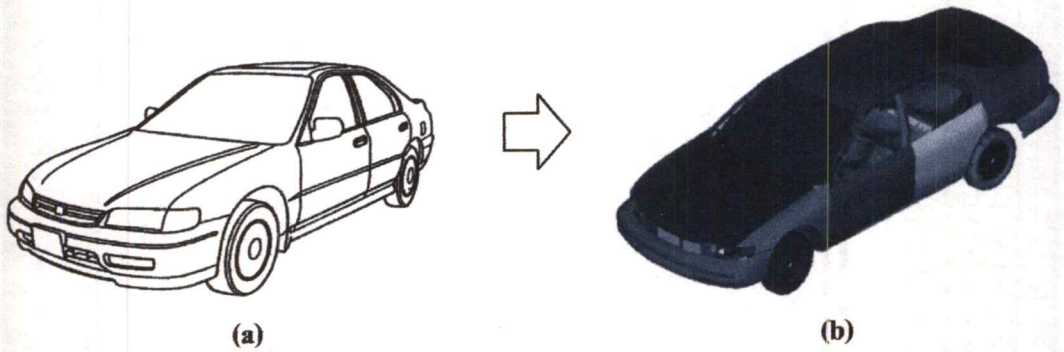

(a) (b)

Figure 2.2 Example of automobile model: (a) wireframe model (b) CAD model [2]

2.2 Finite Element Analysis

Finite Element Analysis (FEA) is a computational technique used to provide an approximate solution of boundary value problems especially the mechanical parts. It is stated that a boundary value problem is a mathematical problem in which one or more dependent variables must satisfy a differential equation everywhere within a known domain of independent variables in specific conditions on the boundary of the domain. An example used finite element analysis solving the structural problem is shown in Figure 2.3.

(a) (b) (c)

Figure 2.3 Finite element procedures: (a) CAD model,

(b) mesh generation, and (c) solution

Figure 2.3 shows a basic concept of finite element analysis for solving structural problem. First, a CAD model is created to represent the physical geometry of the actual model as shown in Figure 2.3 (a). The model is divided into many small pieces called elements as shown in Figure 2.2 (b). The common points sharing from each element are called nodes. An approximate continuous function, namely shape function related to the nodes, is assumed to represent the solution of an element. After the material properties and boundary conditions are applied, the equations governing the behavior of each element connected to other elements are formulated. A

This material is reserved for educational use only, not allowed for commercial use.
Forbidden to modify the content, and cite the document when use.

large set of the finite element equations are simultaneously solved for the unknowns. In stress analysis, it begins solving the displacements at each node and the strain is then calculated. Finally, the derived stress from strain is obtained and displayed throughout the analytical body as the stress distributions shown in Figure 2.3 (c).

In order to understand the finite element process [3], a very simple one-dimensional problem which is a linear truss element is considered. A truss element is a bar loaded in tension or compression and is of constant cross-sectional area (A), length (L), and elastic modulus (E) as shown in Figure 2.4.

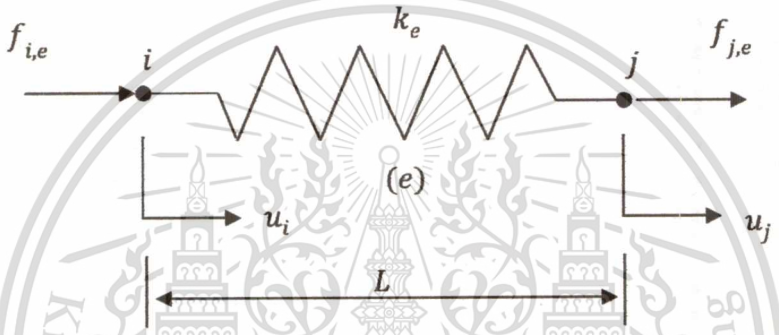

Figure 2.4 Simple spring element

The basic truss element has two nodes and each node contains only one degree of freedom. The derivation for the finite element equations begins with the Hooke's law which describes the relationship between the stress and strain as

$$\sigma = E\varepsilon \tag{2.1}$$

where σ is the stress and ε is the strain. From Figure 2.4, if node i is hold and the force $f_{j,e}$ is applied at node j Equation (2.1) becomes

$$\frac{f_{j,e}}{A} = E\left(\frac{u_j - u_i}{L}\right) \tag{2.2}$$

Under equilibrium conditions the applied forces can be written as

$$f_{i,e} = \frac{AE}{L}(u_i - u_j) \tag{2.3}$$

This material is reserved for educational use only, not allowed for commercial use.
Forbidden to modify the content, and cite the document when use.

$$f_{j,e} = -\frac{AE}{L}(u_i - u_j) \tag{2.4}$$

The spring stiffness can be written

$$k = \frac{AE}{L} \tag{2.5}$$

Consider a spring element e of spring rate k_e, with nodes i and j, as shown in Figure 2.4. The forces f and displacement u directed toward the right as positive, the forces at each node can be written as

$$f_{i,e} = k_e(u_i - u_j) = k_e u_i - k_e u_j \tag{2.6}$$

$$f_{j,e} = k_e(u_j - u_i) = -k_e u_i + k_e u_j \tag{2.7}$$

The two equations can be written in matrix form as

$$\begin{Bmatrix} f_{i,e} \\ f_{j,e} \end{Bmatrix} = \begin{bmatrix} k_e & -k_e \\ -k_e & k_e \end{bmatrix} \begin{Bmatrix} u_i \\ u_j \end{Bmatrix} \tag{2.8}$$

in a brief form as

$$\{F\} = [k]\{u\} \tag{2.9}$$

where $[k]$ is the element stiffness matrix, $\{u\}$ is the vector of nodal displacement, and $\{F\}$ is the vector of nodal forces.

2.2.1 One Dimensional Spring-Damper Element

A spring is an elastic element used to store mechanical energy and retains its original shape after a force is removed. Springs are typically defined in a stress free or unloaded state. This means that no longitudinal loading conditions exist unless preloading is specified. In FEA system, springs are defined as longitudinal and they connect two bodies together or connect a body to ground. Longitudinal springs generate the force that depends on linear displacement. Longitudinal springs could be used as a damping force which is a function of velocity. A spring-damper element that contains two nodes at the ends is shown in Figure 2.5.

This material is reserved for educational use only, not allowed for commercial use.
Forbidden to modify the content, and cite the document when use.

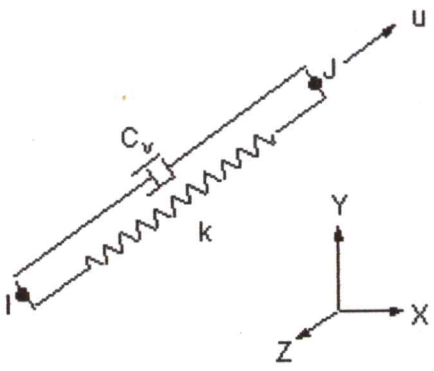

Figure 2.5 Spring-damper element [4]

Consider the case of a single DOF per node. The form of the element stiffness K_e and damping matrices C_e are

$$[K_e] = k\begin{bmatrix} 1 & -1 \\ -1 & 1 \end{bmatrix} \tag{2.10}$$

$$[C_e] = C_v\begin{bmatrix} 1 & -1 \\ -1 & 1 \end{bmatrix} \tag{2.11}$$

where k is the stiffness matrix and C_v is the damping coefficient matrix. The static force of spring-damper element can be computed

$$F_s = k\varepsilon_0 \tag{2.12}$$

where F_s is the static force and ε_0 is the spring stretch. Finally, if a nonlinear transient dynamic analysis is performed, a damping force is computed

$$F_D = C_v v \tag{2.13}$$

According to the Equation (2.13), the damping force F_D involves C_v the damping coefficient and v the relative velocity.

2.2.2 Mixed-Dimensional Elements by Constraint Equations

When the different element types are required, it is necessary to define the relationships among different degrees of freedom using an additional element to connect the node. Establishment such special association among nodal degrees of freedom by constraint equations is

This material is reserved for educational use only, not allowed for commercial use.
Forbidden to modify the content, and cite the document when use.

possible. This techniques enables the models to link degrees of freedom in ways that elements cannot. The technique of constraint equations is described by Figure 2.6.

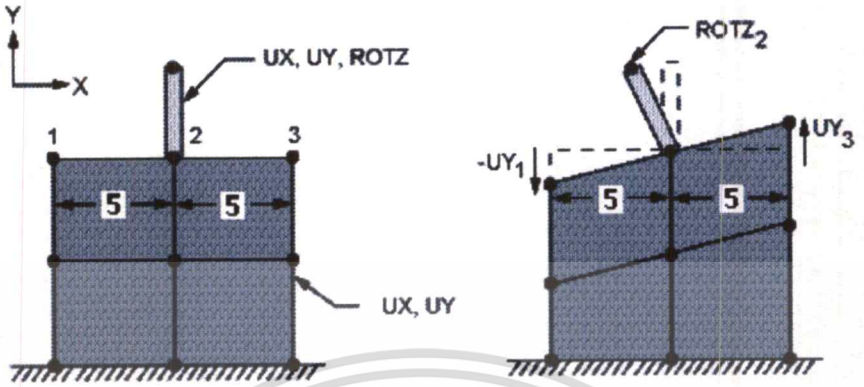

Figure 2.6 Definition of constraint equations [4]

In Figure 2.6, node 2 acts as a hinge if no constraint equations are used. In order to transfer moment between the beam and the plane-stress elements, the constraint equations can be

$$ROTZ_2 = (UY_3 - UY_1)/10 \tag{2.14}$$

This equation would be rewritten in the required format and entered into the finite element program as

$$0 = UY_3 - UY_1 - (10 * ROTZ_2) \tag{2.15}$$

The first unique degree of freedom in the equation is eliminated in terms of all other degrees of freedom in the equation. A unique degree of freedom is one which is not specified in any other constraint equation, coupled node set, specified displacement set, or master degree of freedom set. The mixed dimensional elements are needed in some structural problems because the computational time could considerably be reduced especially the large problem. An example of automobile structure demonstrated the mixed elements between shell and beam element is shown in Figure 2.7. It demonstrated the replacement of beam elements in a vehicle model to achieve the computational time. The constraint equations were employed on several defined geometric cross sections and shell surfaces. In a study, the results obtained from the original model which only used shell elements as shown in Figure 2.7 (a) and the conceptual model employed mixed elements as shown in Figure 2.7 (b) were compared. The comparison showed that small

This material is reserved for educational use only, not allowed for commercial use.
Forbidden to modify the content, and cite the document when use.

differences of 0.46% and 0.22% between the original and the conceptual model were found for the torsion and bending load cases respectively.

(a) (b)

Figure 2.7 Mixed element applied to B-pillars on passenger car: (a) original model (b) conceptual beam model [5]

2.2.3 Static Structural Analysis

Static structural analysis used to determine the displacements, stresses, strains, and forces in structures or components caused by loads that do not induce significant inertia and damping effects. Steady loading and response conditions are assumed to vary slowly with respect to time. In general, the equations that are solved for static linear analysis are

$$\{F\} = [K]\{u\} \tag{2.16}$$

or

$$\{F^a\} + \{F^r\} = [K]\{u\} \tag{2.17}$$

where the static analysis equation consists of $[K]$ the total stiffness matrix, $\{u\}$ the nodal degree of freedom (DOF) vector, $\{F^a\}$ the total applied load vector, and $\{F^r\}$ the nodal reaction load vector. The total load vector is defined by

$$[F^a] = \{F^{nd}\} + \{F^e\} \tag{2.18}$$

where the total load is a summation of $\{F^{nd}\}$ the applied nodal load vector and $\{F^e\}$ the total of all element load vector.

A static analysis calculates the effects of steady loading conditions on a structure while ignoring inertia and damping effects which caused by time-dependent loads. Small deflection and

This material is reserved for educational use only, not allowed for commercial use.
Forbidden to modify the content, and cite the document when use.

small strain assume that displacements are small enough to give the stiffness change insignificance.

2.2.4 Dynamic Structural Analysis

Transient dynamic analysis is sometimes called time-history analysis. It is a technique used to determine the dynamic response of a structure under the action of any general time-dependent loads. It could also be used to determine the time-dependent displacements, strains, stresses, and forces in a structure. The time scale of the loading is that the inertia or damping effects are considered important. If the inertia and damping effects are not important, it is better to use a static analysis instead. The basic equation of motion solved by a transient dynamic analysis is

$$\{F^a\} = [M]\{\ddot{u}\} + [C]\{\dot{u}\} + [K]\{u\} \tag{2.19}$$

Because the dynamic analysis involves the structural mass and damping coefficient, $[M]$ is called the structural mass matrix, $\{\ddot{u}\}$ the nodal acceleration vector, $[C]$ the damping matrix, and $\{\dot{u}\}$ the nodal velocity vector. The Newmark time integration method for implicit transient analysis is used for obtaining the solution of Equation (2.19). It uses finite difference expansions in the time interval Δt in which it is assumed that

$$\{\dot{u_{n+1}}\} = \{\dot{u_n}\} + [\{1-\delta\}\{\ddot{u}_n\} + \delta\{\ddot{u}_{n+1}\}]\Delta t \tag{2.20}$$

$$\{u_{n+1}\} = \{u_n\} + \{\dot{u_n}\}\Delta t + \left[\left(\frac{1}{2} - \alpha\right)\{\ddot{u_n}\} + \alpha\{\ddot{u}_{n+1}\}\right]\Delta t^2 \tag{2.21}$$

where

δ and α are the Newmark integration parameters

Δt is $t_{n+1} - t_n$

$\{u_n\}$ is the nodal displacement vector at time t_n

$\{\dot{u_n}\}$ is the nodal velocity vector at time t_n

$\{\ddot{u}_n\}$ is the nodal acceleration vector at time t_n

$\{u_{n+1}\}$ is the nodal displacement at time t_{n+1}

$\{\dot{u_{n+1}}\}$ is the nodal velocity vector at time t_{n+1}

$\{\ddot{u}_{n+1}\}$ is the nodal acceleration vector at time t_{n+1}

This material is reserved for educational use only, not allowed for commercial use.
Forbidden to modify the content, and cite the document when use.

Since the primary aim is the calculation of displacement $\{u_{n+1}\}$, the governing Equation (2.19) is evaluated at the time t_{n+1} can be

$$\{F^a\} = [M]\{\ddot{u}_{n+1}\} + [C]\{\dot{u}_{n+1}\} + [K]\{u_{n+1}\} \tag{2.22}$$

2.3 Strain Gage

In order to design a structure which ensures the necessary strength while keeping such a safety requirement, it is necessary to know the stress borne by each material part. However, at the present scientific method, there is no technology which enables direct measurement and judgment of stress. Consequently, the strain on the surface is measured in order to know the internal stress. Strain gage is the most common sensing element to measure surface strain. When a material receives a tensile force P, it has a strain ε that corresponds to the applied force. In proportion to the strain, the cross-section elongates by ΔL from the original length L before receiving the tensile force as shown in Figure 2.8.

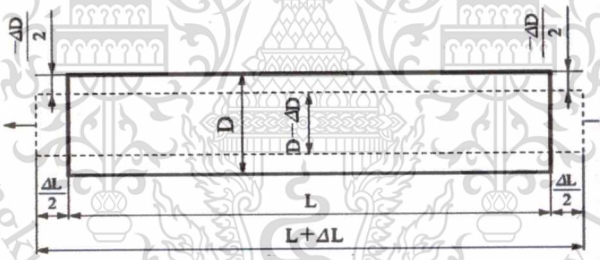

Figure 2.8 Principle of strain gage in tension [6]

The ratio of the elongation to the original length is called tensile strain and it is expressed as

$$\varepsilon = \frac{\Delta L}{L} \tag{2.23}$$

The relation between stress and strain initiated in a material by an applied force could be based on Hooke's law $\sigma = E\varepsilon$.

A common type of strain gage is a foil strain gage. The foil strain gage has metal foil photo-etched in a grid pattern on the electric insulator of the thin resin and gage leads as can be seen in Figure 2.9.

This material is reserved for educational use only, not allowed for commercial use.
Forbidden to modify the content, and cite the document when use.

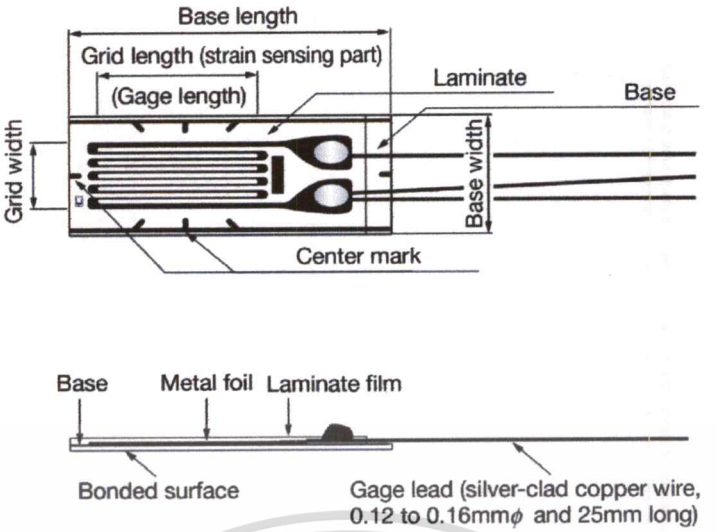

Figure 2.9 Structure of foil strain gage [6]

The strain gage is bonded to the measuring object with a dedicated adhesive. Strain occurring on the measuring site is transferred to the strain-sensing element via the gage base. For accurate measurement, the strain gage and adhesive should match the measuring material and operating conditions including temperature. Each metal has its specific resistance. An external tensile or compressive force increases or decreases the resistance by elongating and contracting it respectively.

The principle of strain measurement involves the resistance change. Strain-initiated resistance change is extremely small. Thus, a Wheatstone bridge is formed to convert the resistance change to a voltage change. In Figure 2.10, the resistances are R1, R2, R3 and Rg. The resistance of strain gage Rg changes by ΔR due to surface deformation with the original resistance R. The gage factor K_s is a coefficient expressing strain gage sensitivity. For a general-purpose strain gage, it use copper-nickel or nickel-chrome alloy for the resistive element and the gage factor provided by these alloys is approximately 2. An output voltage is proportional to a change in resistance i.e. a change in strain. This microscopic output voltage e_0 is amplified for analog recording or digital indication of the strain. The output voltage is obtained with the following equation

$$e_0 = \frac{1}{4} \cdot \frac{\Delta R}{R} \cdot V_{EX} = \frac{1}{4} \cdot K_s \cdot \varepsilon \cdot V_{EX} \tag{2.24}$$

where V_{EX} is the bridge voltage.

This material is reserved for educational use only, not allowed for commercial use.
Forbidden to modify the content, and cite the document when use.

สำนักหอสมุดกลาง พระจอมเกล้าลาดกระบัง

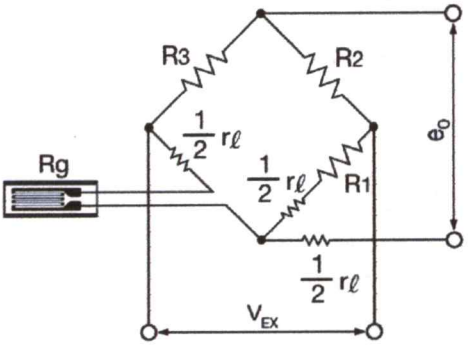

Figure 2.10 Strain gage bridge for 1 active gage in 2-wire system [6]

With the 1-gage system as shown in Figure 2.10, a strain gage is connected to a side of the bridge and a fixed resistor is inserted into each of the other 3 sides. This system could easily be configured and thus it is widely used for general strain measurement. The 1 gage in 2-wire system receives much influence of leads. Therefore, if large temperature changes are anticipated or if the leadwire length is long, the 1 gage in 3-wire system is preferable.

The strain gage in 3-wire system is a common method of compensating temperature effect of leadwire. For effective self-temperature-compensation, strain gages adopt the 1-gage system. However, if the leadwire cable is a 2-wire system, strain output from the bridge is affected by temperature effect of the leadwire. If 3 leads are connected to the strain gage as shown in Figure 2.11, one half the leadwire resistance $r\ell$ is applied to the adjacent side of the bridge to compensate the resistive components of the 2 leads affected by a similar temperature change. Thus, the bridge output is free from any temperature effect of the leadwire. The temperature effect of a third lead connected directly to the amplifier could be ignored since the amplifier provides a high input impedance. As precautions in using the 3-wire system, three leads should be the same type, length, and its cross section to receive the same temperature effect.

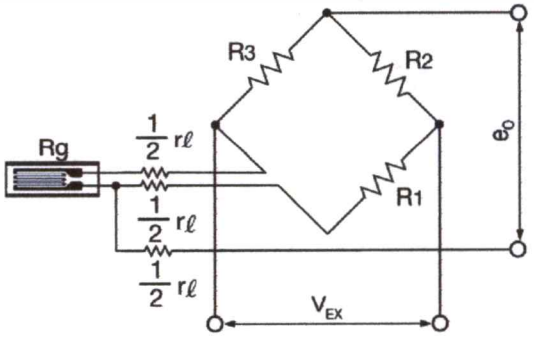

Figure 2.11 Strain gage in 3-wire system [6]

This material is reserved for educational use only, not allowed for commercial use.
Forbidden to modify the content of the document when use.
76491

There have been many applications used strain gage to measure strength of automobile parts such as Dusan M. et al. [7] measured strength of an airport bus structure at the critical area. From the previous study, the analysis results revealed that the critical stress was observed on the door frame during the cornering condition. In order to investigate structural strength around the door frame, three strain gages were attached as shown in Figure 2.12. In experiment, test condition was a cornering at a maximum speed of 40 km/hr in a designated circle. The strain gages measured the deformation change and converted to stress. The maximum stress was calculated to be 65.1 MPa.

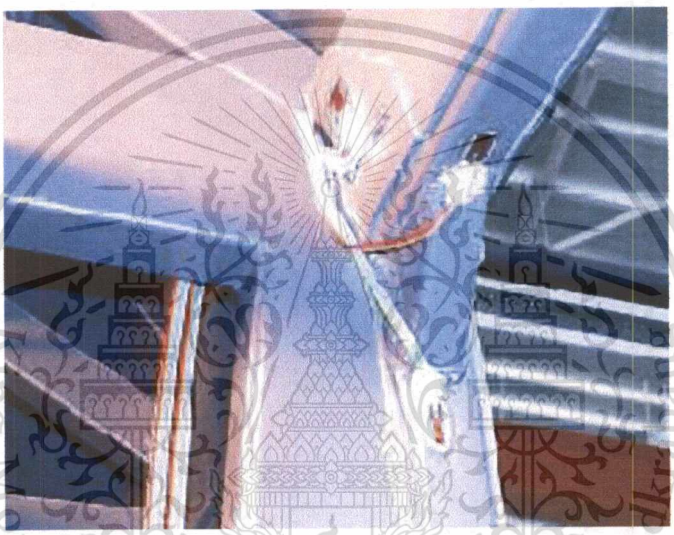

Figure 2.12 Strain gage attachment on the door frame of an airport bus [7]

In addition, strain gage could also be used to obtain the road condition. Emmanuel F. et al. [8] implemented a ride quality criteria, which was specified by the Texas Department of Transportation, using dynamic data collected from different load conditions. Dynamic load from the road surface was measured on the pavement section. Strain gages were mounted on the left and right side of the axles as shown in Figure 2.13. It was found that the pavement response was relatively constant during the experiment and the amplitude of the dynamic load was related to several factors such as axle weight, road condition, and tire pressure. The results from measurement were used for statistical calculation to obtain the standard deviation and the absolute difference. It was showed that a maximum standard deviation of repeatability profiles was 21, which were not exceeded 35, and the absolute difference of the accuracy profile was 13 that were also within 20. Therefore, the small vehicle met the ride quality requirements.

This material is reserved for educational use only, not allowed for commercial use.
Forbidden to modify the content, and cite the document when use.

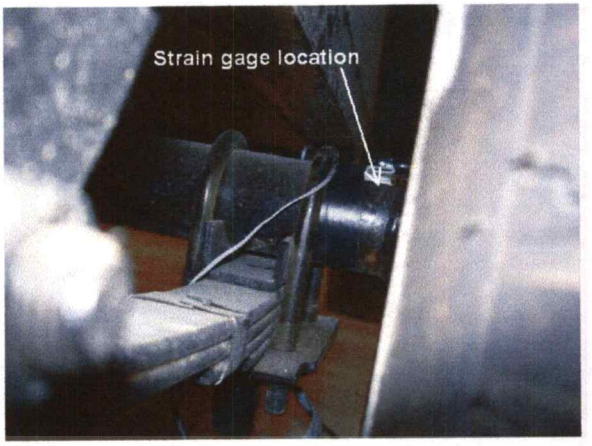

Figure 2.13 Dynamic load measurement using strain gages [8]

Ilankamban et al. [9] used strain gages to obtain the dynamic load on a lower control arm. In the past, conventional measurement was that the load cells were attached on the critical areas of the component. This method could change the stiffness and mass of the component that directly affected the load environment. Resulting loads in the system could become a major source of discrepancy between the measured load and the load in the actual system. In order to identify the proper location for measuring the dynamic load from strain gage on a lower control arm, software developed in-house called BLC (Back Load Calculator) was used in conjunction with numerical analysis. The strain gage attachment at various appropriate locations is illustrated in Figure 2.14. This technique of strains converted to loads is a common use in an automobile suspension component. The resulting loads showed excellent correlation between the loads calculated by strains and the loads obtained from simulation. The proposed method consistently showed considerable improvement over the conventional method.

Figure 2.14 Strain gage attachment on suspension lower control arm [9]

This material is reserved for educational use only, not allowed for commercial use.
Forbidden to modify the content, and cite the document when use.

2.4 Accelerometer

An accelerometer is used to measure acceleration or vibration characteristics of the components such as an acceleration of a car body and a vibration of machinery parts. A common accelerometer employs a semiconductor and strain gage as the sensing elements to measure acceleration. The basic configuration of acceleration measurement is illustrated in Figure 2.15.

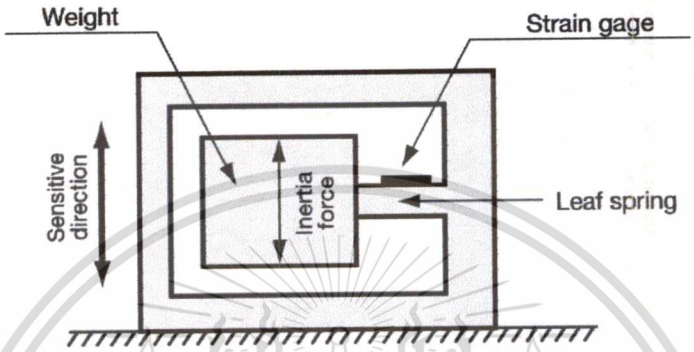

Figure 2.15 Basic configuration of strain gage accelerometer [10]

Figure 2.15 shows configuration of a uniaxial accelerometer. The strain gage attached on the leaf spring detects the surface deformation of the leaf spring as a strain quantity proportional to the acceleration. The strain gage signal is amplified to enable acceleration measurement. However, several applications such as vehicle testing require 3-axis accelerometer. The 3-axis accelerometer is shown in Figure 2.16. This model employed a sputtering technique mounting 3 uniaxial accelerometers on the 3-axis bracket. Consequently, it allowed simultaneous detection of accelerations in three directions which were X, Y and Z coordinates.

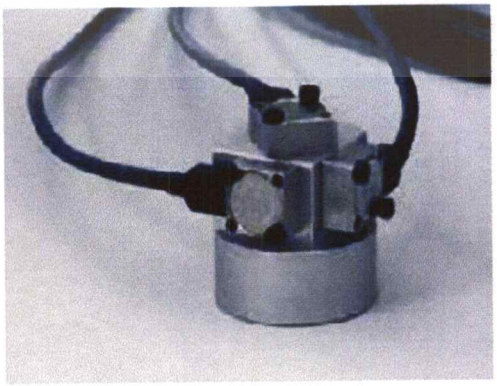

Figure 2.16 Multiple accelerometers mounted on 3-axis bracket [11]

This material is reserved for educational use only, not allowed for commercial use.
Forbidden to modify the content, and cite the document when use.

Mujahid A. [12] attached four accelerometers at four corners of the racing car. It was for the motion parameter measurement during the drifting situation as shown in Figure 2.17. A drift racing challenges drivers to navigate a course in a sustained sideslip by exploiting coupled nonlinearities in the tire force response. Several physical parameters affecting the drift motion that related to performance and handling qualities were studied. The comparison between data collected during drifting against data from the estimation revealed a small discrepancy in the magnitude of the yaw acceleration incurred during turning maneuver.

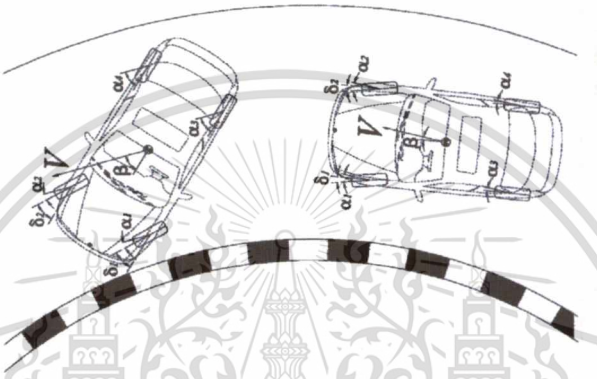

Figure 2.17 Drift vehicle performing a left-hand drift on the test track [12]

Timothy J. et al. [13] reported an experimental study of a vehicle vibration response. In general, the vehicle characteristics are very useful for several research fields such as vibration analysis, vehicle comfort, and structural analysis. The characteristics could be determined by an acceleration response. In this study, two accelerometers were mounted on the frame above the wheel and at the end of the front axle to capture the sprung-mass and unsprung-mass acceleration respectively. The attachment of the accelerometers is shown in Figure 2.18.

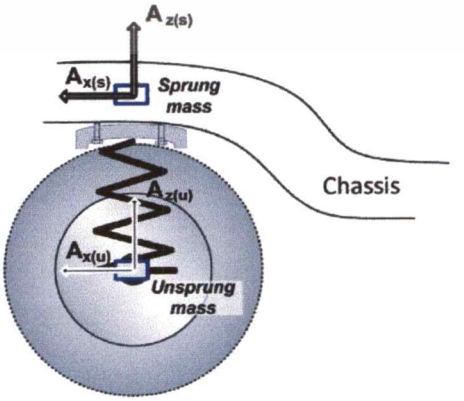

Figure 2.18 Acceleration measurement on the vehicle chassis and the axle [13]

This material is reserved for educational use only, not allowed for commercial use.
Forbidden to modify the content, and cite the document when use.

2.5 Data Acquisition

The purpose of data acquisition (DAQ) is to measure an electrical or physical phenomenon such as voltage, current, temperature, pressure, or sound that are generated from the sensors. Computer-based data acquisition uses a combination of modular hardware, application software, and a computer to complete measurements as shown in Figure 2.19. While each data acquisition system is defined by its application requirements, every system shares a common goal of acquiring, analyzing, and presenting information.

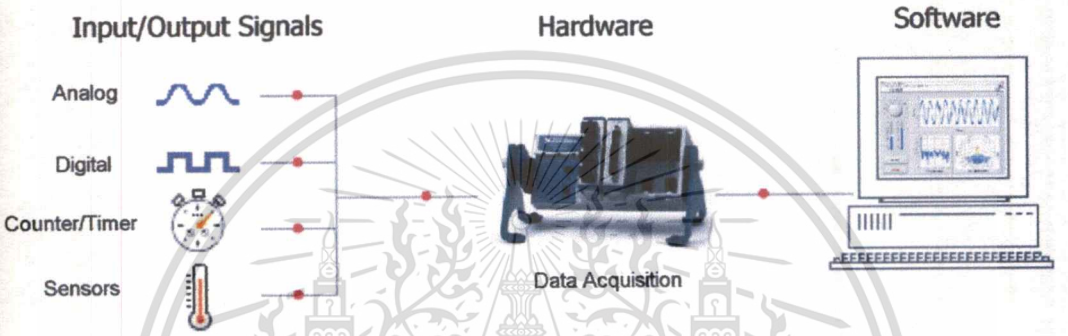

Figure 2.19 Data acquisition system [14]

From Figure 2.19, the analog physical input and output signals involve gathering signals from measurement sources. The signals are then digitized by data acquisition for storage and analysis before presenting on a computer screen. The data acquisition installed in a test vehicle is shown in Figure 2.20.

Figure 2.20 Data acquisition in testing of vehicle dynamics [15]

This material is reserved for educational use only, not allowed for commercial use.
Forbidden to modify the content, and cite the document when use.

From Figure 2.20, the data acquisition VFRICOM VC3000 was selected to obtain the dynamic characteristics of the vehicle body. It allows acceleration measurement with 1.5 g range as a maximum. The VC3000 also enables the user interface to use the front panel buttons on the display screen without a need of computer. The real-time measured data was also displayed when operating.

2.6 Structural Deformation of Vehicle

The first step to design a vehicle frame or any structure is to understand the loads acting on the structure. The deformation modes of automobile chassis are illustrated in Figure 2.21.

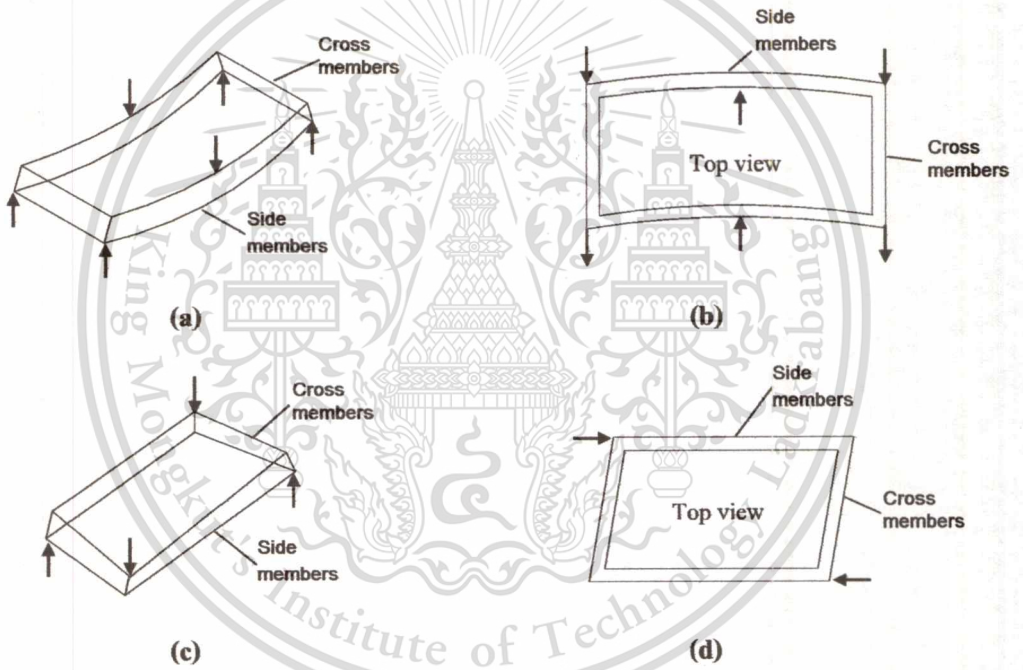

Figure 2.21 Deformation modes of vehicle frame: (a) vertical bending, (b) lateral bending, (c) torsion, and (d) lozenging [16]

In Figure 2.21 (a), the weight of the passengers and all components mounted to the vehicle frame including engine, electrical devices are carried in vertical bending because the reactions are taken up at both front and rear axles. The lateral bending as shown in Figure 2.21 (b) is introduced on the vehicle frame for various reasons such as road camber, side wind loads, and centrifugal forces during cornering. The lateral bending generally comes from sideway forces acting along the length of the vehicle and resisted at the tires. The torsion is produced by the

This material is reserved for educational use only, not allowed for commercial use.
Forbidden to modify the content, and cite the document when use.

vertical loads acting on one or two oppositely opposed corners of the vehicle as shown in Figure 2.21 (c). Torsional loads corresponding to torsional deformation of the vehicle frame could affect the handling performance. Figure 2.21 (d) illustrates lozenging deformation that could observe during a braking condition due to unequal forces at each side of the vehicle frame.

2.7 Vehicle Testing

Now a day, market conditions are forcing manufacturers to reduce the time to develop and market new products to reduce costs with value analysis and to produce higher standards of reliability to satisfy the expectations of consumers. Thus, products still need to be tested in order to back up predictions of the analytical models and to answer questions that they simply cannot answer satisfactorily. Two forms of product testing might be identified, namely performance testing and endurance testing. Performance testing evaluates the functional and performance characteristics of the product against the product design specification. Endurance testing evaluates the durability characteristics of the product. In automotive industries, the endurance testing might involve laboratory testing, proving ground testing, and field testing [17]. The testing conditions together with some basic equations supporting the study are demonstrated in the next sections.

2.7.1 Braking

When the vehicle decelerates, the mass times acceleration or inertia force is generated in longitudinal direction. As the centre of gravity of the vehicle is above the road surface, the inertia force provides a load transfer from rear axle to front axle as shown in Figure 2.22.

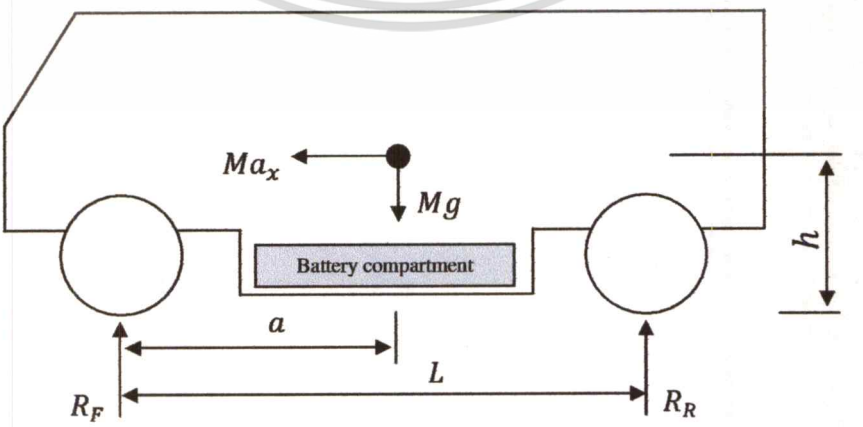

Figure 2.22 Longitudinal loading

This material is reserved for educational use only, not allowed for commercial use.
Forbidden to modify the content, and cite the document when use.

From Figure 2.22, the heights of the centers of gravity of all components are required in order to obtain a complete view of all the forces acting on the body. A simplified model considering one braking inertia force generated at the vehicle center of gravity could provide useful information about the local loading at the axle positions. The braking force generated during deceleration can be calculated from

$$F_b = Ma_x \tag{2.25}$$

where F_b is the braking force, M is the vehicle mass, and a_x is the linear deceleration. At constant deceleration, it can be obtained from

$$a_x = \frac{v_0^2 - v_f^2}{2S} \tag{2.26}$$

where v_0 and v_f are the vehicle velocity before braking and the final velocity of the vehicle (= 0 m/s) respectively. S is the brake distance. The reactions on the axles are

$$R_F = \frac{Mg(L-a) + Mh\left(\frac{dv}{dt}\right)}{L} \tag{2.27}$$

$$R_R = \frac{Mga - Mh\left(\frac{dv}{dt}\right)}{L} \tag{2.28}$$

where R_F and R_R are the reaction forces on front and rear axle respectively. g is the acceleration of gravity and h is the height of center of gravity.

2.7.2 Cornering

Lateral load is a result of a cornering inertia force acting at the centre of gravity of the vehicle. This lateral load also reacts against the mounting points of the front and rear suspension systems. The vertical loads on the outer wheels increase while those on the inner wheels decrease. Consequently, the load acting above the ground plane could cause a moment. This moment might lead to changes in vertical loads at the tires that affect vehicle handling and stability. A simplified model considering one cornering inertia force generated at the vehicle center of gravity and

This material is reserved for educational use only, not allowed for commercial use.
Forbidden to modify the content, and cite the document when use.

balanced by the forces at the contact patches between the outer tires and the ground is shown in Figure 2.23.

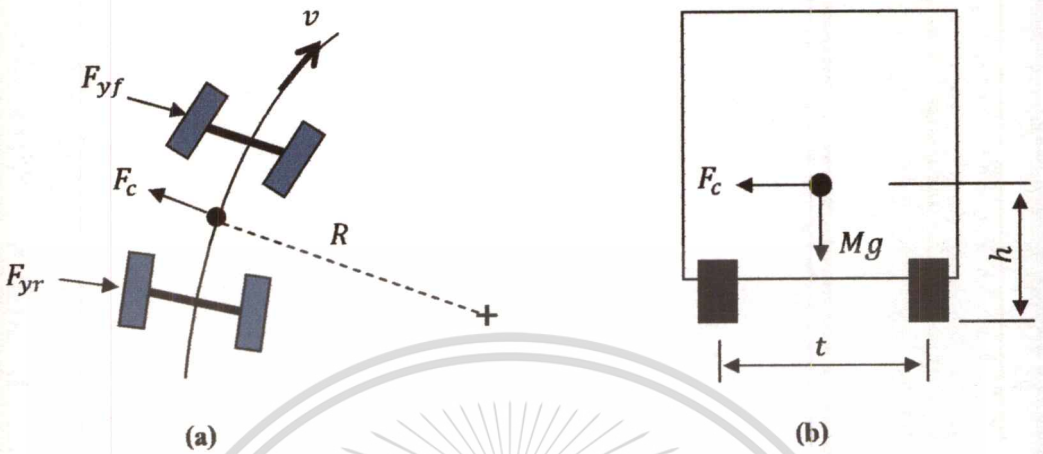

Figure 2.23 Lateral loading: (a) top view (b) front view

When cornering, the centrifugal force generated at center of the gravity of vehicle can be calculated from

$$F_c = \frac{Mv^2}{R} = \frac{Mgt}{2h} \tag{2.29}$$

where F_c is the centrifugal force at the center of gravity, v is the forward velocity, R is the radius of the turn, t is the track width, and h is the height of the center of gravity. The centrifugal force can also be determined as a combination of the contact patch loads

$$F_c = F_{yf} + F_{yr} \tag{2.30}$$

where F_{yf} and F_{yr} are the lateral forces at the outer front tire and rear tire respectively.

2.7.3 Double Lane Change

A double lane change is used to determine handling and stability of the bus by measuring speed through a double lane change test. The bus is driven through a double lane change course at increasing speed until the test is considered unsafe or a speed of 45 mph is reached. As can be seen in Figure 2.24, the bus begins in one lane, change to another lane, and return to the original lane.

This material is reserved for educational use only, not allowed for commercial use.
Forbidden to modify the content, and cite the document when use.

Figure 2.24 Right-hand approach of double lane change maneuver [18]

2.7.4 Structural Integrity

The structural integrity is to determine static characteristics of the bus structure subjected to the vertical loading. In this test, the bus is isolated from the suspension by blocking the vehicle movement at the suspension points. The bus is then loaded and unloaded with a distributed load equal to 2.5 times designed passenger loads. The loads are applied to every passenger seats and the floor space. The permanent deflection is measured at several locations after unloading. Structural integrity test using sandbags loaded the bus structure is shown in Figure 2.25.

Figure 2.25 Bus loaded to 2.5 times passenger weight [18]

2.7.5 Torsional Stiffness

The torsional stiffness could be evaluated for specific criteria while other criteria could be based on experience and development. If the stiffness is low, driver perception is that the front of the vehicle appears to shake with the front wing structures tending to move up and down.

This material is reserved for educational use only, not allowed for commercial use.
Forbidden to modify the content, and cite the document when use.

Practical problems of doors failing to close properly occur when the vehicle is parked on uneven ground such as with one wheel on a curb. Open-top sports cars with no structural roof panel are likely to have poor torsional stiffness unless the underbody is reinforced. Therefore, it is important that the vehicle structure contain adequate torsional stiffness. The torsional stiffness can be calculated as

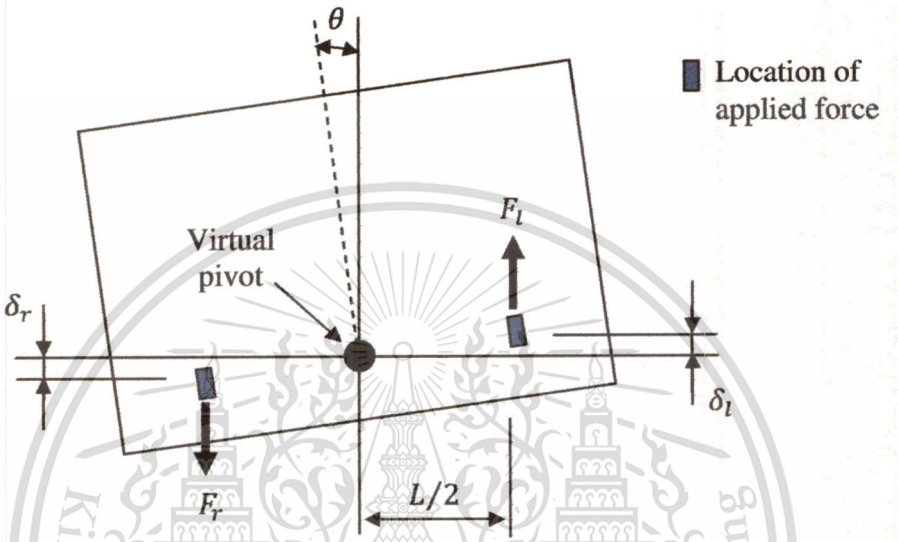

Figure 2.26 Front view of vehicle body subjected to vertical loads in opposite directions

In order to calculate the torsional stiffness, the applied torque T and the twist angle θ are measured.

$$K = \frac{T}{\theta} \tag{2.31}$$

The torque and the twist angle can be expressed as

$$T = \left(\frac{|F_r| + |F_l|}{2}\right) L \tag{2.32}$$

$$\theta = \tan^{-1}\left(\frac{|\delta_r| + |\delta_l|}{L}\right) \tag{2.33}$$

where F_r and F_l are the applied forces at the right front and the left front suspension mounting point respectively, L is the lateral distance between the applied force positions. The right δ_r and left δ_l vertical displacements are measured for calculating the twist angle.

This material is reserved for educational use only, not allowed for commercial use.
Forbidden to modify the content, and cite the document when use.

Steven et al. [19] displayed the torsional stiffness of an automobile chassis obtained from finite element analysis. Two different approaches such as analytical and numerical calculation were considered. A disadvantage of analytical method is that a large number of long calculations to determine the torsional stiffness is required and it was only based on the geometry. Thus, the present FEA-based method was more practical to apply loads and measure the resulting deflections. The applied loads were applied at the suspension mounting points as shown in Figure 2.27. Loads in the same magnitudes but opposite in direction were applied to both sides of front suspension mounting points ranging from 1500 N-m to 3750 N-m with increments of 375 N-m. This loading condition created the pure torsion to the structure. The fixed constraints were applied at both rear suspension mounting points. A graph of applied torque against the angle of rotation was generated. The slope of the graph was the overall torsion stiffness of the body. The overall torsion stiffness was found to be 3000 N-m/rad. The result obtained was a reasonable value compared to an actual vehicle that had numerous structural members missing such as cross members and all panels were of uniform thickness and material. It was suggested that the torsional stiffness obtained from the numerical analysis should be verified by experimental measurement.

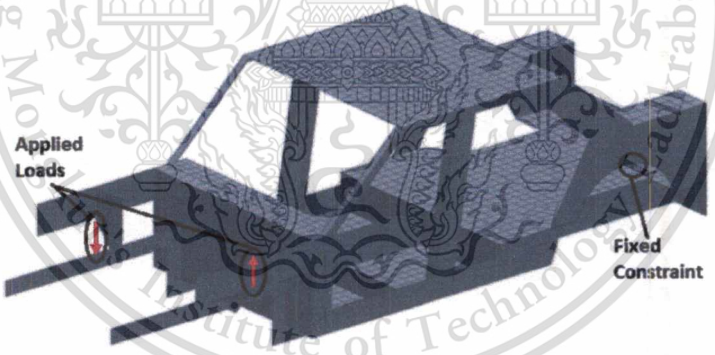

Figure 2.27 Applied loads and constraints for torsional analysis [19]

Another remarkable research used torsional stiffness as a constraint in structural optimization was done by Boada et al. [20]. This presented a methodology to obtain a lightweight bus model using genetic algorithm of structural optimization. A simplified bus model was created as shown in Figure 2.28. In analysis, the simplified bus structure was generated by line bodies before treating to the beam elements. The force was applied at the right front position of the model while other 3 locations were fixed all translations. This would create a torsional load which was represented the actual forces acting on the real structure. Such that the torsion stiffness was

This material is reserved for educational use only, not allowed for commercial use.
Forbidden to modify the content, and cite the document when use.

calculated by the applied force and twist angle. In optimization, structural weight, torsional stiffness, and thicknesses were the optimization parameters. The structure of the bus was optimized by means of genetic algorithms. It was found that mass and torsional stiffness of the optimized structure were reduced by 68.7% and 66.1% respectively. In addition, a maximum improvement of the design variables was 75%.

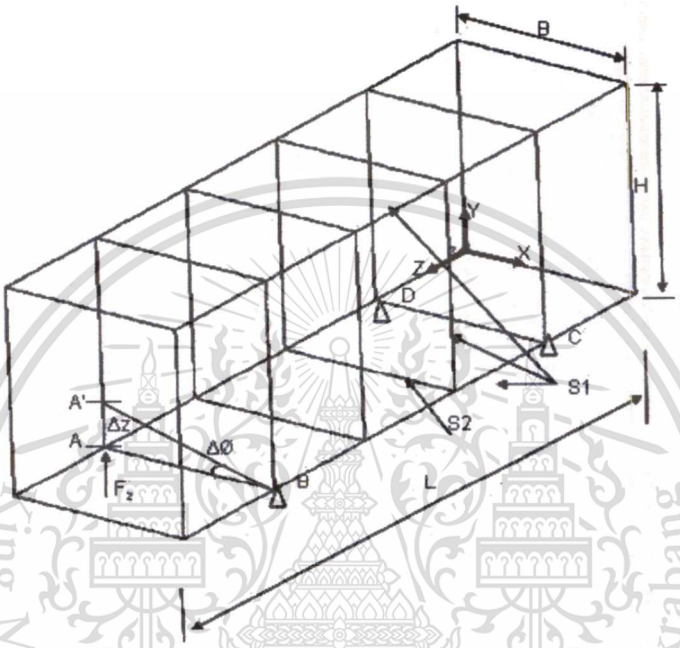

Figure 2.28 Simplified bus structure subjected to torsional load [20]

However, few studies have been carried out on experimental measurement of torsional stiffness using the real structure. John S. [21] setup the test for the torsional stiffness measurement on a CAV GT chassis as shown in Figure 2.29. In order to measure the torsional stiffness, the rear suspension was locked to the floor by means of a jig while the front suspension was allowed to rotate around a specified pivot point as shown in Figure 2.29 (a). A vertical load was applied to the end of the torque arm to create torsion to the chassis. The load was applied by a hydraulic cylinder and a loadcell was used to obtain the load path. The twist angel was measured by two dial gages. From the measurements, the torsional stiffness of the chassis was calculated to be 32,154 N-m/degree by the slope of an applied torque and the angle as shown in Figure 2.29 (b). Little nonlinearity of the torsional stiffness was observed that was next to the zero coordinate due to a hypothesis in several welding joints on the structure.

This material is reserved for educational use only, not allowed for commercial use.
Forbidden to modify the content, and cite the document when use.

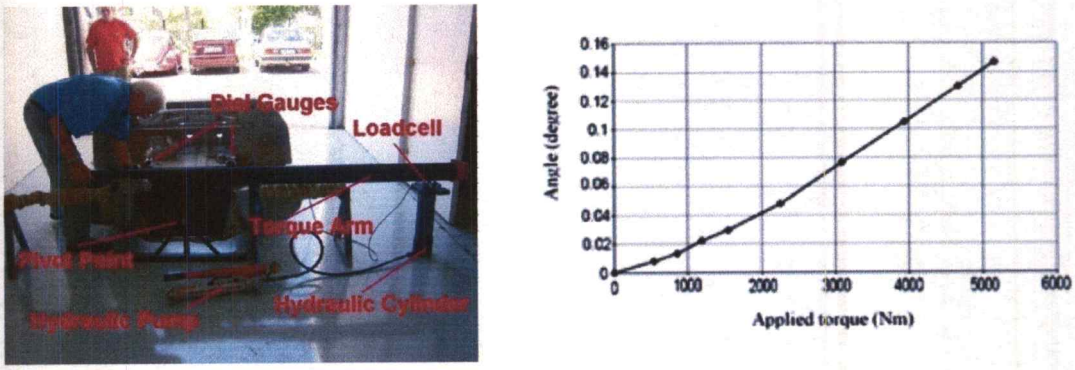

Figure 2.29 Torsion test: (a) experimental setup (b) torsional stiffness [21]

Lonny L.T. et al. [22] fabricated and verified the twist fixture which could be used for torsion stiffness measurement. The fixture was relatively lightweight and portable with the ability to be transported and set-up by one person as shown in Figure 2.30. The test was carried out on several chassis at different manufacturers. The deflections of the chassis at several locations were detected by dial indicators. The accuracy of twist fixture was validated through finite element analysis. It was found that the error between torsional test and simulation was about 6% due to uncertainty in the measured data and small changes in stiffness contributed by the welding joints.

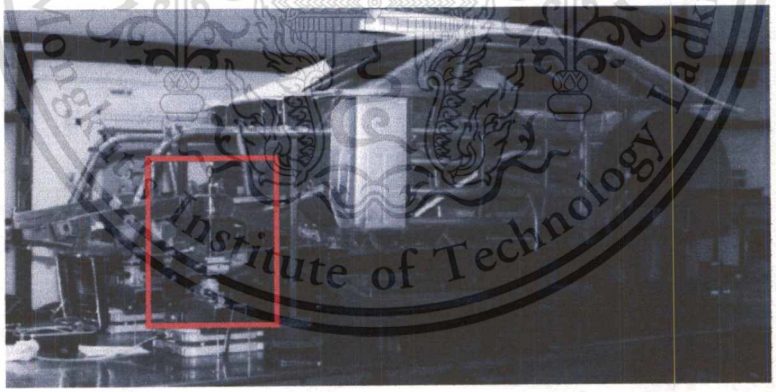

Figure 2.30 Portable twist fixture for torsional stiffness measurement [22]

2.8 Structural Optimization

Structural optimization deals with engineering design problems with the aim of finding an optimal point that satisfies a number of given constraints. Structural optimization problems are characterized by various objective and constraint functions which are generally non-linear

This material is reserved for educational use only, not allowed for commercial use.
Forbidden to modify the content, and cite the document when use.

function of design variables. These functions are usually implicit, discontinuous, and non-convex. The mathematical formulation of the structural optimization problem with respect to the objective, design variables, and constraint functions depends on the type of application. However, the general engineering constrained optimization is stated as follows [23]

Minimize

$$f = f(x) \tag{2.34}$$

Subject to

$$g_k(\{x\}) \leq 0 \qquad k = 1,2,\dots,K \tag{2.35}$$

$$h_l(\{x\}) = 0 \qquad l = 1,2,\dots,L \tag{2.36}$$

where f is the objective function, g is the inequality constraints, and h is the equality constraints. K and L are the numbers of inequality and equality constraints respectively. The design variable is given as

$$\{x_L\} \leq \{x\} \leq \{x_U\} \tag{2.37}$$

where $x = (x_1, x_2, \dots, x_n)^T$ is the column vector of n design variables. Each variable contains upper and lower bound with x_U and x_L respectively.

2.8.1 Design of Experiment (DOE)

In process of engineering design, it is very important to understand how many input variables are contributing factors to the output variables of interest. It is a lengthy process before a conclusion is made as to which input variables play a role in influencing the output variables. Design of Experiment (DOE) helps revolutionize the lengthy process of costly and time-consuming trial-and-error search to a powerful and cost-effective statistical method in terms of computational time. The Central Composite Designs (CCD) is commonly used in the DOE process. The Face-Centered CCD is a special case of central composite designs. As a result, the Face-Centered CCD becomes a three-level design that is located at the center of each face formed by any two factors. The geometry representation of Face-Centered CCD of three factors is shown in Figure 2.31.

This material is reserved for educational use only, not allowed for commercial use.
Forbidden to modify the content, and cite the document when use.

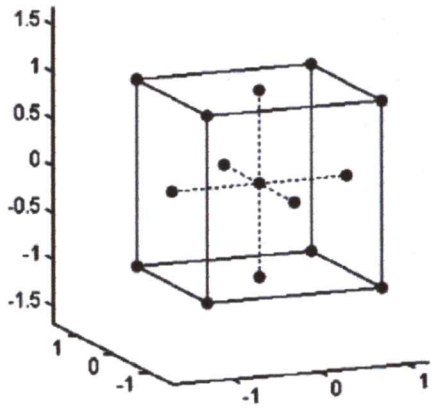

Figure 2.31 Central composite designs [4]

2.8.2 Sensitivity Analysis

The sensitivity plot is to display how sensitive the output parameters are to the input parameters. The sensitivity could help innovate toward a more reliable and better quality design. The sensitivity analysis is based on a statistical correlation using the generated sample points which are located throughout the entire space of input parameters. The true response $y(x)$ is approximated by the first order polynomial $f(x)$ which is defined as

$$f(x) = \sum_{j=1}^{L} b_j \phi_j(x) \tag{2.38}$$

where L is the size of basis function vector $(\phi_j = [1, x_1, \dots, x_n]^T)$. The vector of constant b is determined through minimization of summation of the square errors computed by

$$\sum_{i=1}^{P} \{[y_i(x) - f_i(x)]^2\} = \sum_{i=1}^{P} \left\{ \left[y_i(x) - \sum_{j=1}^{L} b_j \phi_j(x) \right]^2 \right\} \tag{2.39}$$

where $f_i(x)$ is the response predicted by metamodel, $y_i(x)$ is the response obtained from the optimization code, and P is the total number of sampling point.

2.8.3 Multi-Objective Genetic Algorithm (MOGA)

The engineers often deal with simultaneously minimizing or maximizing different criteria. The structural engineers would like to minimize weight together with maximize stiffness. In finite element based optimization, it might desire to optimize the nodal locations in the mesh

This material is reserved for educational use only, not allowed for commercial use.
Forbidden to modify the content, and cite the document when use.

based on distortion parameter, aspect ratio, or several other mesh quality criteria simultaneously. Mathematically, the problem with multiple objectives might be stated as

Minimize

$$f = [f_1(x), f_2(x), \dots, f_m(x)] \tag{2.40}$$

Subject to

$$x \in \Omega \tag{2.41}$$

where $\Omega = \{x: g(x) \leq 0,\ h(x) = 0,\ x_L \leq x \leq x_U\}$. Ω is a subset of R^n called feasible region or entire space.

The criteria sometimes do not conflict with one another. In that case, a single optimum x minimizes all the objectives simultaneously. More often, there is a conflict between the different criteria. A central concept in multiobjective optimization involves the concept of Pareto Optimality that was introduced by V. Pareto in 1896. There have been several methods developed to solve multiobjective optimization problems. Multi-Objective Genetic Algorithm (MOGA) is one of the methods that has widely used. In ANSYS DesignXplorer, it is also employed the MOGA to generate a set of Pareto optimal solutions based on a certain specific criterion or rule. It is only available for continuous input parameters that could handle multiple goals.

2.9 Previous Studies on Bus Analysis and Structural Optimization

Structural analysis of a bus structure has been studied by several authors such as Kim H.S. et al. [24] presented a method of prediction a dynamic stress response on a bus structure. This employed a hybrid superposition of pseudostatic stresses. The time history of road data generated by flexible multibody dynamic analysis was used in finite element system for predicting the dynamic stress. In addition, a bus structure analyzed under dynamic condition was accomplished a fatigue life at a pillar joint. This method could serve as an initial stage of durability consideration of a prototype vehicle. Another studies involved with a dynamic response was shown by Zhang D. et al. [25]. It was a study of structural reliability of a bus structure. External loads were taken as stochastic variables by fundamental theories of structural system reliability. The dynamic load coefficients in bending and torsional conditions were considered.

This material is reserved for educational use only, not allowed for commercial use.
Forbidden to modify the content, and cite the document when use.

The reliability of strength and stiffness of the bus structure was based on the design average checking points of Taylor expansion stochastic finite element method (SFEM). Both bending and torsional loads had significant influence on the bus structure reliability but less influential effect revealed on a small cross-sectional thickness area. Jin Yi-Min et al. [26] employed finite element analysis to evaluate strength of a minivan structure. The structure was subjected to static and dynamic loads. The static analysis was conducted using the bending and torsion loads. The dynamic analysis comprised of two sources i.e. tire unbalance and engine excitation. The structural analysis of the minivan structure was accomplished by comparing the dynamic analysis with experimental test. The comparison showed that the maximum deviation between analysis and experiment was 3.23%. Chandna P. et al. [27] analyzed a city bus structure under static condition. The FE model was created by mid-surface extraction which was appropriate for shell element meshing. The structure was divided into 6 parts such as roof, front stair, middle stair, middle floor, and seat. The applied load was calculated from 46 sitting and 40 standing passengers and it was distributed throughout the structure. The stress and displacement could observe individually on each divided parts. This bus analysis could be an alternative approach which used less computational performance compared to analysis on the whole model.

In addition to a bus analysis described previously, Dario C. [28] showed stress analysis of an articulated bus structure. An articulated bus consisting of 2 structures connected by a flexible joint is shown in Figure 2.32.

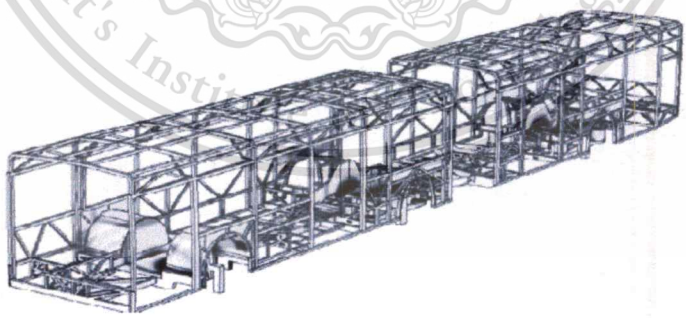

Figure 2.32 Articulated bus structure [28]

Both structures were analyzed under braking, and cornering conditions. From analysis, several structural members underneath the floor frame and those close to the articulation device were influence by braking effect with stress mean values of about 100 MPa. The right side pillars

This material is reserved for educational use only, not allowed for commercial use.
Forbidden to modify the content, and cite the document when use.

that connected the roof to the right body side revealed the stress about 130 MPa at cornering condition. It was reported that the cornering case was the most severe condition compared to braking case at the same acceleration magnitudes.

Apart from bus analysis reviewed above, there have also been many studies on structural optimization of a bus structure. Since, the UNECE R66 regulation [29] has been entitled for safety consideration of a passenger bus, much research in structural analysis and optimization has been generated. The UNECE R66 refers to integrity of a bus roof and is based on a rollover test. The purpose of the test is to ensure a superstructure of sufficient strength, so that the residual space stays unbroken on both during and after the dynamic rollover test. In experiment, the entire vehicle resting on the tilt table is quasi-statically rotated on one side as illustrated in Figure 2.33 (a). When the center of gravity reaches its highest point, the bus begins falling due to gravity.

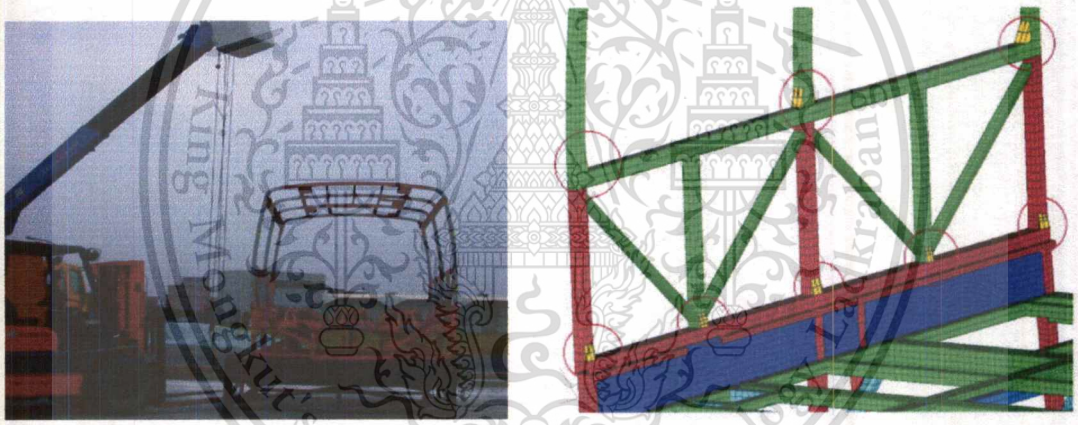

(a) (b)

Figure 2.33 Rollover test: (a) actual experiment (b) reinforcement on bus body [30]

Cheng Y. et al. [30] considered improving strength of the bus body section to prevent a rollover condition. Comparison of the rollover test and analysis were done after the body section rolling and deformation were recorded. The measured data showed that the maximum deformation in compression and tension were 510 mm and 440 mm respectively. From the analysis results, the modified body section was carried out by increasing the thickness from 2 mm to 3 mm at the pillar members and creating the reinforcement plates at all intersections as shown in Figure 2.31 (b). From modification, the structural mass was increased by 22 kg or 2.11%

This material is reserved for educational use only, not allowed for commercial use.
Forbidden to modify the content, and cite the document when use.

changed from the original model but maximum deformation was significantly reduced by 53-55%.

Lan F. et al. [31] investigated strength and showed structural weight reduction of a medium-sized bus body structure via finite element analysis and experimental measurement under torsion and bending case. In addition, the modal analysis was analyzed in order to understand lower-order vibration modes. The sensitivity analysis was done before optimization. It was found that the upper and lower cross-beam of the chassis, the vertical middle column, and the bridging bars of the chassis to cover the front wheels were more sensitive to the structural stiffness. These were selected to be the four design variables in parametric optimization. The objective function was to minimize structural weight. The constraints of structural stiffness and fundamental frequency were defined. It was shown that structural weight was reduced by 5.7%.

Zhang X. et al. [32] conducted the lightweight bus model by means of shape optimization. The stiffness sensitivity of the whole body structure parts were analyzed for torsion and bending loads. The mass of original body structure was decreased by 8.9 kg or 2.95 %. Butdee S. et al. [33] used the TRIZ method to achieve a lightweight bus structure. TRIZ is a problem solving method based on logic and data which accelerates the project team's ability to solve these problems creatively. The TRIZ principle and parameters were applied to assist a lightweight bus body design that is compared to the existing design. The bus was re-analyzed under same finite element method as the original structure. The comparison of mass before and after improvement was reduced by 0.93%.

Kim M.H. et al. [34] proposed a new approach for optimum design of the bus window pillar member. The bus was subjected to the torsional load and stress concentration exhibited at the window pillar of the right side frame. The window pillar was modeled individually. The B-spline was used for shape optimization of the pillar in order to carry out the joint strength against the torsional loads. The maximum stress and the deformation of the optimized window pillar member were decreased by 43% and 28% respectively.

Zhang Y. et al. [35] studied automotive front-side rail by means of robust optimization to obtain a lightweight model. The robust design is the variation of design variable that is transferred to the performance functions leading to the variation of objective and constraint functions. The variation in sheet gauge, geometrical size, and material parameters caused the environmental factors. The response surface method accompanied by the Design-of-Experiment (DOE)

This material is reserved for educational use only, not allowed for commercial use.
Forbidden to modify the content, and cite the document when use.

technique was employed. The robust optimization was executed by the Sequential Quadratic Programming (SQP) algorithm. The weight reduction was achieved by 29.96%.

Manokruang S. et al. [36] presented an approach of lightweight bus design using the original model. The Capitalization Knowledge Check Sheet was used to consider which structural element was not important, less important, moderate, important, or very important. The original structure was redesigned by eliminating less priority parts based on the capitalization knowledge. As a result, overall vehicle weight was decreased by 4.62%.

Osvaldo R. et al. [37] illustrated the reduction of bus structure mass using torsional load as analysis condition. After analysis, the components contained stress below 50 MPa were eliminated and cross-sectional areas of the components contained stress lower than 150 MPa were reduced. The modifications were proceeded in two zones which were the luggage compartment and the rear seats. It was found that 29 components at the luggage compartment and at the rear seat for 21 and 8 components were removed respectively. The results showed that structural mass was reduced by 250 kg or 8%.

Gauchia A. et al. [38] employed genetic algorithm for an optimization of a bus structure. The process of the optimization was a combination between MATLAB and ANSYS software as shown in Figure 2.34.

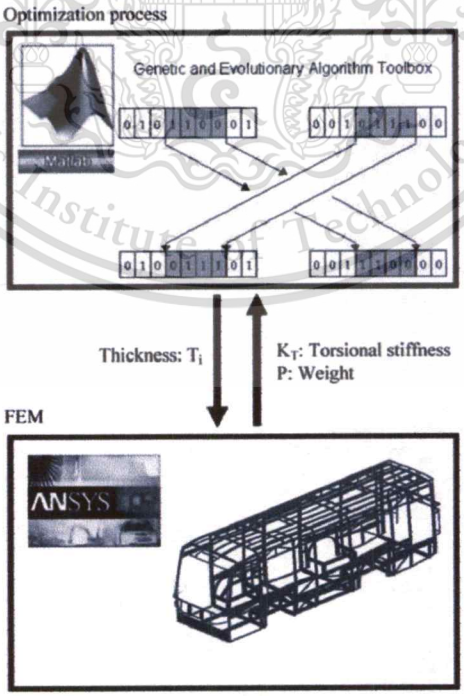

Figure 2.34 Structural optimization process [38]

This material is reserved for educational use only, not allowed for commercial use.
Forbidden to modify the content, and cite the document when use.

The method for reducing the structural mass was to optimize an appropriate cross-sectional thickness without losing structural stiffness. The advantage of the proposed approach was that the bus weight was reduced while unchanging the structural configuration. In Figure 2.34, the thickness of selected beams was design variables defined as outputs of MATLAB. The weight and torsional stiffness were calculated in ANSYS and forwarded to MATLAB in order to carry out the optimization process. The optimization was executed by genetic algorithm. From sensitivity analysis, four structural members from a total of 55 members were chosen to optimize. As a result, both structural mass and torsional stiffness were slightly improved by 4% decrease and 0.23% increase respectively.

In previous literature, the method of achieving weight reduction focused on a change of the cross-sectional thickness or configuration. However, there have been some studies considered using alternative lighter materials. Asnafi N. et al. [39] provided new material for fabricating the bus body. The metal-composite-metal (MCM) panel exhibited slightly smaller stiffness than that from the aluminum panel but higher than that from the carbon steel panels. Although the MCM panel was 46% heavier than the aluminum panel, it was 60% lighter than the carbon and stainless steel panels. In order to produce the MCM pane, low-pressure pressing and the electromagnetic rapid heating indicated possibilities of economical production. For these reasons, the MCM panel was expected to apply to many applications in manufacturing parts, car, train and bus body.

Cruz M.G.H. et al. [40] presented the replacement of conventional steel ZAR 230 by microalloyed steel ZSTE 380 in bus structure. The steel ZAR 230 is widely used by the Brazilian bus industry due to cost effective. However, the microalloyed steel contained higher yield strength and higher in fatigue limit by 49% and 45.7% compared to those of the conventional steel respectively. The validation of the methodology was based on the ECE R66 regulation. In experiment, the structures made of two different materials were tested according to the regulation and analyzed to confirm the present methodology. The results showed that the maximum deformation was reduced by 29.23% on the microalloyed bus structure and the strain from the calculations were lower than 10% compared to that obtained from the experiment. It was concluded that that the structural mass was reduced by 358.3 kg on the bus structure made of microalloyed steel.

Belure S.B. et al. [41] estimated the failure of a bus structure when it was subjected to the front impact condition. The aluminum material was given to the analytical structure in order to

This material is reserved for educational use only, not allowed for commercial use.
Forbidden to modify the content, and cite the document when use.

study the strength to weight ratio of an aluminum bus structure. In analysis, the bus structure impacted the rigid wall which is applicable in the front impact regulation of a small vehicle. It was shown that the passenger compartment after the impact was not failed due to the absorption of the front portion of the bus body. The deformed shape in crumbled zone was observed to be 124.4 mm. The bus structure constructed by aluminum material could save the structural weight by 37% with satisfied strength compared to that calculated by common steel.

Antero K. et al. [42] studied the use of stainless steel (AISI 304) on bus structure. In general, the stainless steel contains excellent corrosion properties and toughness. These could result in a better resistance for crash situation. Safety aspects were carried out based on fracture mechanics and impact toughness testing by laboratory scale. The study reported that the stainless city bus was slightly lighter than the aluminum city bus by 11%. The calculation of life cycle cost (LCC) showed that the stainless steel (AISI 304) was more competitive for bus structure compared with carbon steel and aluminum.

Haibin N. et al. [43] investigated strength of the roof door of a mass transit bus that was made of thermoplastic composite material as shown in Figure 2.35.

Figure 2.35 Roof door of mass transit bus [43]

In general, the composite material presents high specific strength and high modulus of elasticity. It has also been used in various applications such as transportation, marine, and aerospace. The replacement of metallic components with reinforced composites in mass transit helps reduce weight. A novel design using thermoplastic composites materials and thermoforming technology

This material is reserved for educational use only, not allowed for commercial use.
Forbidden to modify the content, and cite the document when use.

were demonstrated to form the part. Innovative composite materials, namely thermoplastic polyolefin (TPO), as the outer skin and a ribbed lofted glass mat thermoplastic (GMT) inner liner could improve structural stiffness and strength. The strength and deflection of the thermoplastic composite roof door were investigated via numerical simulation and experiment. It was shown that the weight of the thermoplastic composite roof door was lower than that obtained by the conventional metallic roof door by 39% and a maximum deflection was reduced by 42%.

From the literature reviewed above, it could be classified as two research areas i.e. stress analysis and lightweight optimization. Additionally, there have been two approaches to obtain a lightweight structure which were structural configuration change and material change. However, no one has reported clearly an accuracy of the FE bus model used in analysis especially the constraints for representing the bus suspensions. In finite element analysis, the constraint plays an important role in obtaining an accurate solution so that these applied constraints on the FE model could be investigated precisely. The purposes of this thesis were to investigate the FE model of the studied bus via finite element analysis and experimental measurement and to reduce structural mass using structural optimization. This thesis illustrated all stages of bus structural improvement in term of strength and stiffness such as simulation, experiment, and optimization. It was hoped that the thesis could be useful in development and a further study in finite element analysis of bus body structure and optimization.

This material is reserved for educational use only, not allowed for commercial use.
Forbidden to modify the content, and cite the document when use.

CHAPTER 3

EXPERIMENTAL PROCEDURES

3.1 Electric Bus Prototype

In this study, the structural strength and torsional stiffness of an electric bus prototype was examined by means of experiments and simulations. An employed bus, shown in Figure 3.1, was an 8-meter bus powered by electricity from battery sources. A main difference in structural configuration from conventional buses driven by internal combustion engines was location of a primary load i.e. the batteries. For a studied bus, a group of battery packs was designed to situate at the center of the chassis for a good stability as shown in Figure 3.2.

Figure 3.1 An electric bus prototype

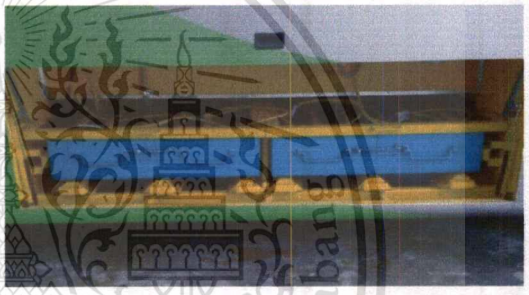

Figure 3.2 Battery packs (300 V.)

Figure 3.3 Electric motor drive

Figure 3.4 Interior for 20 passengers

Figure 3.3 shows an electric induction motor with rated 97 kW peak power located at the rear end of the chassis. The motor was electrically connected with a high electricity voltage of

This material is reserved for educational use only, not allowed for commercial use.
Forbidden to modify the content, and cite the document when use.

approximately 300 V, supplied from battery packs consisting 24 cells of 12 V lead-acid batteries. In addition, the internal layout of the bus for a passenger space of 20 passengers is displayed in Figure 3.4.

3.2 Experimental Setup

In this work, corresponding strains and accelerations were the main parameters of interest as shown in experimental setup procedures in Figure 3.5.

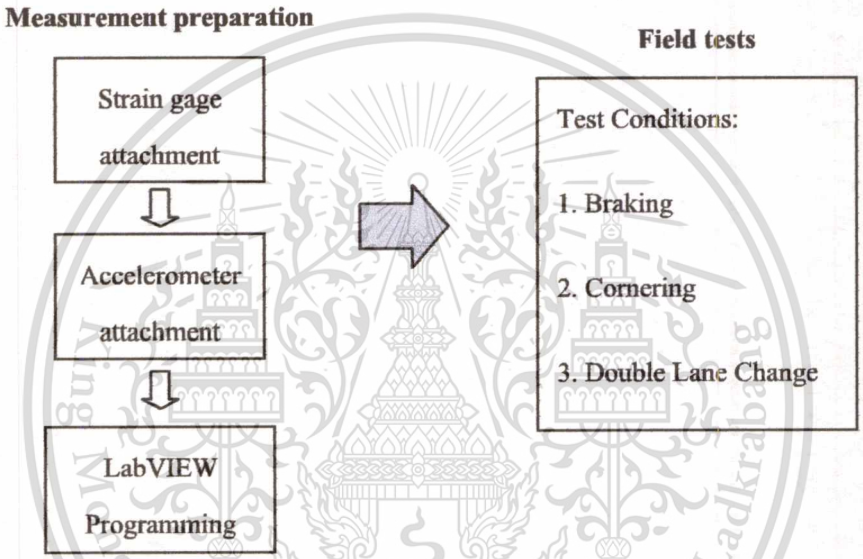

Figure 3.5 Experimental procedure flow chart

From Figure 3.5, this study was divided into 2 sections: a measurement preparation and a field test. In a measurement preparation, strain gages were attached at several specified locations to detect a minute strain on those particular surfaces of the bus structures. A 3-axis accelerometer was then placed around the vicinity of the center of gravity of the bus. After both strain gage and accelerometer attachments were completed, a data acquisition protocol was then created to make an interface between a laptop computer and sensors for logging the measured data via LabVIEW. Three test conditions of braking, cornering, and double lane change maneuver were selected for this study. A complete set of an experimental setup for a real-time data monitoring is shown in Figure 3.6. During the test, additional weights by means of sandbags were added onto the bus for

This material is reserved for educational use only, not allowed for commercial use.
Forbidden to modify the content, and cite the document when use.

a purpose of representing a passenger mass as shown in Figure 3.7. The measurement preparations and testing conditions are explained in details in the next sections.

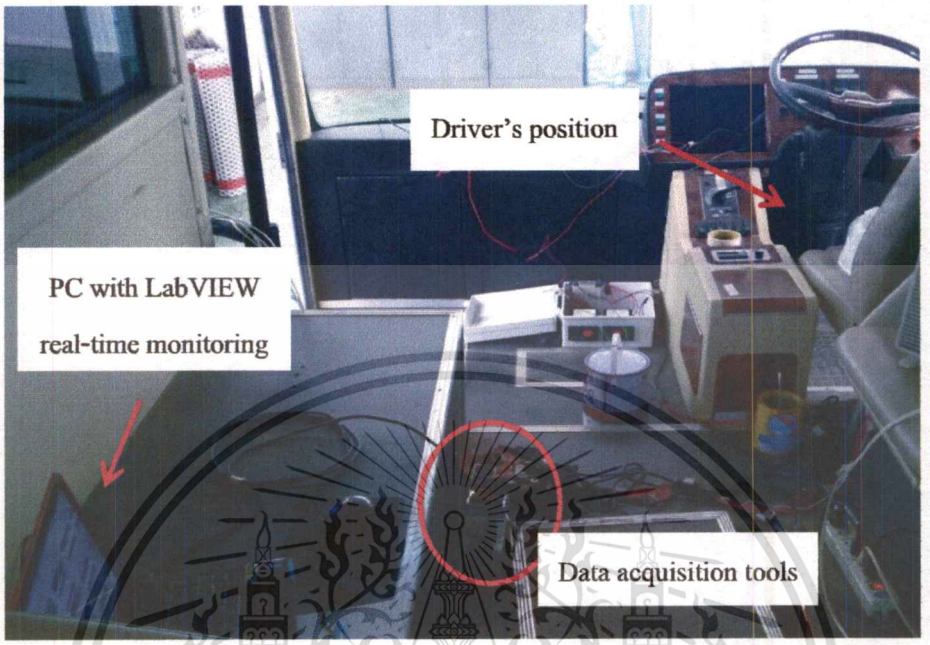

Figure 3.6 Experimental configuration of strain and acceleration measurement on the bus

Figure 3.7 Additional loads provided by sandbags (total of 845 kg)

This material is reserved for educational use only, not allowed for commercial use.
Forbidden to modify the content, and cite the document when use.

3.2.1 Strain Gage Attachment

In general, strain gage is used to detect a small surface deformation. In a bus application, a strain response could be generated from the structure when the bus is running under either normal or certain driving conditions such as braking, cornering, and double lane change. These responses vary continuously with time indicating a dynamic nature of the applications. Therefore, the aim of the current work was to measure dynamic strain responses on structural members of the electric bus prototype. For strain gage attachment, uniaxial strain gages in 3-wire system were used. Effectively, 3-wire system has been developed to eliminate a thermal effect of leadwires [44] and generally has a wiring configuration as displayed in Figure 3.9. A quarter bridge type of strain gage configuration was considered to collect the bending strain at all measurement locations. In addition, a calibration for correcting the generated strain values was carried out by means of balancing the Wheatstone bridge that was constructed inside the data acquisition module. Eight different locations on both chassis and body structure were specified to attach the strain gages as shown in Figure 3.8. An example of stain gage attachment at location S7 is demonstrated in Figure 3.10.

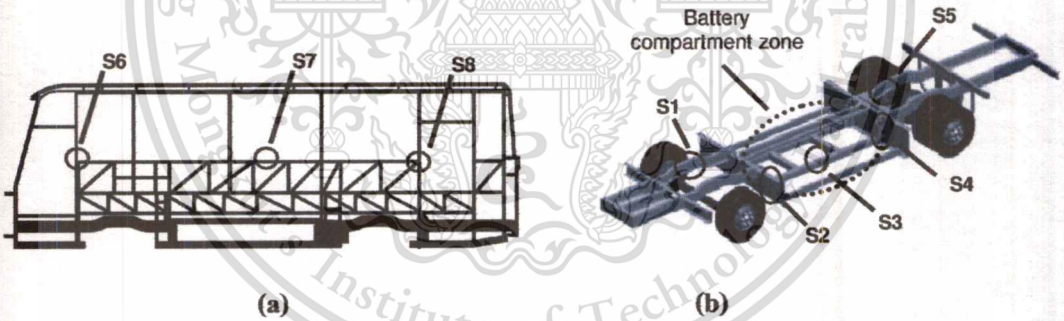

Figure 3.8 Strain gage attachment locations: (a) right side of body frame (b) bus chassis

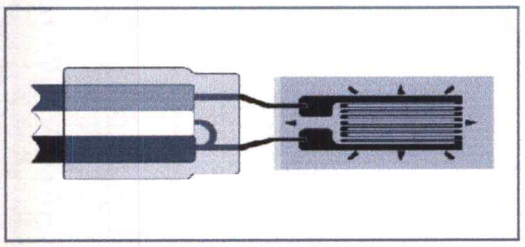

Figure 3.9 Uniaxial strain gage (3-wire system)

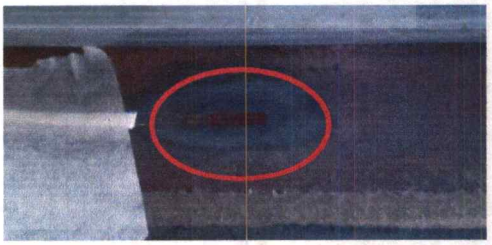

Figure 3.10 An example of strain gage attachment at location S7

This material is reserved for educational use only, not allowed for commercial use.
Forbidden to modify the content, and cite the document when use.

3.2.2 Acceleration Measurement

In order to measure vehicle acceleration during a braking, cornering, and double lane change manoeuvres, a 3-axis accelerometer was used. Furthermore, it was necessary to place the sensor at approximately the location of a centre of gravity of the bus. A corresponding position of the centre of gravity was identified from a bus model through computer-aided-design software as shown in Figure 3.11.

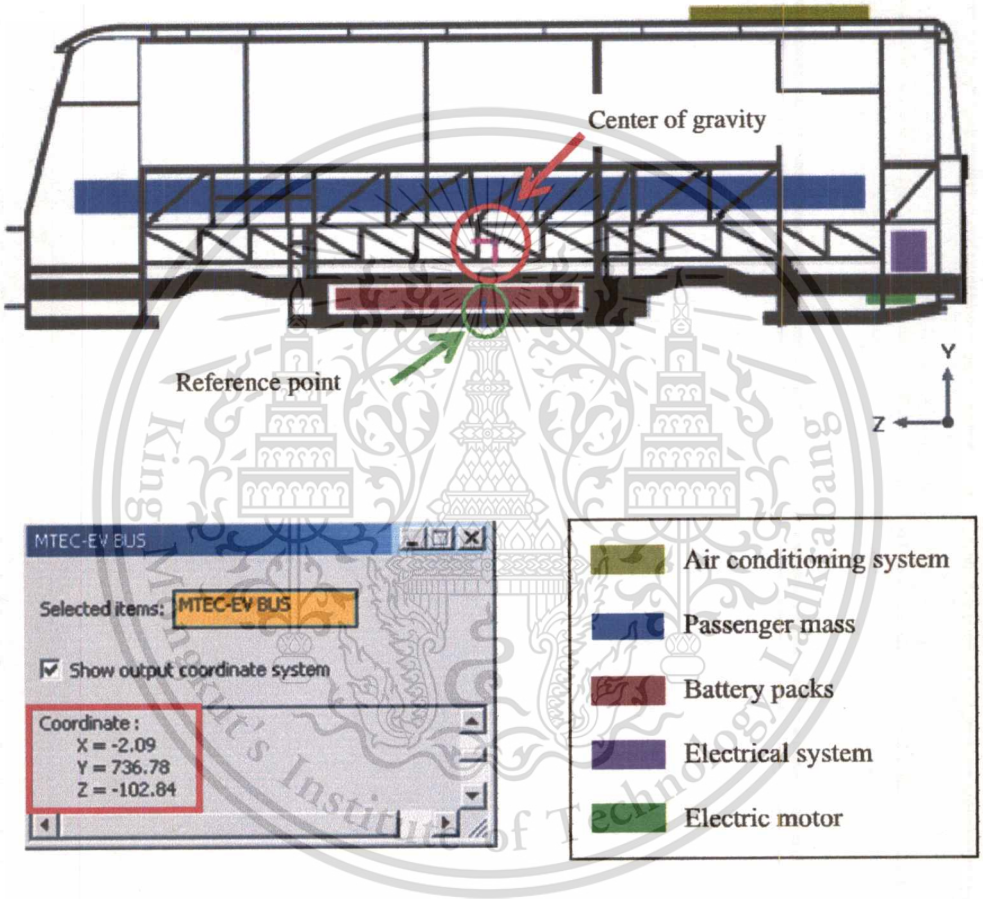

Figure 3.11 Center of gravity determination

(X = -2.09 mm , Y = 736.78 mm , Z = -102.84 mm)

It could be seen in Figure 3.11 that the center of gravity of the studied bus was located at -2.09 mm, 736.78 mm, and -102.84 mm for X, Y, and Z coordinate system according to a reference point respectively.

This material is reserved for educational use only, not allowed for commercial use.
Forbidden to modify the content, and cite the document when use.

3.2.3 Data Acquisition

Data acquisition (DAQ) is a process of measuring an electrical or physical quantity such as voltage, current, temperature, pressure, or sound with an aid of a computer. Typically, a DAQ system is consisted of sensors, DAQ measurement hardware, and a computer with programmable software. In this study, the sensors were the strain gages and the accelerometer, which were to generate analog signals to the DAQ hardware before measured data being displaying by LabVIEW software on the laptop screen. The details of data acquisition process could be shown graphically in Figure 3.12.

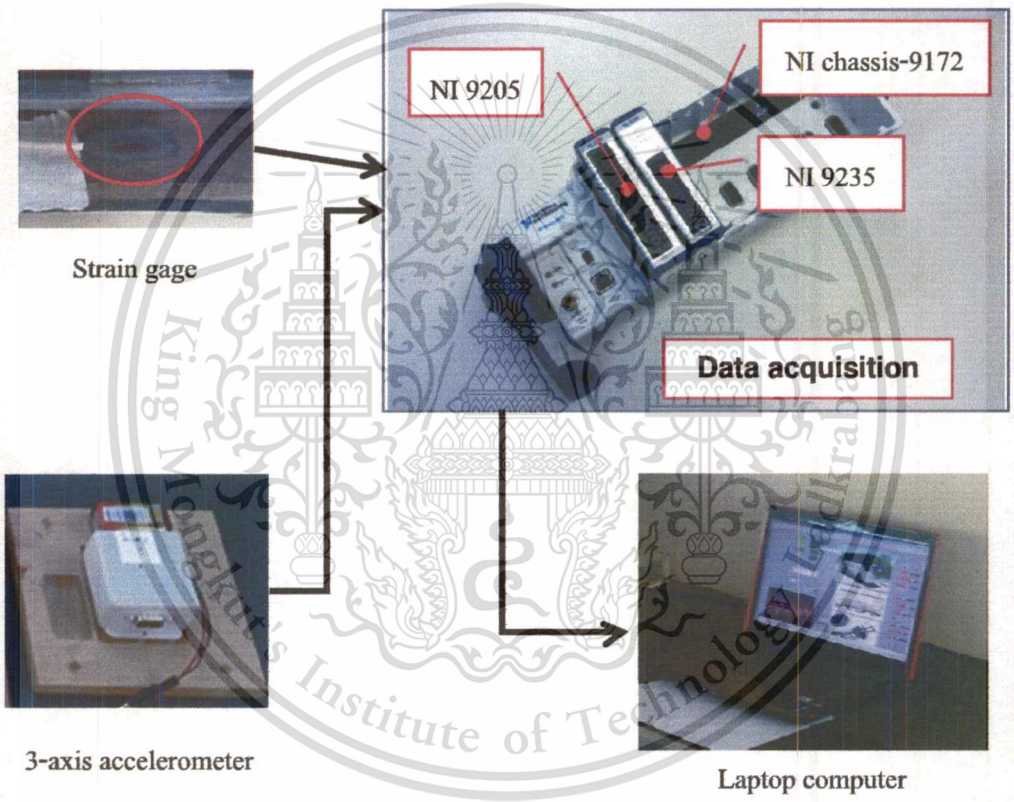

Figure 3.12 Data flow of strain and acceleration measurement using data acquisition tools

3.2.4 Graphical LabVIEW Programming

LabVIEW is the graphical programming software that uses the data flow programming language to support National Instruments (NI-DAQ) devices. In this work, LabVIEW was used to communicate between the measured data, which was transferred to the laptop computer via DAQ devices.

This material is reserved for educational use only, not allowed for commercial use.
Forbidden to modify the content, and cite the document when use.

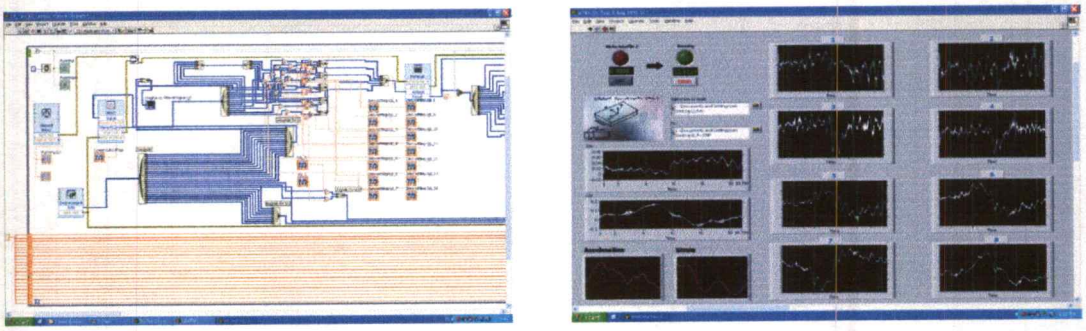

(a) (b)

Figure 3.13 (a) LabVIEW programming codes (b) Front panel for DAQ devices interface

Figure 3.13 (a) shows block diagrams that contained graphical source codes to read and to display the measured data. In detail, block diagrams were consisted of three main features i.e. acquire data, strain conversion, and graph generation. The acquire data feature was the first block for reading the measured data from both strain gages and acceleration attached on the bus. In the strain conversion, the measured strains were converted to stresses using Hooke's law. In order to improve accuracy of the measurement, a low-pass filter with the specified cut-off frequency of 300 Hz was selected to filter both converted stresses and measured acceleration. Finally, the waveform of the measured data was generated to graphically present the converted stresses and acceleration. All data were then generated on the front panel screen as shown in Figure 3.13 (b).

3.3 Experimental Conditions

In the tests, there were 3 configurations for dynamic stains and an acceleration measurement i.e. braking, cornering, and double lane change maneuver. The experimental data obtained from these testing conditions were then used in comparison with calculated solutions from the finite element analysis in order to verify the computational bus model employed in this study.

3.3.1 Braking Maneuver

The braking test was conducted in a straight-line braking maneuver as shown in Figure 3.14.

This material is reserved for educational use only, not allowed for commercial use.
Forbidden to modify the content, and cite the document when use.

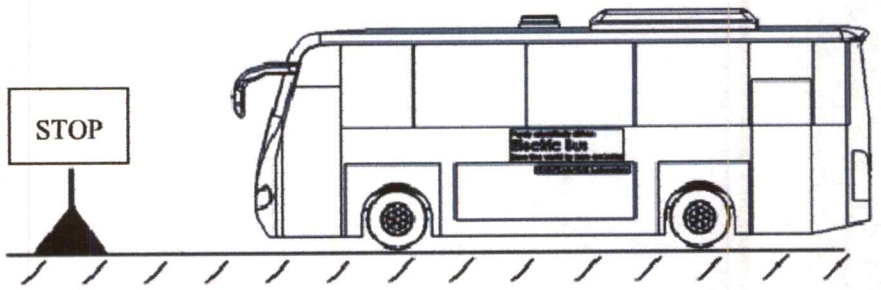

Figure 3.14 Braking configuration

During the test, the bus was accelerated up to 40 km/hr before the brake was suddenly applied until the bus came to a complete stop. The objective of this test was to measure strains detected from strain gages in several areas on both chassis and body structure and deceleration generated at the center of the bus during a braking test.

3.3.2 Cornering Maneuver

The main aims of this test were to study structural strength through collected strains from strain gage attachment and to measure lateral acceleration of the vehicle during a bus turning.

Figure 3.15 Cornering configuration

This material is reserved for educational use only, not allowed for commercial use.
Forbidden to modify the content, and cite the document when use.

Figure 3.16 Cornering maneuver

Figure 3.15 shows the top view of the bus for cornering maneuver. Figure 3.16 illustrates an example of the bus going through the cornering test with a turning radius of 30 m at 30 km/hr. The vehicle inclination from an effect of a centrifugal force could be clearly noticed.

3.2.3 Double Lane Change Maneuver

A double lane change maneuver was configured according to the Pennsylvania Transportation Institute test for handling performance [18]. However, there were a few adjustments in configuration and operating parameters due to driving characteristics of the electric bus prototype.

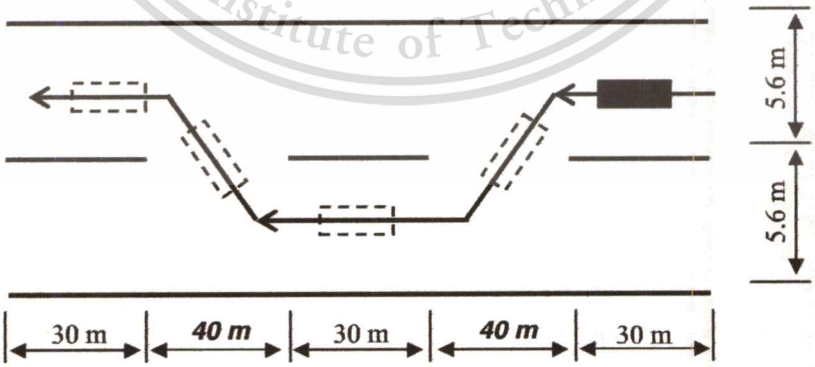

Figure 3.17 Double lane change configuration

This material is reserved for educational use only, not allowed for commercial use.
Forbidden to modify the content, and cite the document when use.

Figure 3.18 Double lane change maneuver

The double lane change test was the last physical experiments to obtain both strains and acceleration. The double lane change profile was shown in Figure 3.17. In the test, the bus was driven in a straight line at a specified speed before four different approaches such as left-,right-,right-, and left-hand approach were done sequentially. An example of the real test is shown in Figure 3.18 where the bus was about to be driven through the objects (traffic cones) which were places to configure the double lane change maneuver. The vehicle speed was kept constant at 30 km/hr throughout the tests.

3.4 Conclusions

Three physical tests were carried out on the electric bus prototype and were comprised of braking, cornering, and double lane change to measure the corresponding strains and accelerations in order to compare with those obtained from the computational simulations. Such comparison between both experimental and simulation results could be carried out for the FE model validation. In the measurement preparation, uniaxial strain gages in 3-wire system were attached at 8 specified locations on both chassis and body structure to detect minute strains, which would be generated when the bus was driven. Moreover, for the 3-axis accelerometer, a position around the center of gravity of the bus was identified by a computational approach. The data acquisition tools together with LabVIEW software were used to monitor and record the real-time strains and acceleration responses occurred during each test.

This material is reserved for educational use only, not allowed for commercial use.
Forbidden to modify the content, and cite the document when use.

CHAPTER 4

FINITE ELEMENT ANALYSIS AND OPTIMIZATION

4.1 FE Model of Electric Bus Structure

An electric bus prototype was employed in this study as shown in Figure 4.1 (a). For finite element analysis, a wireframe CAD body shown in Figure 4.1 (c) represented the actual bus geometry. It was also shown that an electric motor was located at the rear end of the chassis and the battery packs that stored high electricity voltage supplying to the motor to drive a bus was placed at the center of the chassis for a good stability.

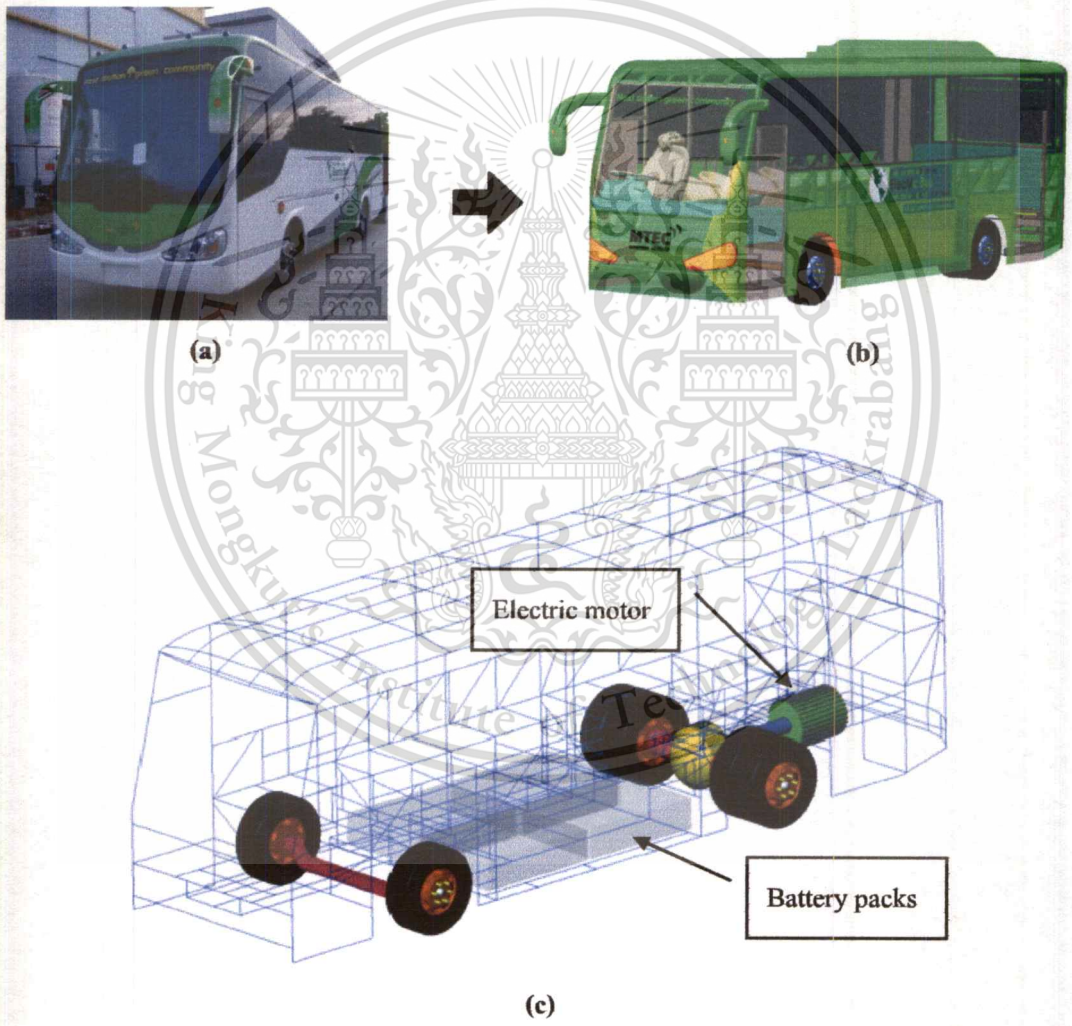

Figure 4.1 Electric bus prototype: (a) actual bus, (b) CAD model, and (c) wireframe bus structure for FE modeling

This material is reserved for educational use only, not allowed for commercial use.
Forbidden to modify the content, and cite the document when use.

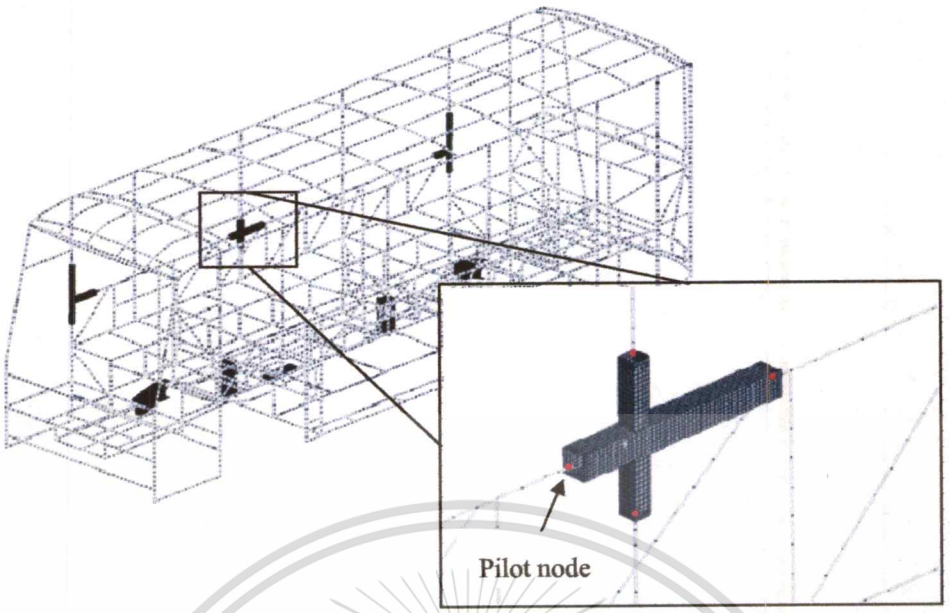

Figure 4.2 FE model and local areas for stress monitoring

In order to build an actual bus structure, several factors need to be considered such as structural strength, fabrication difficulty and structural configuration. In fabrication process, a bus structure is generally divided into two sections. One is a chassis construction which is a main component built by steel sheets designing to resist an external loads either from the upper or lower structure such as reaction forces from the ground. Another part that placed on the top of the chassis is called a body structure creating to accommodate passengers and bus utilities. The body structure is constructed similar to a skeleton frame that consists of many members with various cross-sectional shapes. The finite element (FE) model was generated to convert a physical geometry of the actual bus structure into an analytical model. It is suggested that if the length of the members is 10 times larger than the largest dimension of its cross section, the beam element is more suitable for an FE model generation [45]. As a result, the FE bus model was meshed by beam elements to perfectly represent the actual bus geometry and to optimize a performance and accuracy in computational simulation. Moreover, several areas of shell elements on the FE model were focused where the strain gages were attached as presented in Chapter 3 "Strain Gauge Attachment." These specified locations were to assess normal stresses along its longitudinal axis in comparison with converted stress collected from experiment. Figure 4.2 shows a combination of beam and shell elements used in the FE model and statistical information is given in Table 4.1.

This material is reserved for educational use only, not allowed for commercial use.
Forbidden to modify the content, and cite the document when use.

Table 4.1 FE model summary

Component	Value
Number of node	37,238
Number of element	31,909
Number of equation (DOF)	224,196

4.1.1 Mixed Element Verification

The FE bus was a combination between beam and shell elements for an assessment of the calculated stresses in local areas. This generated model could not be used directly. The problem was theoretically the difference in the number of degree of freedoms, so that how to connect the beam and shell elements was questioned. The Multipoint Constraints (MPC) was used to handle this problem. In fact, the MPC uses the rigid elements to connect between a nodal beam and a surface of the shell element to transmit the force. In order to have a precise solution of the whole bus analysis, a study of the mixed elements between beam and shell elements by the MPC connections was necessary by means of displacement comparison among other element types. A sample model for mixed element verification is shown in Figure 4.3.

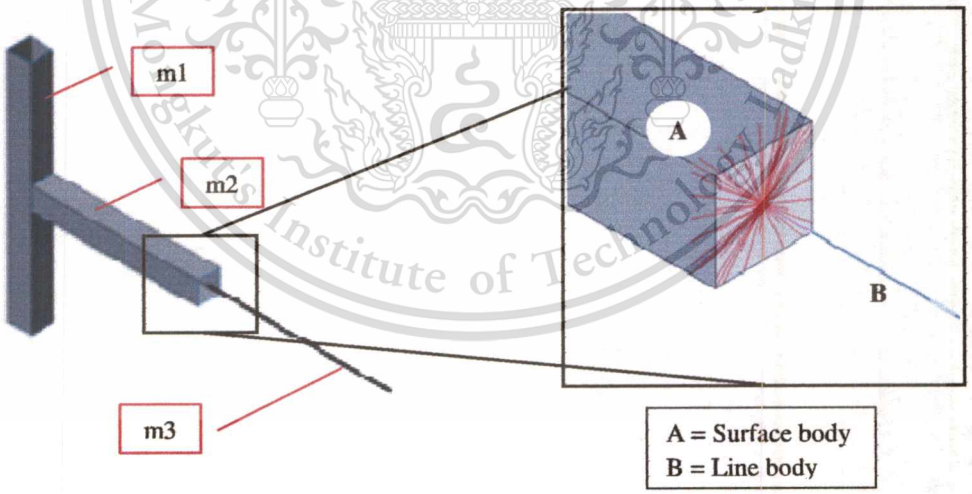

Figure 4.3 Mixed element of T-joint specimen by Multipoint Constraints (MPCs) approach

A simple model consisted of 3 parts denoted m1, m2, and m3. Each part was modeled by using different element types as listed in Table 4.2. In fact, the objective of this simple test was to

This material is reserved for educational use only, not allowed for commercial use.
Forbidden to modify the content, and cite the document when use.

verify the mixed elements, which was a combination between beam and shell element. Three models were created such a pure shell element model, a pure beam element model, and a mixed element model called model A, model B, and model C respectively. In addition, material properties applied to all models was a common steel that had Young's modulus of 210 GPa, mass density of 7900 kg/m^3, and Poisson's ratio of 0.3.

Table 4.2 Element types for T-joint specimens

Model	Element type		
	m1	m2	m3
A	Shell	Shell	Shell
B	Beam	Beam	Beam
C	Shell	Shell	Beam

Mixed element

In order to verify the calculated deformation of the mixed element model in 3 directions, the 3 components of forces were applied to the end of the sample as shown in Figure 4.4. A linear static analysis was employed to obtain deformations in 3 directions on parts m2 and m3. The accuracy of the mixed dimensional element using the MPC was given by comparison of calculated deformations of model C to those obtained from model A and B. The deformations in 3 directions of different models are plotted in Figure 4.5-4.7.

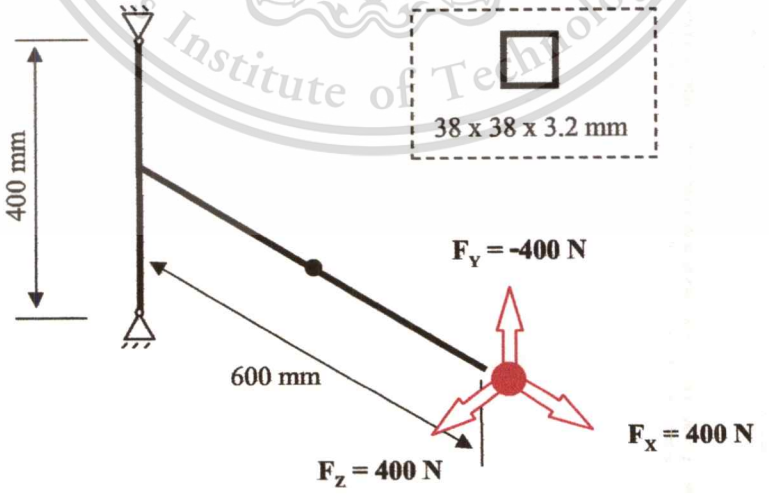

Figure 4.4 T-Joint connection of square tubes subjected to 3 components of force

This material is reserved for educational use only, not allowed for commercial use.
Forbidden to modify the content, and cite the document when use.

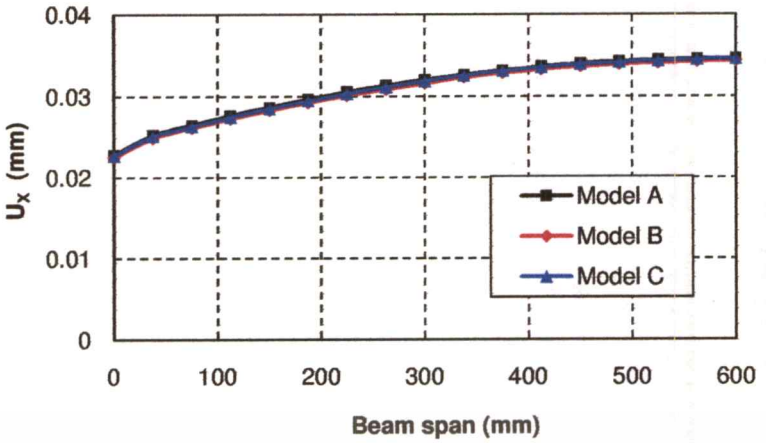

Figure 4.5 Comparison of X-deformation in different element types

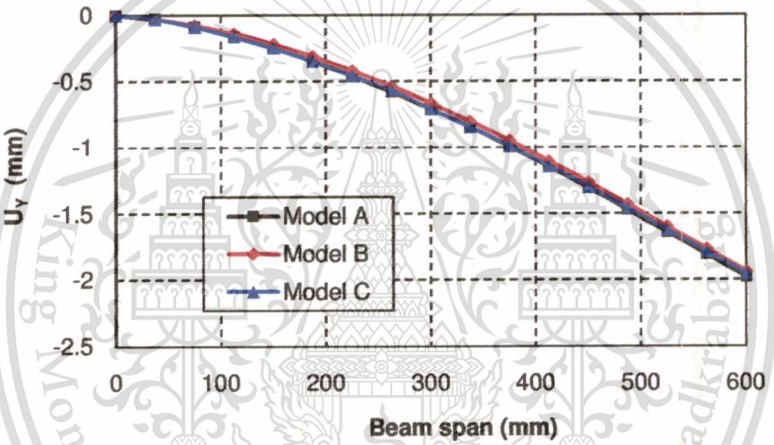

Figure 4.6 Comparison of Y-deformation in different element types

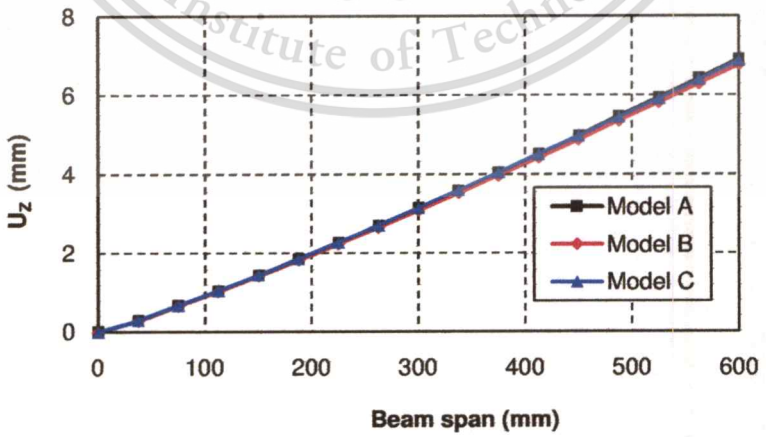

Figure 4.7 Comparison of Z-deformation in different element types

This material is reserved for educational use only, not allowed for commercial use.
Forbidden to modify the content, and cite the document when use.

It could be seen that all corresponding deformations among 3 models shown in Figure 4.5-4.7 illustrated a very similar trend despite a small discrepancy. However, comparison of Y-deformation components shown in Figure 4.6 was an obvious variation measured when the sample was subjected to a bending load. At the middle of the beam span, the deformations for model A, B, and C were 0.578, 0.535, and 0.568 mm respectively. These results showed that model A, B, and C had different structural strength classified as weakest, strongest, and medium respectively. Theoretically, shell element could obtain more precise solution than that from beam element due to a higher degree of freedoms a better the solution accuracy. Therefore, the deviations of each directions of model B and model C respected to model A were calculated and displayed in Table 4.3.

Table 4.3 Deviation of deformation in different element types respecting to shell element

Model	Deformation	Deviation (%)		
		U_X	U_Y	U_Z
A (Shell element)	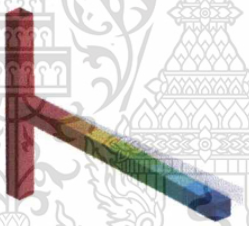	-	-	-
B (Beam element)		0.93	7.34	2
C (Mixed element)	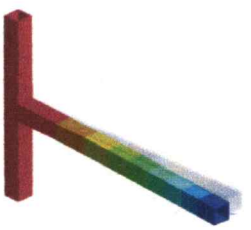	0.13	1.72	0.24

This material is reserved for educational use only, not allowed for commercial use.
Forbidden to modify the content, and cite the document when use.

In Table 4.3, model B and C relatively exhibited small deviations in all deformation directions compared to those from model A of pure shell element. This was clearly identified that the mixed element model by MPC approach could have an equivalent solution to other element types. Thus, the mixed element model was acceptable to use in the FE bus model to examine a stress in local areas.

4.1.2 Suspension Modeling

There have been many studies in the literature focusing on a bus design and analysis using Computer-Aided Engineering (CAE). However, no one has clearly reported an FE bus model including with spring suspensions. Generally, many studies used the constraints for a bus simulation as simply supported constraints to represent both front and rear suspensions. In this thesis, it was called "without suspension" constraint as shown in Figure 4.8.

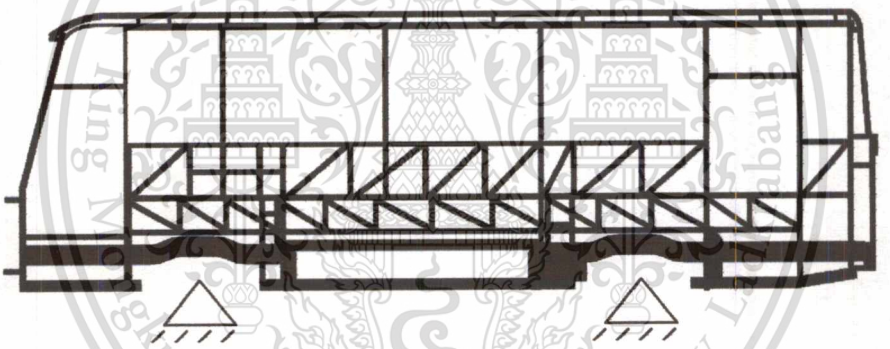

Figure 4.8 Simply supported constraints for bus analysis

In simply supported constraints, four locations above front and rear wheels on the chassis were allowable to rotate about its axis. However, any translational direction was unmovable. This unmovable translation of supports could cause a stress concentration or significant variation of predicted results at both locations compared to those obtained by experiment. Consequently, another method to constrain the bus structure was proposed. It was used spring-damper elements to simplify the actual suspensions as the actual suspensions of a studied bus shown in Figure 4.9. The accuracy of a structure without suspension and with suspension was investigated for justifying which model was suitable for bus analysis and leading to obtain a precise solution.

This material is reserved for educational use only, not allowed for commercial use.
Forbidden to modify the content, and cite the document when use.

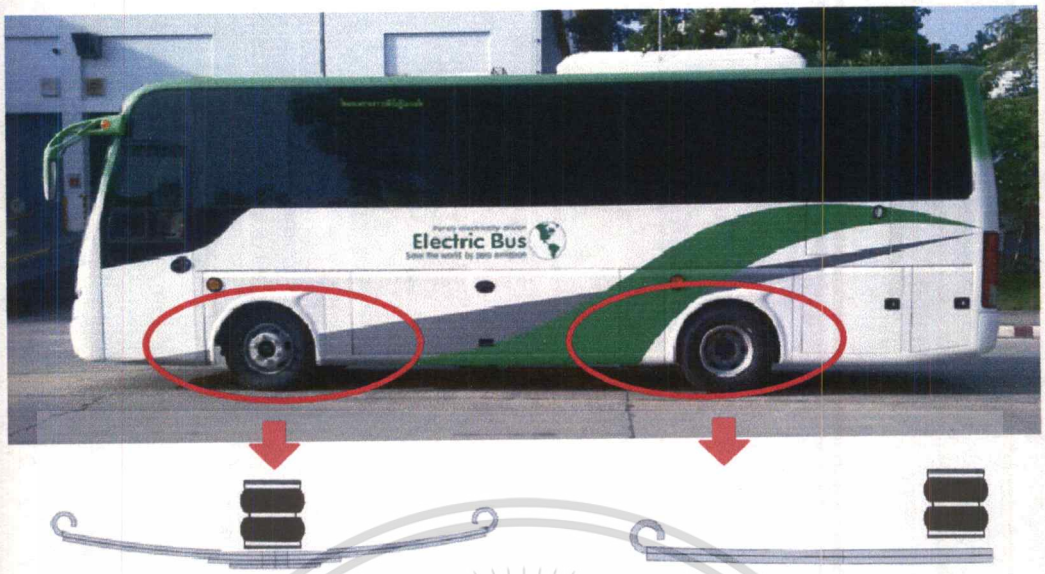

Figure 4.9 Suspensions of studied bus

The air suspensions of a studied bus consisted of two components such as leaf springs and air bellows. In fact, both components naturally have nonlinear characteristics. This work presented linear spring elements for both leaf spring and air bellows representation. In this section, the leaf spring stiffness and maximum deflection verification on both front and rear leaves of an electric bus prototype were illustrated for obtaining precise suspension parameters before applying to the FE bus model. Maximum deflection and spring stiffness were specified by means of comparison between theoretical and numerical solutions. At the end of this section, all parameters involved with suspensions were revealed. Front and rear suspension configurations considered a static equilibrium are displayed in Figure 4.10 and Figure 4.11 respectively.

Front Suspension

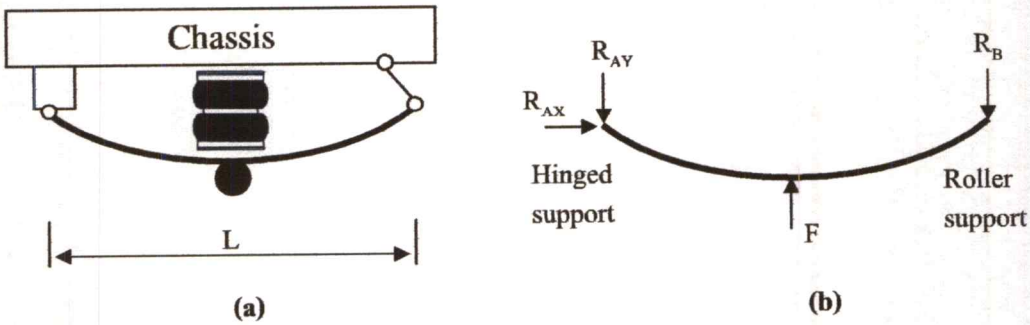

Figure 4.10 (a) Configuration of front suspension and (b) Static equilibrium of front leaf

This material is reserved for educational use only, not allowed for commercial use.
Forbidden to modify the content, and cite the document when use.

The equation used to calculate maximum deflection of the front leaf was

$$\delta_{max} = \frac{3FL^3}{8Enbt^3} \tag{4.1}$$

Rear Suspension

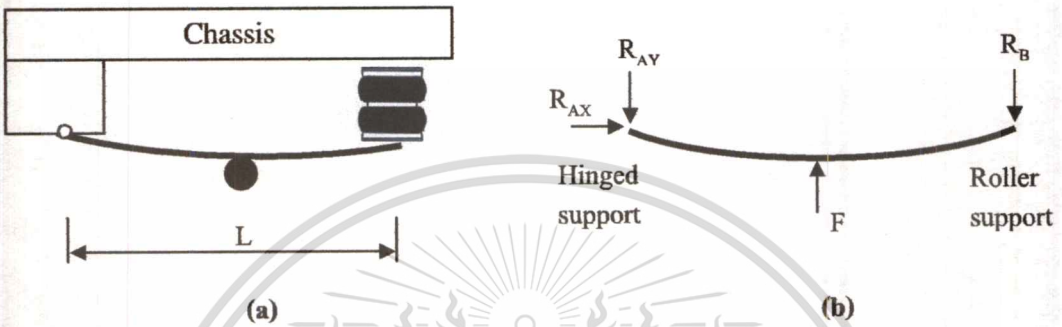

Figure 4.11 (a) Configuration of rear suspension and (b) Static equilibrium of rear leaf

The equation used to calculate maximum deflection of the rear leaf was

$$\delta_{max} = \frac{FL^3}{4Enbt^3} \tag{4.2}$$

where F is the applied force, L is the leave span, E is the Young's modulus, n is the number of leaves, b is the leaf width, and t is the thickness of leaves.

In Figure 4.10 and Figure 4.11, it was seen that both suspensions were supported by a hinged support on the left side of the leaves and a horizontal translation was allowable at another side as a roller support. An applied load was introduced at the center of the leaves to simulate the load from the axle which was again transmitted from the road surface. The material properties and parameters used for leaf spring calculation are defined in Figure 4.4 and Figure 4.5 respectively.

Table 4.4 Material properties of leaf springs [46]

Material	Young's modulus, E	Yield strength, σ_y	Poisson's ratio
AISI 6150 Steel	205 GPa	1160 MPa	0.29

This material is reserved for educational use only, not allowed for commercial use.
Forbidden to modify the content, and cite the document when use.

Table 4.5 Parameters for leaf spring calculation

Variable	Front leaf	Rear leaf	Unit
E	205	205	GPa
n	4	2	-
b	70	80	mm
t	18	32	mm
L	1520	1320	mm

Finite Element Analysis of Leaf Springs

In analysis, leaves were treated as solid elements with assigned contact to be pure penalty at each small clearance between the lower leaf and another upper leaf. Both front and rear models were constrained by a hinged and a roller support at the left side end and the right side end respectively. In addition, an applied force was introduced at the center of the leaves in vertical direction. The calculated deflections of leaves analyzed under static analysis were illustrated in Figure 4.12 and Figure 4.13.

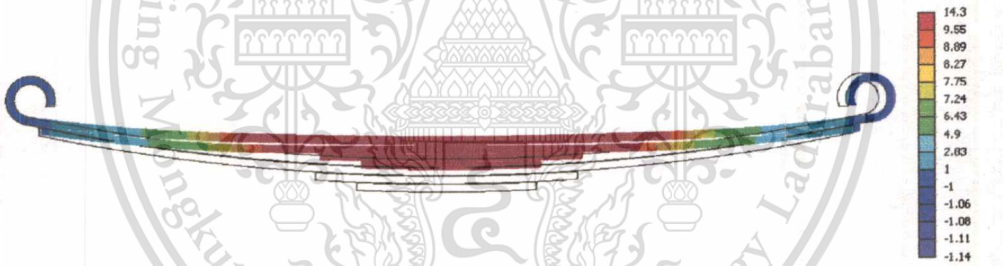

Figure 4.12 Deflection of front leaf

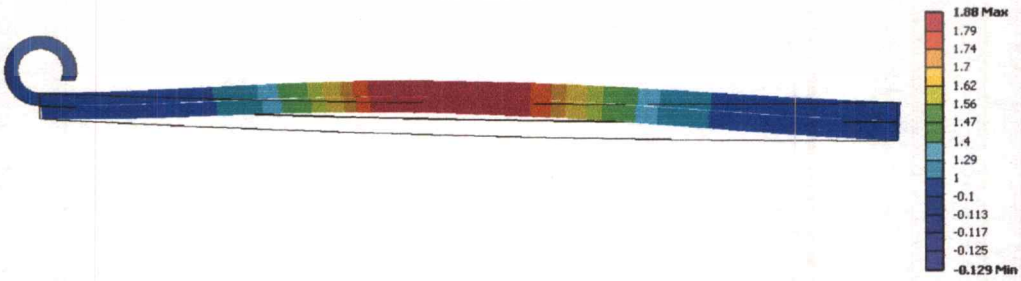

Figure 4.13 Deflection of rear leaf

This material is reserved for educational use only, not allowed for commercial use.
Forbidden to modify the content, and cite the document when use.

In Figure 4.12 and Figure 4.13, it was found that the maximum deflections were approximately exhibited at the center of leaves where the forces were applied. In addition, a small translation was observed according to an applied movable translation at the right side of the leaves. Spring stiffness could be considered from a slope between an applied force and predicted maximum deflection. Comparisons between numerical and analytical methods for spring stiffness determination of front and rear leaf are shown in Figure 4.14 and Figure 4.15 respectively.

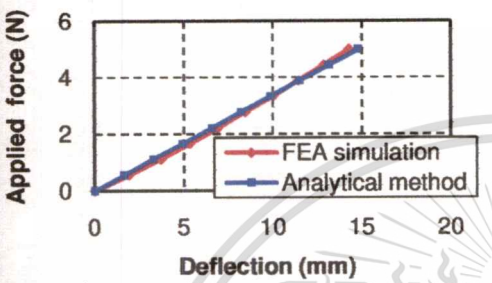

Figure 4.14 Spring stiffness of front leaf

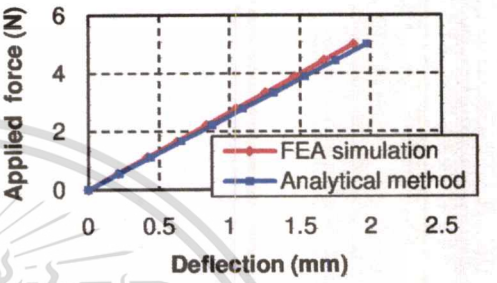

Figure 4.15 Spring stiffness of rear leaf

The calculations from Equations (4.1), Equation (4.2) and numerical solutions on both front and rear suspensions were compared for the variations as shown in Table 4.6.

Table 4.6 Investigation of leaf spring stiffness

Leaf	Max. deflection (mm)		Deviation %	Spring stiffness (kN/m)		Deviation %
	Theory	FEA		Theory	FEA	
Front	14.79	14.27	3.57	338.01	350.18	3.53
Rear	1.97	1.87	5.2	2535.53	2661.41	4.84

In Figure 4.6, it was reported that comparisons of maximum deflection and spring stiffness on both front and rear suspensions appeared a small deviation. Thus, the leaf stiffness obtained from both theoretical and numerical results were acceptable. In order to damp the vibration magnitude from the spring elements during a calculation, a damping coefficient was included. This damping coefficient was taken into account when a bus was analyzed under dynamic procedure as a part of this thesis.

This material is reserved for educational use only, not allowed for commercial use.
Forbidden to modify the content, and cite the document when use.

Damping Coefficient of Bus Suspensions

Critical damping coefficient related to sprung mass and spring stiffness calculated by

$$C_c = 2\sqrt{K_S M_s} \tag{4.3}$$

where C_c is the critical damping coefficient, K_S is the spring stiffness of suspension, and M_s is the sprung mass. Damping ratio is calculated from damping coefficient of the system and critical damp.

$$\zeta = \frac{C_s}{C_c} \tag{4.4}$$

where ζ is the damping ratio, C_s is the damping coefficient of suspension. For vehicle ride comfort, the damping ratio ranges between 0.2 and 0.3 [47]. Therefore, damping coefficient of bus suspension could be calculated as

$$C_s = 0.25 \times 2\sqrt{K_S M} \tag{4.5}$$

All parameters involved with both front and rear suspension are given in Figure 4.16 and Table 4.7. The obtained suspension model was then utilized to form the FE bus with spring suspension for the purpose of enhancing the solution accuracy.

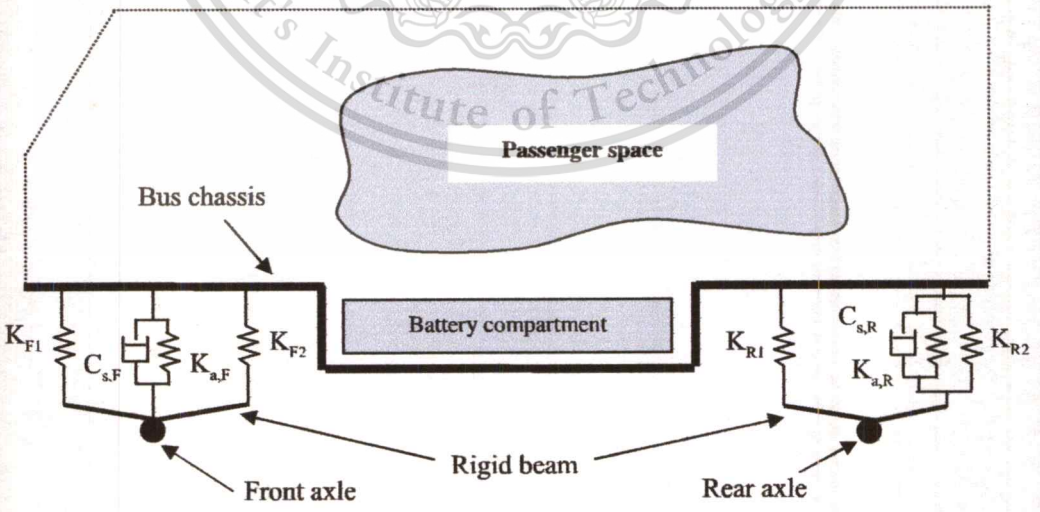

Figure 4.16 Suspension model of the bus

This material is reserved for educational use only, not allowed for commercial use.
Forbidden to modify the content, and cite the document when use.

Table 4.7 Parameters of electric bus suspension calculated from 1/4 bus

Front suspension		Rear suspension	
K_{F1}	122 kN/m	K_{R1}	1300 kN/m
K_{F2}	122 kN/m	K_{R2}	1300 kN/m
$*K_{a,F}$	318 kN/m	$*K_{a,R}$	318 kN/m
$C_{s,F}$	3000 N-s/m	$C_{s,R}$	3000 N-s/m

* Firestone Industrial Products Company [48]

where K_F and K_R are the spring stiffness of front and rear suspension respectively. K_a is the dynamic stiffness of air bellows at gauge pressure 5 bars and C_s is the damping coefficient.

4.2 Assigned Material and Distributed Loads

The material properties applied to all components on the bus structure were a common steel as the properties shown in Table 4.8. The distributed load applied on the bus structure is shown in Figure 4.17.

Table 4.8 Material properties of common steel [49]

Young's modulus, E	Mass density	Yield strength, σ_y	Poisson's ratio
210 GPa	7850 kg/m^3	350 MPa	0.3

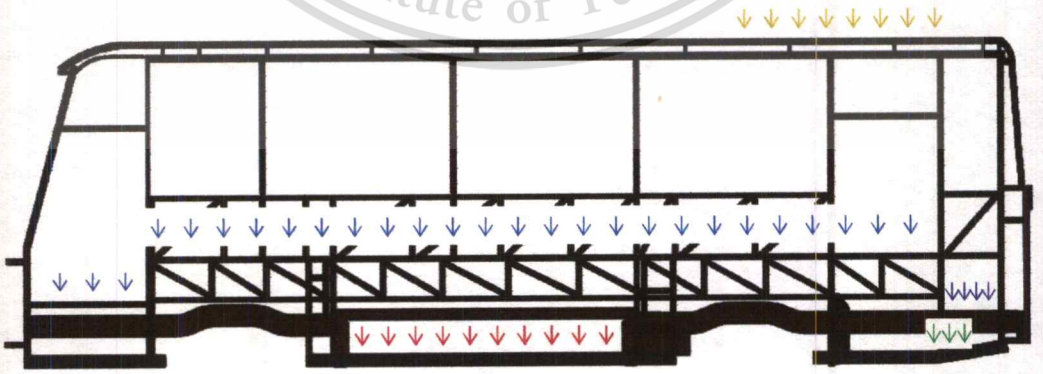

Figure 4.17 Loads on the bus structure

This material is reserved for educational use only, not allowed for commercial use.
Forbidden to modify the content, and cite the document when use.

Table 4.9 External loads for bus analysis

Symbol	Item	Mass (kg)	
		Normal case	Severe case
⟶	Passengers + Sandbags	1300	2040*
⟶	Battery packs	2000	2000
⟶	Air conditioning system	50	50
⟶	Electrical system	150	150
⟶	Electric motor	190	190

* In bending case, this number was changed.

Table 4.9 summarizes the external loads used in bus analysis and specified before the calculation from several boundary conditions was done. It could be seen that the passengers mass including the sandbags was increased from 1300 kg to 2040 kg as a loading level was increased from a normal to severe loading conditions respectively. This was because the number of 1300 kg was definitely used in a physical test. In analysis of normal case, the structure must be subjected to the same number of mass as in the test in order to compare the calculated results to the experimental data. The number 2040 kg using in severe case was calculated from 68 kg times 30 passengers that determined both sitting and standing passengers.

4.3 Boundary Conditions

In finite element analysis, the boundary conditions must be specified to solve the system equations before the solutions were given. There are many types of constraints used in structural analysis such as enforced displacements, forces, and accelerations. In an enforced displacement, this constraint allows the definition of the location where nodes or elements will end up at the end of the analysis. This enforced displacement was used in torsional case to simulate a wheel of a bus lifted off the ground by a specified height. In general, an acceleration constraint uses to simulate a load resulting from inertia of the component or system. For example, in order to determine the effect on the bus structure during a braking, an acceleration load could be applied to take an effect of the bus components. In this study, two constraints i.e. enforced displacement, and acceleration load were used to analyze the bus structure under different normal and severe loading conditions as given in Table 4.10.

This material is reserved for educational use only, not allowed for commercial use.
Forbidden to modify the content, and cite the document when use.

Table 4.10 Boundary conditions for finite element analysis

Analysis condition		Loading level	
		Normal case (Dynamic load)	Severe case (Static load)
Braking	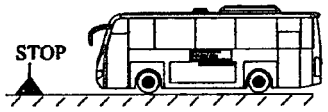	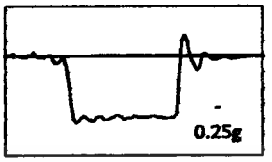	a = -0.75g (longitudinal)
Cornering		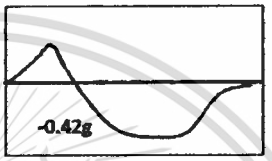	a = -0.75g (lateral)
Double Lane Change	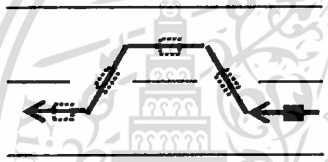	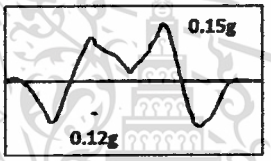	-
Bending		-	Passenger weight x 2.5
Torsion (stress)		-	u_y = 200 mm
Torsion (stiffness)	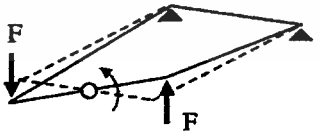	-	Force increment

Driving situations affecting either small or large deformation could appear in two main modes [51]. First, it was a bending case happened when the bus was subjected to the vertical load or displacement. Another was a torsional case, an external load attempted to deform the bus structure in rotating fashion along a longitudinal axis. In this case, a twist angle was utilized to calculate a torsional stiffness. In previous study, it was found that a large torsional deformation

This material is reserved for educational use only, not allowed for commercial use.
Forbidden to modify the content, and cite the document when use.

directly influenced the fatigue fracture of window pillar members [34]. In order to determine structural strength of the bus body operating in the different situations, several boundary conditions were considered as follows:

In braking case, it was a situation where the bus was driven at constant velocity and a brake pedal was suddenly pressed. In this case, a measured deceleration response from the physical test around 0.25 g during deceleration was employed as an acceleration load to the bus structure. Technically, the measured acceleration response was divided into 111 parts before assigning into the FEA environment in order to obtain a better-simulated response. For a severe case, the calculation was reduced to 1 step because the calculated result was only focused on the peak of the applied acceleration. A severe acceleration load in longitudinal direction was increased to be 0.75 g [50].

In cornering case, a lateral acceleration was used to simulate the cornering maneuver. In normal case, there were two distinct features. A small peak showed on the left side of the chart was collected just before the bus making turn by adjusting the wheel to the left. This was followed by an opposite acceleration during the actual right turn according to the test circuit. The majority of this test was the right turn. From the experiment, lateral accelerations of the left and right turn measured at the peaks were 0.26 g and 0.42 g respectively. For a severe drive, a lateral acceleration of 0.75 g [50] was employed for a turning analysis.

In double lane change, it was similar to the cornering maneuver but only severity of a drive and the direction of a drive were different. The dynamic response of measured acceleration during double lane change maneuver classified as a normal loading level was shown in Figure 4.10 (double lane change). The test began with a right-hand approach followed by the doubles of left-hand approaches and ended again by right-hand approach. The drive approaches displayed the lateral acceleration to be 0.12 g, 0.12 g, 0.15, and 0.13 g on right-, left-, left-, and right-hand approach respectively. However, a severe loading case of double lane change case was not determined due to the same loading effect as the cornering case.

In bending case, the objective of this test was to determine certain static characteristics of the bus structure such a permanent structural deformation by 2.5 times the passenger load. In fact, a studied bus was designed to accommodate 30 passengers including the standing passengers. Therefore, the passenger load was calculated to be 5100 kg by 68 kg per a passenger. This load was distributed evenly over the passenger space instead of 2040 kg specified in Table 4.9. In this case, a maximum deflection and a maximum stress were measured.

This material is reserved for educational use only, not allowed for commercial use.
Forbidden to modify the content, and cite the document when use.

In torsion (stress), it was a study of a wheel climbed up a curb accidentally. A preliminary study suggested that an applied displacement to the left front wheel displayed the most significant effect to the bus structure compared to those from other wheels. Therefore, a vertical displacement was applied to the left front wheel in upward direction by 200 mm while other three wheels were attached at the ground. In this case, a maximum stress was a main focus.

In torsion (stiffness), it was different from the torsional (stress) case in an applied load. In this case, the opposite vertical forces were employed activating at both locations of front air bellows. These loads twisted the structure along a longitudinal axis of the bus. Many literatures suggested that this case is the most severe situation compared to longitudinal and lateral load found in braking and cornering respectively. A structural stiffness was assessable through a torsional stiffness.

Three dynamic acceleration responses of braking, cornering, and double lane change shown in Table 4.10 were collected from acceleration measurement that was the bus driven in normal situations. These normal loading cases were only used to predict stress at specified areas before comparing to those obtained from experiments in order to validate the FE model. In severe drive, the purpose was to observe the structural performance when it was subjected to the severe loading conditions. It should be noted that the FE model used in bending and torsion (stiffness) cases was necessary to be isolated from the spring suspensions according to the regulation [18].

4.4 Lightweight Optimization

In previous sections, the creation of the FE model and several boundary conditions on both normal and severe loading levels were clearly described. In order to achieve a better electricity consumption and vehicle performance, this section provided a structural optimization by means of Multi Objective Genetic Algorithm (MOGA) to minimize the structural mass. The optimization formulation of finite element base was expressed in Figure 4.18.

Objective function :	Minimize the total structural mass
Subject to :	$22{,}000 \leq \max(\text{TSF}) \leq 32{,}095$
Design variables:	Structural thicknesses

Figure 4.18 Optimization formulation for an improvement of the bus structure

This material is reserved for educational use only, not allowed for commercial use.
Forbidden to modify the content, and cite the document when use.

From Figure 4.18, the objective function was to minimize the weight of the bus structure and torsional stiffness (TSF) of the whole structure was a constraint function. Both lower and upper bounds of the constraint were specified based on the range of the torsional stiffness for a bus structure given by [31] as 18,000-40,000 N-m/degree. However, the torsional stiffness of 20,267 N-m/degree was reported from an engine bus [31]. For the upper bound of the constraint, it was obtained from the previous study that the current bus contained 32,095 N-m/degree. Therefore, the torsional stiffness could be reduced from the current model in order to achieve the structural weight reduction. The lower bound was limited at 22,000 N-m/degree compared to that from the torsional stiffness of a current model or approximately 10% higher than that given from the torsional stiffness of an engine bus. Table 4.11 shows details of optimization parameters based on initial design.

Table 4.11 Lightweight optimization of bus structure

Optimized variable	Code	Initial	Lower limit	Upper limit
Objective	W (kg)	1962.5	-	-
Constraint	TSF (N-m/deg)	32,095	22,000	32,095
Design Variables	T1 (mm)	3.2	1.6	3.2
	T2 (mm)	3.2	1.6	3.2
	T3 (mm)	6	3	6
	T4 (mm)	4.5	2.6	4.5

From Table 4.11, four design variables were the wall thicknesses of structural members in specified areas. T1 was a group of central tubular body that contained many members as illustrated in Figure 4.20 (a). T2 was the roof frame that was also constructed by many cross-sectional members as shown in Figure 4.20 (b). The members underneath the battery compartment, the side members and the central members were defined as T3 and T4 respectively as shown in Figure 4.20 (c).

This material is reserved for educational use only, not allowed for commercial use.
Forbidden to modify the content, and cite the document when use.

4.5 Conclusions

In this chapter, there were four main topics such as mixed dimensional elements, suspension simplification by spring elements, boundary conditions, and lightweight optimization. The mixed element was an important part to determine accuracy of a connection between the shell surface and a nodal beam. This was implemented using T-joint connection. The calculated deformations in 3 directions of mixed elements were compared to those obtained by shell and beam elements. As a result, the mixed element modelling by MPC approach was acceptable according to a small deviation. In suspension modelling, both front and rear bus suspensions were simplified using spring elements with the aim of improving the solution accuracy. Before analysis, several boundary conditions both normal and severe loading levels were considered. The last topic was a lightweight optimization which clearly identified the optimization parameters. The purpose of the optimization was to lighten the structural mass while maintaining the sufficient torsional stiffness. The procedure of structural optimization is shown in Figure 4.21.

King Mongkut's Institute of Technology Ladkrabang

This material is reserved for educational use only, not allowed for commercial use.
Forbidden to modify the content, and cite the document when use.

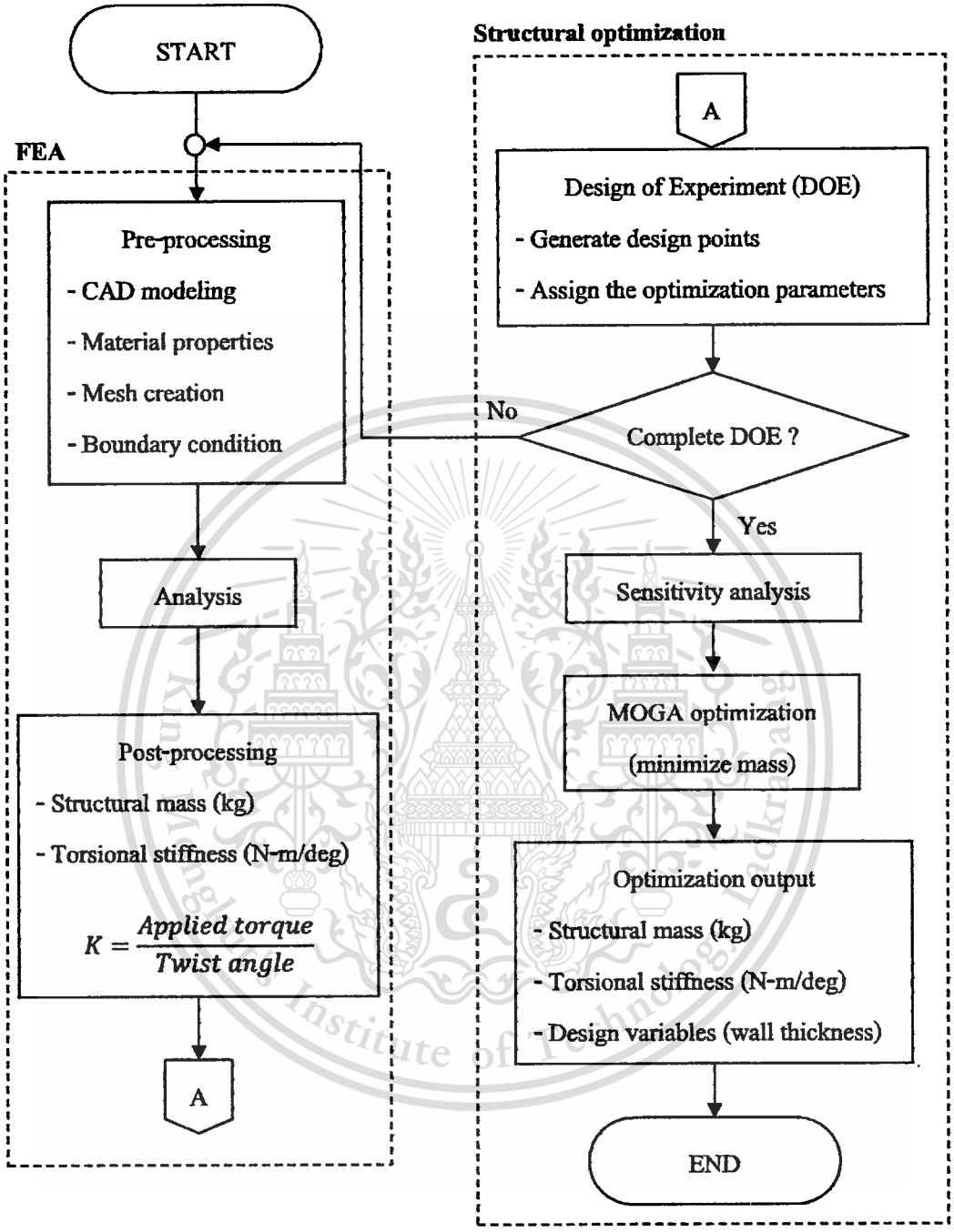

Figure 4.21 Optimization procedure

This material is reserved for educational use only, not allowed for commercial use.
Forbidden to modify the content, and cite the document when use.

CHAPTER 5

RESULTS

5.1 Experimental Investigation of Computational Bus Model

In this section, the data obtained from dynamic tests and finite element analysis are presented and compared. The stress comparison is carried out on three different boundary conditions i.e. braking, cornering, and torsional cases. In addition, the FE models of structures with and without suspensions are verified via experimental data.

5.1.1 Braking Maneuver

The braking test was conducted in a straight-line braking maneuver. During the test, the bus was accelerated up to a required test speed before the brake was suddenly applied until the bus came to a complete stop. The objective of this test was to measure deceleration generated at the center of the bus. The measured deceleration by means of 3-axis accelerometer is shown in Figure 5.1

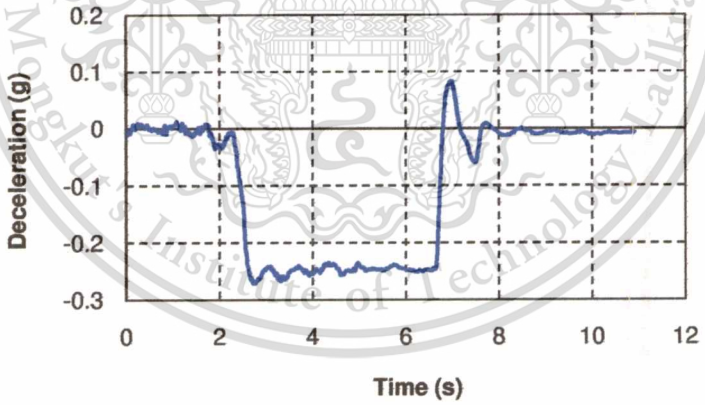

Figure 5.1 Deceleration measured during a braking maneuver at test speed of 40 km/hr

Figure 5.1 shows deceleration response measured at the centre of gravity of the vehicle during a braking test. It could be seen that the constant deceleration of approximately 0.25 g occurred within 4 seconds while a peak of small vibration just before a complete stop was around 0.09 g.

This material is reserved for educational use only, not allowed for commercial use.
Forbidden to modify the content, and cite the document when use.

In order to present the dynamic stress responses, the experimental data was plotted together with all the computational results from different simulation setups. Definitions of each line color used in the following comparison graphs are listed in Table 5.1.

Table 5.1 Definition of lines for dynamic stress responses representation

Color	Definition
	Experimental data
	Static **with** suspension
	Dynamic **with** suspension
	Static **without** suspension

The blue line was the experimental stress converted from measured strains by employing the Hooke's law while other three stress responses were directly received by numerical simulation. The term "with suspension" for either static or dynamic analysis indicated that the spring suspensions were included in the FE bus model. In contrast, a "without suspension" term was where a simply supported constraint was used instead of the spring suspensions.

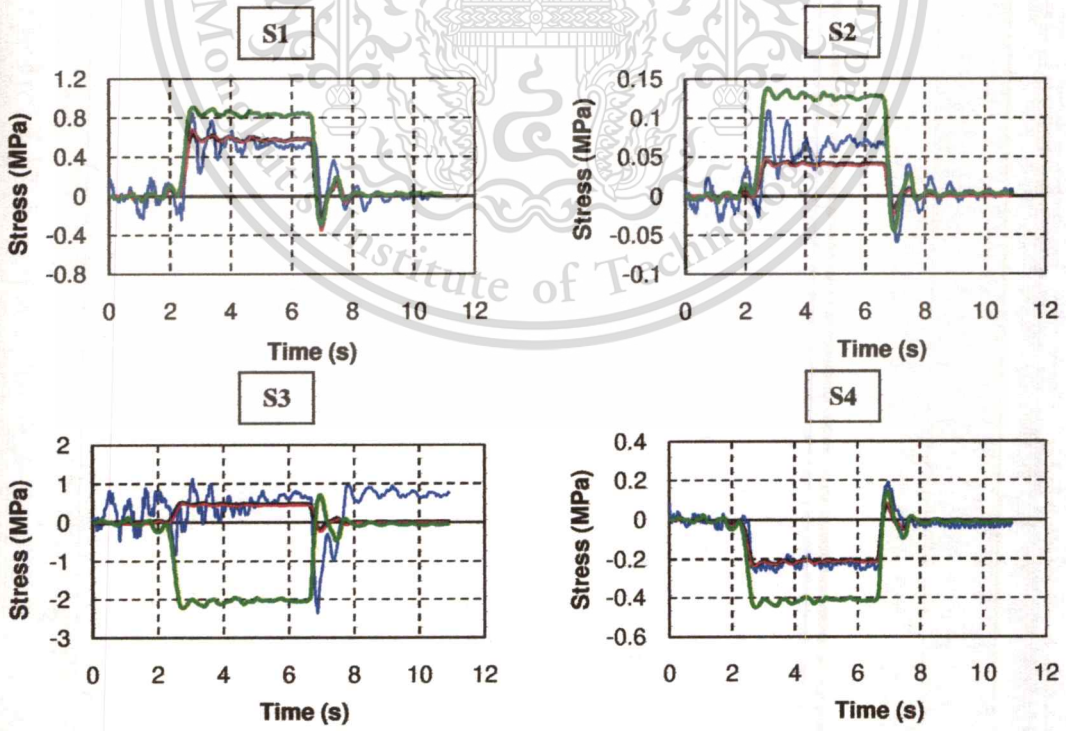

Figure 5.2 Dynamic stress responses measured during a braking maneuver

This material is reserved for educational use only, not allowed for commercial use.
Forbidden to modify the content, and cite the document when use.

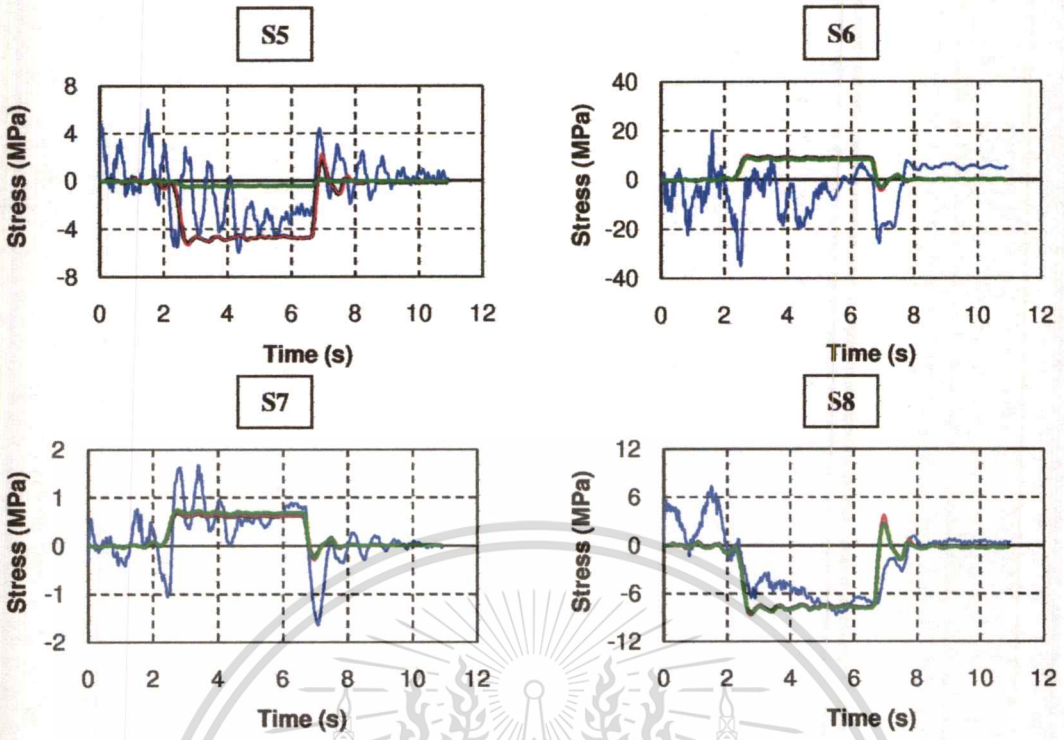

Figure 5.2 Dynamic stress responses measured during a braking maneuver (cont.)

In Figure 5.2, eight locations of stress monitoring responses were ranged from S1 to S8 measured at the same locations as strain gage attachment described in Chapter 3. For each stress location, four different data were included in order to make comparison visibly. The degrees of stress levels were shown in positive and negative values to indicate tensile and compressive stress respectively. It could be seen that the maximum magnitude of measured stress at location S1-S8 was 0.52, 0.073, 0.83, 0.23, 3.97, 7.12, 0.83, and 7.24 MPa respectively. The stress calculated from static with suspension and dynamic with suspension conditions demonstrated a very similar trend compared with the experimental data. However, despite a similar trend, the set of green lines displayed various degrees of discrepancy compared to the rest at location S1, S2, and S4 by calculated stress of 0.86, 0.13, and 0.41 MPa respectively. Furthermore, a significant difference in stress response appeared at location S3 with static without suspension result exhibited opposite stress value and large difference of stress magnitude. The possible reasons for observed difference between stress comparisons will be discussed in Chapter 6.

This material is reserved for educational use only, not allowed for commercial use.
Forbidden to modify the content, and cite the document when use.

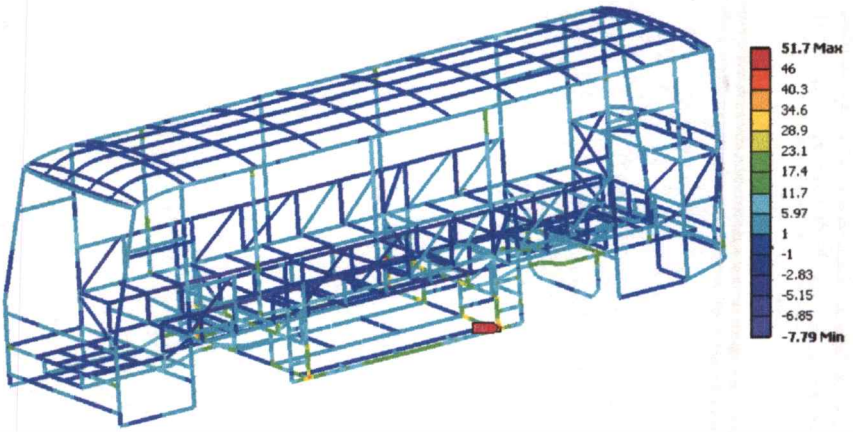

Figure 5.3 Stress distributions in normal braking case using static analysis with suspension

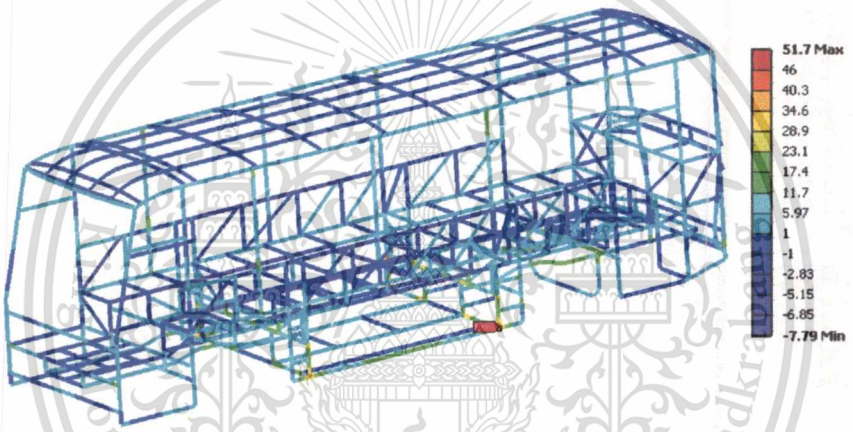

Figure 5.4 Stress distributions in normal braking case using dynamic analysis with suspension

During a braking test, the bus structure was subjected to a longitudinal load. From the computational results, the maximum stress of 51.7 MPa was observed on the left side of the bus near a battery compartment as shown in Figure 5.3. The roof frame and the central tubular members showed a small effect from the deceleration load. On the other hand, noticeable stresses were mostly exhibited around the battery compartment members, the rear suspension, and the top of the column members. In addition, Figure 5.4 illustrates the calculated stress using dynamic analysis. It could be seen that the results of bus structure analyzed by static and dynamic analysis depicted very similar distributions.

This material is reserved for educational use only, not allowed for commercial use.
Forbidden to modify the content, and cite the document when use.

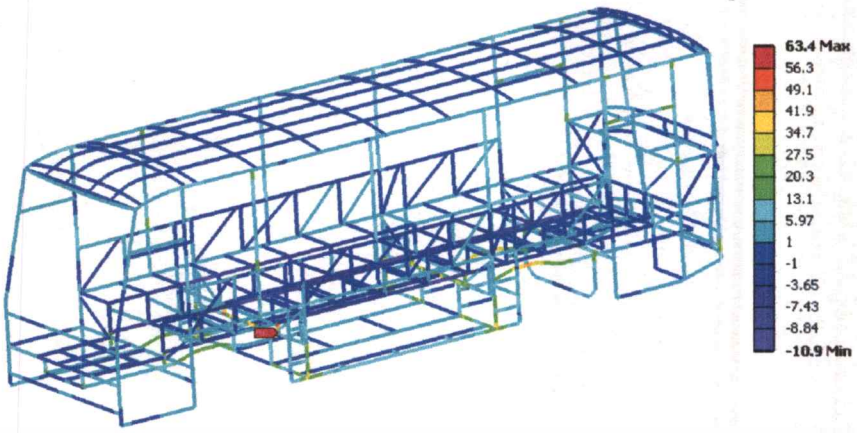

Figure 5.5 Stress distributions in normal braking case using static analysis without suspension

On the other hand, the analysis solution shown in Figure 5.5, in which the FE model was not consisted of spring suspension, was considerably different from Figure 5.3 and Figure 5.4. The maximum stress of 63.4 MPa was predicted to occur at the frontal part of the battery compartment. This was a tubular member located between the chassis and the body structure. In this case, a minute stress level was still generated on the roof, central members, and the central members underneath the battery packs.

5.1.2 Cornering Maneuver

A cornering maneuver was measured during the right turn according to the track configuration. The main aim was to measure lateral acceleration of vehicle during a bus turning for a use in the FE for stress analysis.

This material is reserved for educational use only, not allowed for commercial use.
Forbidden to modify the content, and cite the document when use.

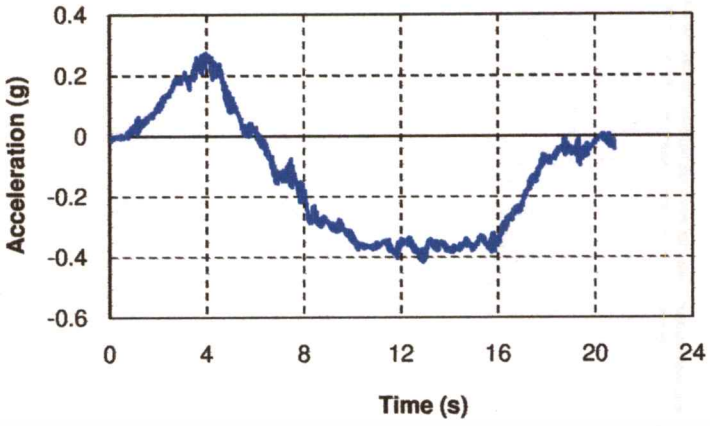

Figure 5.6 Lateral acceleration measured during a cornering maneuver at test speed of 30 km/hr

In Figure 5.6, there were two distinct features. A small peak showed on the left side of the chart was collected just before the bus making turn by adjusting the wheel to the left. This was followed by an opposite acceleration during the actual right turn according to the test circuit. The majority of this test was the right turn. From the experiment, lateral accelerations of the left and right turn measured at the peaks were 0.26 g and 0.42 g respectively. Under the test speed of 30 km/hr, the overall cornering maneuver took about 20 seconds to complete with 4 and 12 seconds for the left and right cornering peaks respectively.

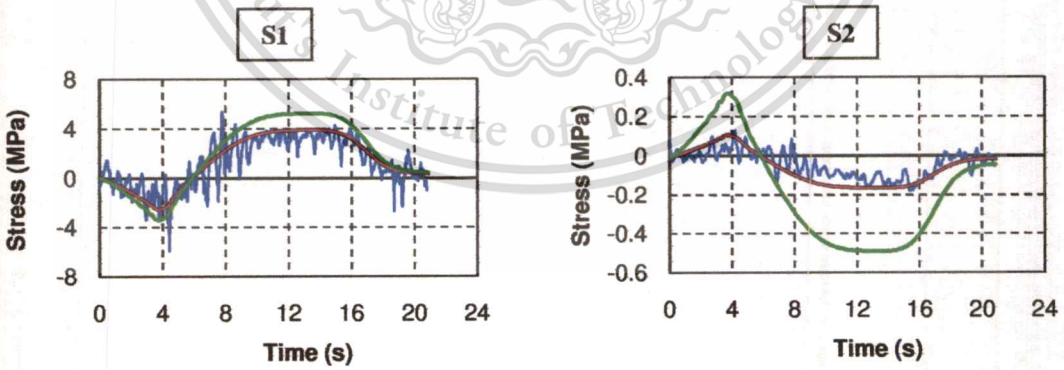

Figure 5.7 Dynamic stress response measured during a cornering maneuver

This material is reserved for educational use only, not allowed for commercial use.
Forbidden to modify the content, and cite the document when use.

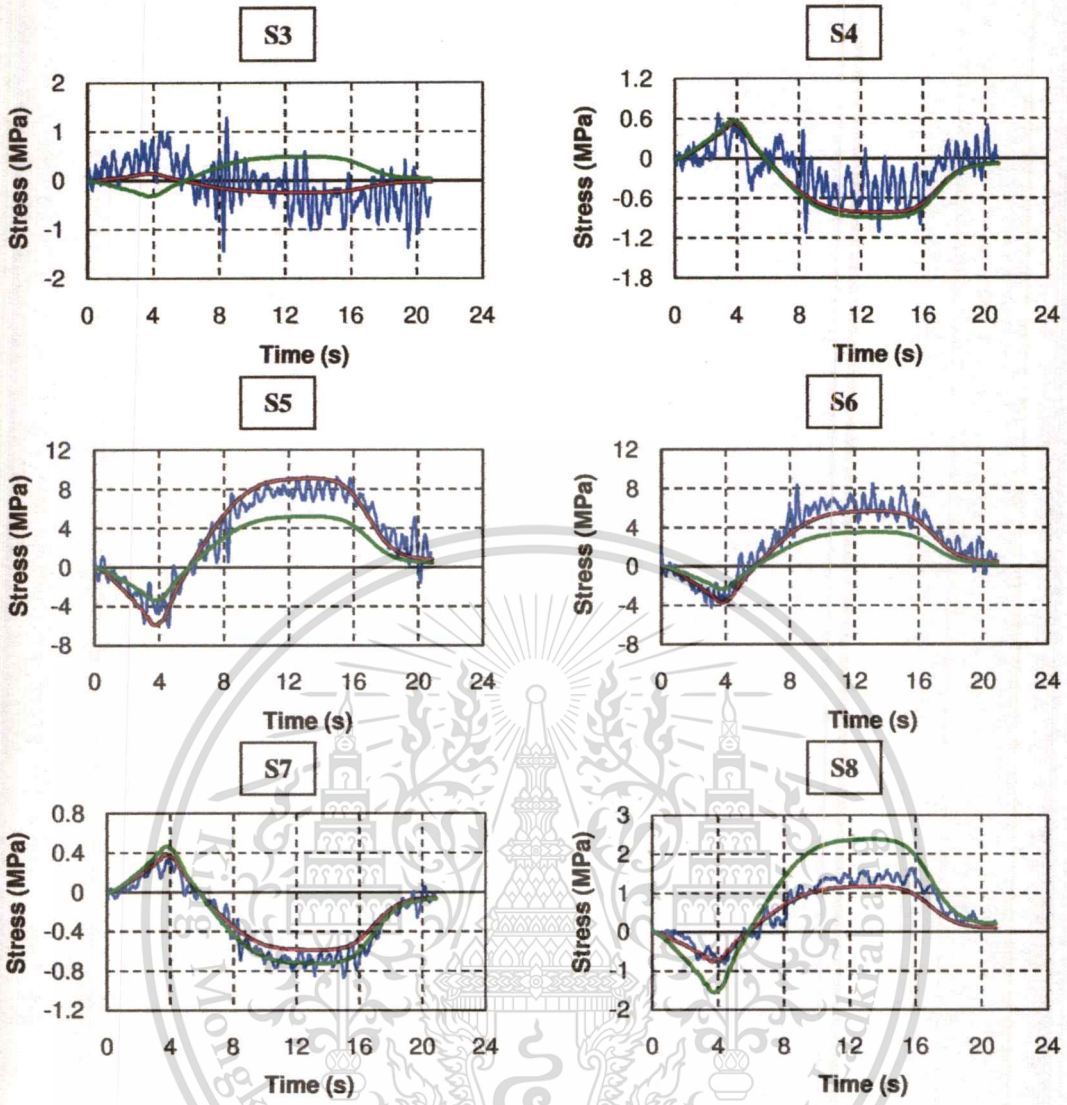

Figure 5.7 Dynamic stress response measured during a cornering maneuver (cont.)

The cornering responses from 8 measurement locations were exhibited in Figure 5.7. Most responses analyzed by static without suspension condition displayed considerable variations at S2, S5, S8 and a reversed stress at S3 with stress of 5.01 MPa, 5.17 MPa, 2.41 MPa, and 0.49 MPa respectively. In experimental data, the maximum magnitude of measured stress at location S1-S8 was found to be 3.86, 0.18, 0.46, 0.63, 7.92, 5.93, 0.75, and 1.42 MPa respectively. In general, calculated stress from both static and dynamic cases with suspension illustrated a small difference compared to the experimental data.

This material is reserved for educational use only, not allowed for commercial use.
Forbidden to modify the content, and cite the document when use.

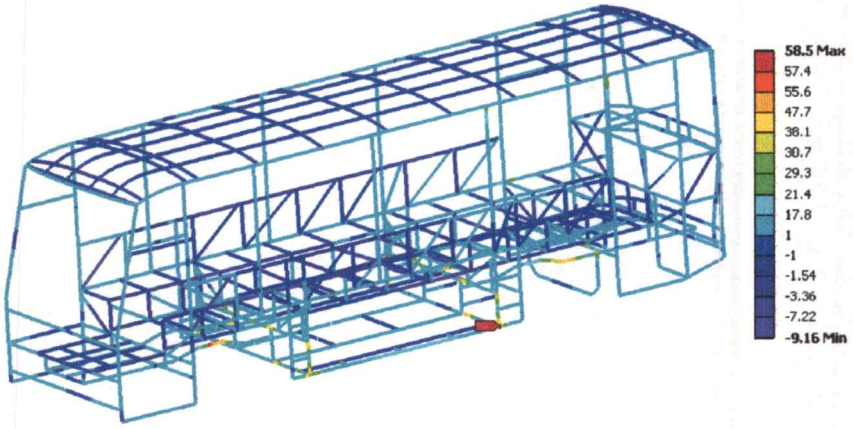

Figure 5.8 Stress distributions in normal cornering case using static analysis with suspension

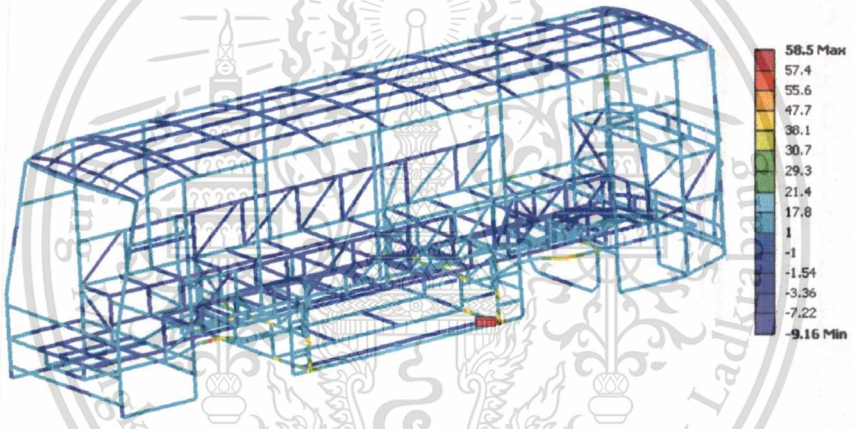

Figure 5.9 Stress distributions in normal cornering case using dynamic analysis with suspension

Figure 5.8 and Figure 5.9 shows computed stress distributions from the analyses using the suspensions simplified by spring elements. Although, they were different in selection of analysis type, both static and dynamic analysis with suspension models predicted the same maximum stress of 58.5 MPa which both appeared at the left side connection of the battery compartment. This was the same location as those found in braking maneuver. Overall, the significant stress could be observed in the left chassis on both front and rear suspension locations while the roof frame and the central body construction were subjected to an insignificant stress level.

This material is reserved for educational use only, not allowed for commercial use.
Forbidden to modify the content, and cite the document when use.

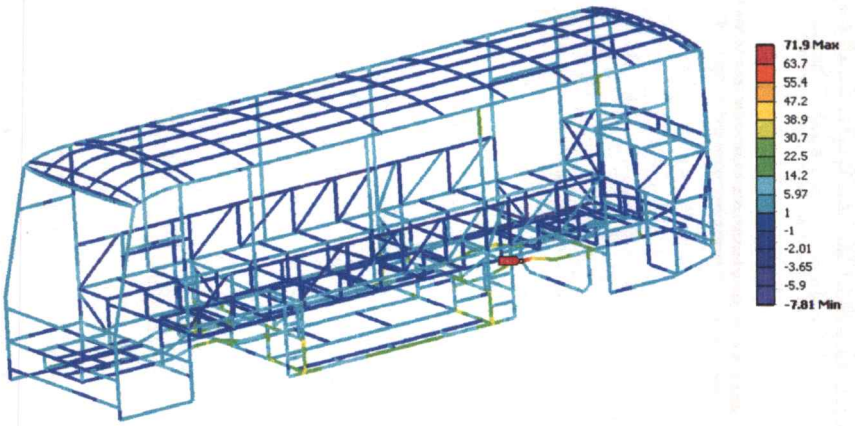

Figure 5.10 Stress distributions in normal cornering case using static analysis without suspension

On the other hand, the analysis solution shown in Figure 5.10, in which the FE model was not consisted of spring suspension, the highest stress level of 71.9 MPa could be seen on the left chassis where the rear suspension was installed. The considerable resulting stress was mostly concentrated at the left front chassis and connections of battery compartment.

5.1.3 Double Lane Change Maneuver

A double lane change test was the last of physical experiments that would be used in comparison with numerical solutions for the FE bus model validation. In this test, the test configuration was conducted with referring to Pennsylvania Transportation Institute for lateral stability test [18]. The following figure illustrates lateral acceleration which was measured at the centre of gravity of the vehicle.

This material is reserved for educational use only, not allowed for commercial use.
Forbidden to modify the content, and cite the document when use.

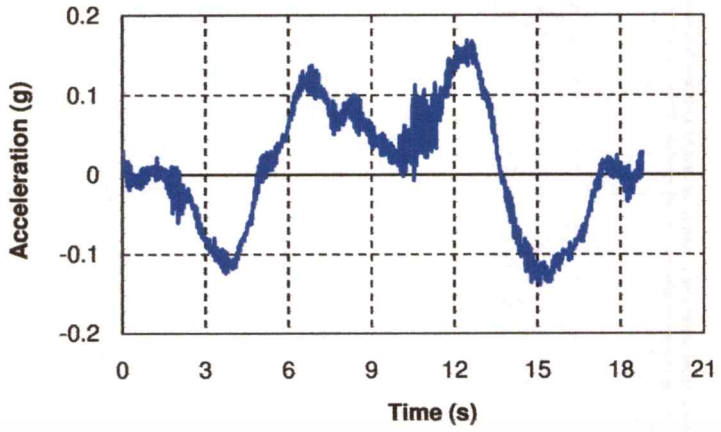

Figure 5.11 Lateral acceleration measured during a double lane change maneuver at test speed of 30 km/hr

The dynamic response of measured acceleration is shown In Figure 5.11. The test began with a left-hand approach followed by the doubles of right-hand approaches and ended again by left-hand approach. All approaches displayed the lateral acceleration to be 0.12 g, 0.12 g, 0.15, and 0.13 g on left-, right-, right-, and left-and approach respectively. It could be seen that the maximum lateral acceleration appeared while performing the second of right-hand approach or at the test duration about 13 seconds. Total duration time used for the double lane change maneuver was 18 seconds with the test path length of 110 m and the test speed of 30 km/hr.

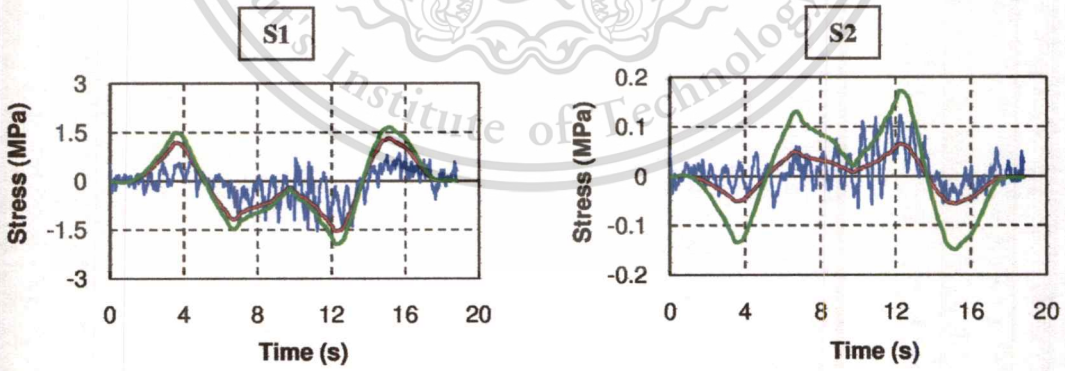

Figure 5.12 Dynamic strain response measured during a double lane change maneuver

This material is reserved for educational use only, not allowed for commercial use.
Forbidden to modify the content, and cite the document when use.

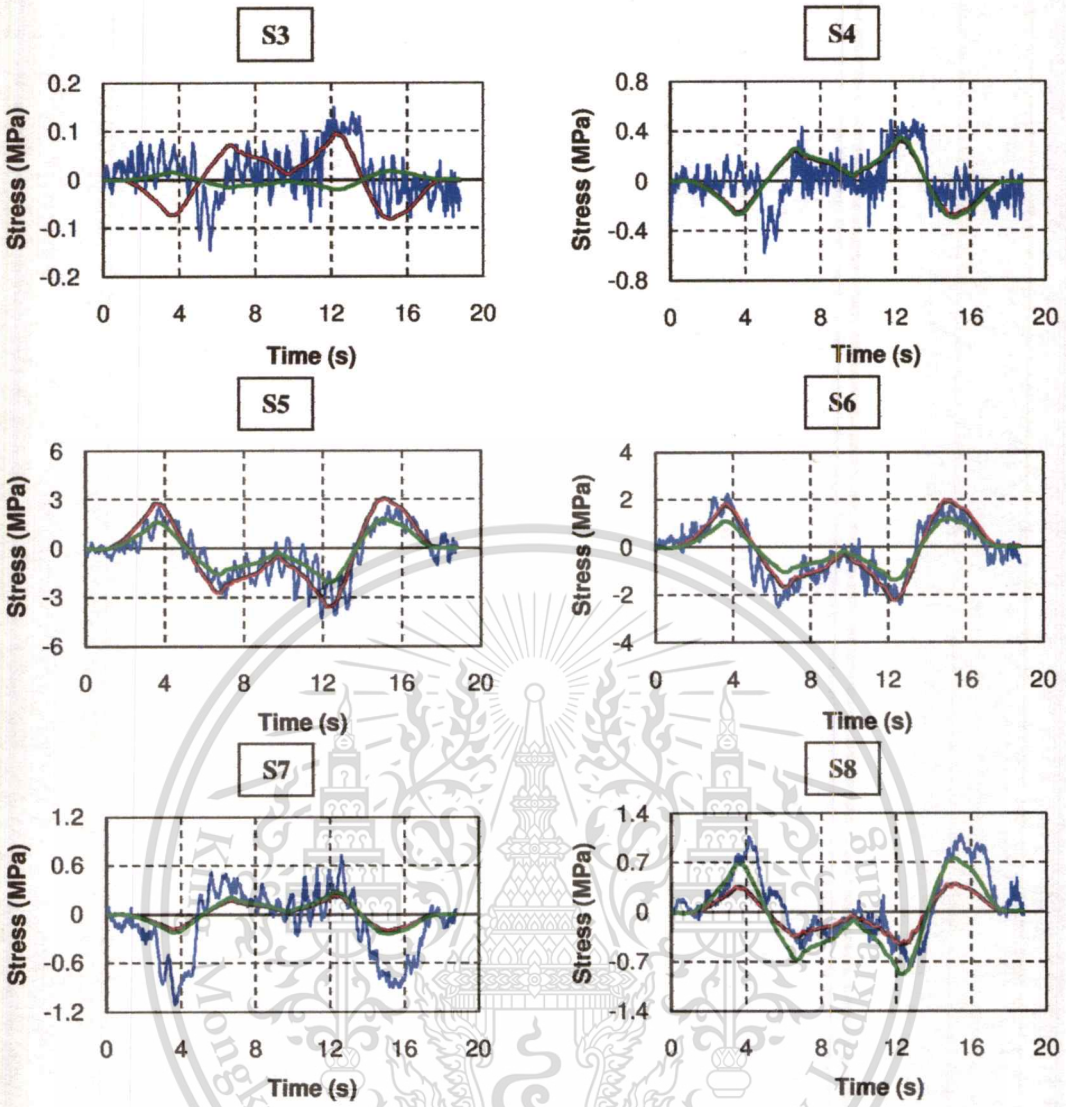

Figure 5.12 Dynamic strain response measured during a double lane change maneuver (cont.)

Figure 5.12 shows resulting stress comparison at 8 different locations monitored throughout the bus structure. In general, the stress responses exhibited four distinct stress peaks at all measurement locations according to the test configuration. The maximum experimental stress was observed at 12th second to be 1.14, 0.1, 0.11, 0.42, 3.21, 2.09, 0.42, and 0.65 MPa at S1-S8 respectively. The calculated stress without suspension at location S2 and S3 were significant because of a higher variation and the opposite direction of stress respectively. Both calculated stress of S2 and S3 displayed the stress of 0.16 MPa and 0.02 MPa respectively.

This material is reserved for educational use only, not allowed for commercial use.
Forbidden to modify the content, and cite the document when use.

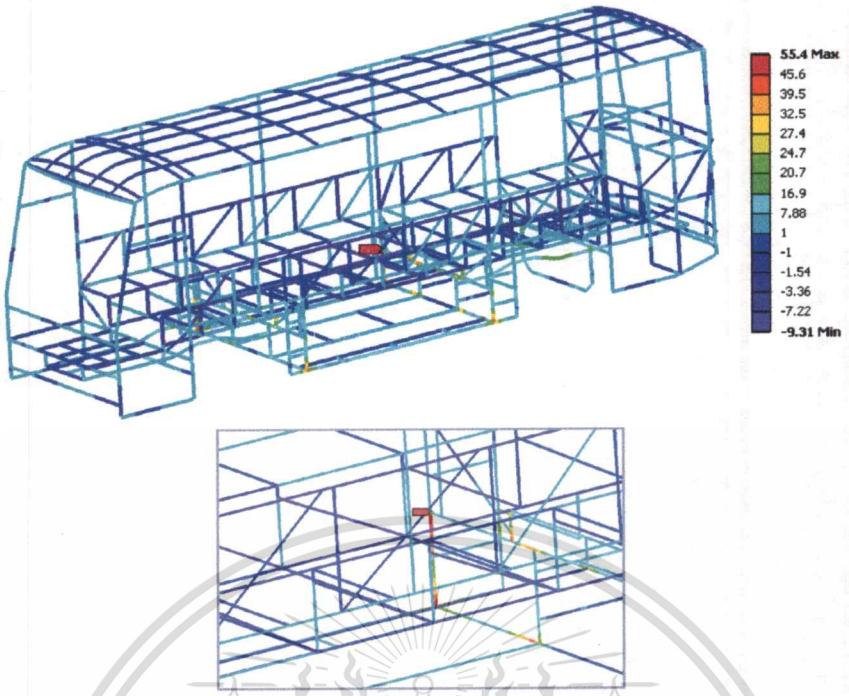

Figure 5.13 Stress distributions in normal double lane change case using static analysis with suspension

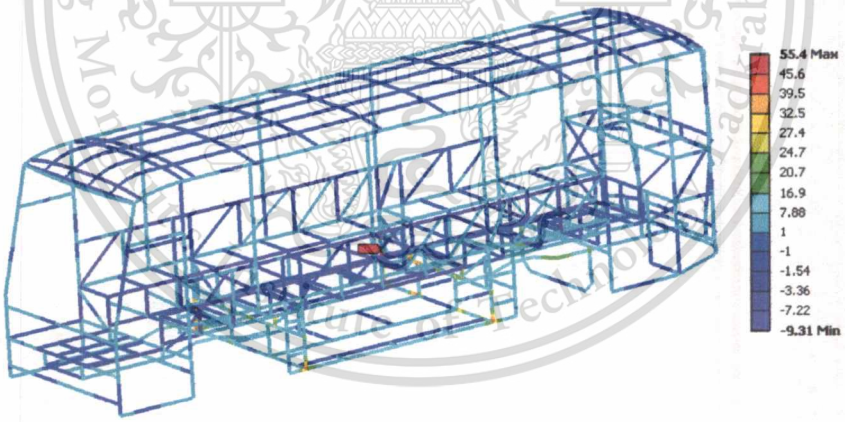

Figure 5.14 Stress distributions in normal double lane change case using dynamic analysis with suspension

In Figure 5.13 and Figure 5.14, the maximum stress was predicted to be 55.4 MPa on both cases and happened during the 12th second as shown in Figure 5.12. Additionally, it was observed at the right member on the rear part of battery compartment while performing the second right approach. The significant stress level exhibited in several connecting joints that used

This material is reserved for educational use only, not allowed for commercial use.
Forbidden to modify the content, and cite the document when use.

to form the battery compartment. The compressive stress could be seen in some longitudinal members placed around the central tubular bodies by 9.31 MPa.

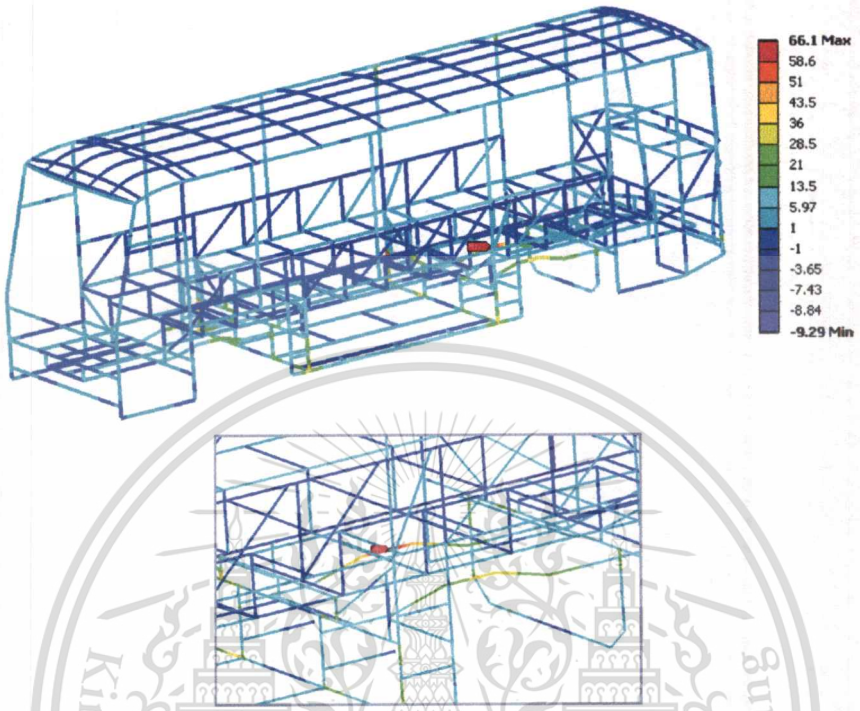

Figure 5.15 Stress distributions in normal double lane change case using static analysis without suspension

The maximum stress of 66.1 MPa calculated by the use of FE model without suspension occurred at the right chassis on the rear suspension. Generally, it could be seen that this lateral load had relatively insignificant effect to most members of the bus structure. Additionally, both constructions of central body and roof frame could be candidates for further structural improvement due to a very low resulting stress level.

5.2 Bus Analysis under Severe Load Conditions

In a previous section, three different boundary conditions were applied to verify the computational models of the bus structure. These employed conditions were the normal loading levels which were collected from physical experiments. However, in a real application, the bus may be subjected to various loading magnitudes. Therefore, a severe loading level for three driving maneuvers considered in previous section was applied together with bending and torsional

This material is reserved for educational use only, not allowed for commercial use.
Forbidden to modify the content, and cite the document when use.

cases. The objective of this section is to present calculated stresses and a torsional stiffness of the bus structure under severe loading conditions.

5.2.1 Braking Maneuver

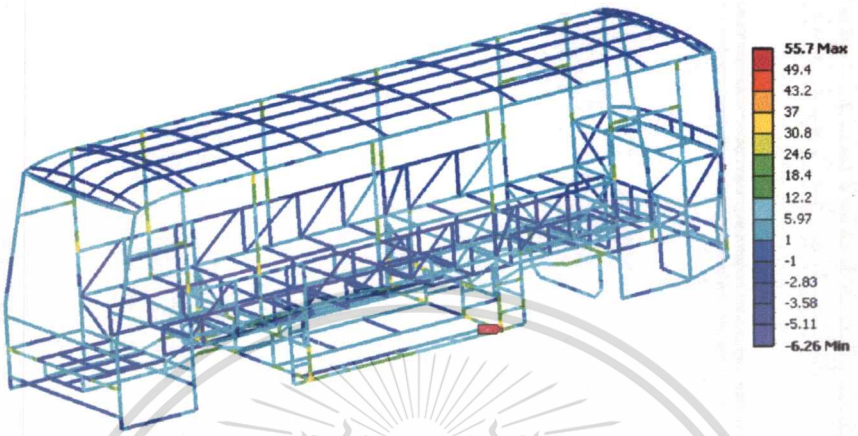

Figure 5.16 Stress distributions in severe braking case on original structure

The stress in severe braking condition of 55.7 MPa was observed as shown in Figure 5.16. The maximum stress occurred at the same location as in the normal loading condition i.e. the left connecting point of battery compartment closed to a left rear wheel. In this case, the resulting significant stress also took place at the top of the most column members.

5.2.2 Cornering Maneuver

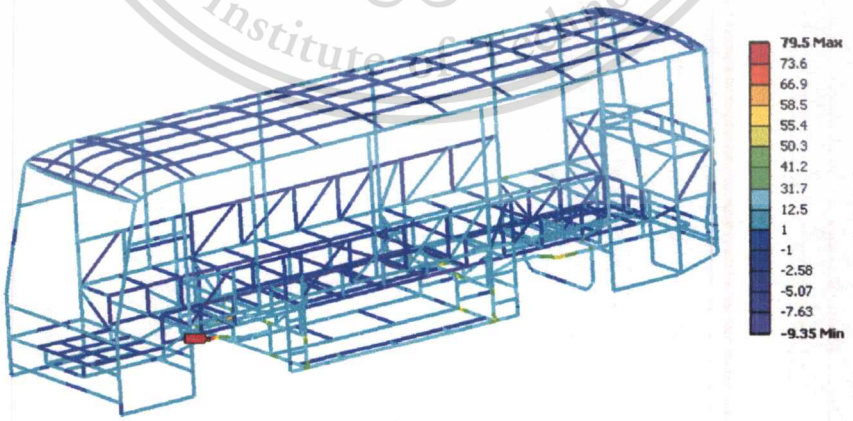

Figure 5.17 Stress distributions in severe cornering case on original structure

This material is reserved for educational use only, not allowed for commercial use.
Forbidden to modify the content, and cite the document when use.

By a lateral loading effect resulting from a cornering maneuver, a maximum stress of 79.5 MPa was identified at the front left chassis or at the installation position of the front left air bellows as shown in Figure 5.17. It could be seen that the stresses were mostly exhibited on the left side of both front and rear suspension areas.

5.2.3 Bending Case

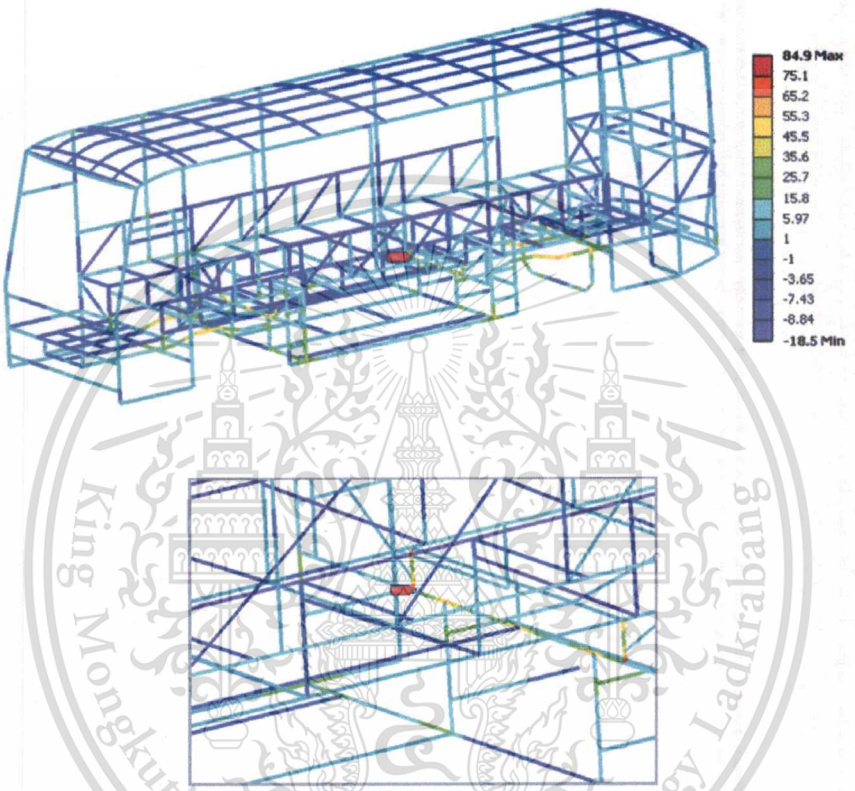

Figure 5.18 Stress distributions in bending load

The bending case was an additional condition used to determine stresses and deflections of the vehicle structure subjected to a vertical load of 2.5 times the passenger load. In this case, an increased distributed load was applied to the floor and the passenger seats. The bus structure was isolated from the suspensions by changing the bus restraints from the spring suspension to a simply supported configuration according to the test regulation. The maximum stress of 84.9 MPa was calculated at the connecting member linking the floor and the battery compartment frame as shown in Figure 5.18. In general, both front and rear suspensions were mainly subjected to a bending load.

This material is reserved for educational use only, not allowed for commercial use.
Forbidden to modify the content, and cite the document when use.

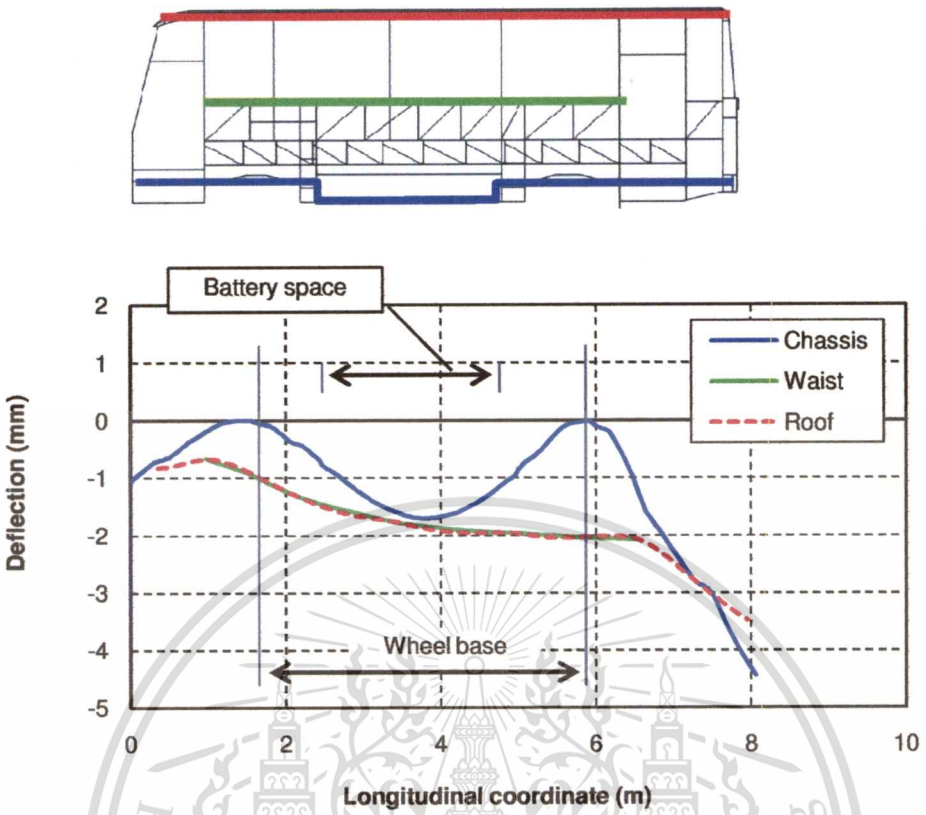

Figure 5.19 Vertical deflections along longitudinal members of left-side chassis and frame in bending case

The vertical deflections in 3 different component areas were plotted as shown in Figure 5.19. The chassis structure displayed an obvious deflection compared to the rest. Noticeable deflections were placed at the center of battery supporting members and at the rear end of the chassis by 1.7 mm and 4.42 mm respectively. It was seen that at the mounting points of both front and rear suspensions, the zero deflection on both areas were found due to isolated spring suspensions. On the other hand, the waist and the roof structure displayed a similar deformed shape with maximum deflections of 2.1 mm and 3.4 mm respectively.

This material is reserved for educational use only, not allowed for commercial use.
Forbidden to modify the content, and cite the document when use.

5.2.4 Torsional Case (stress)

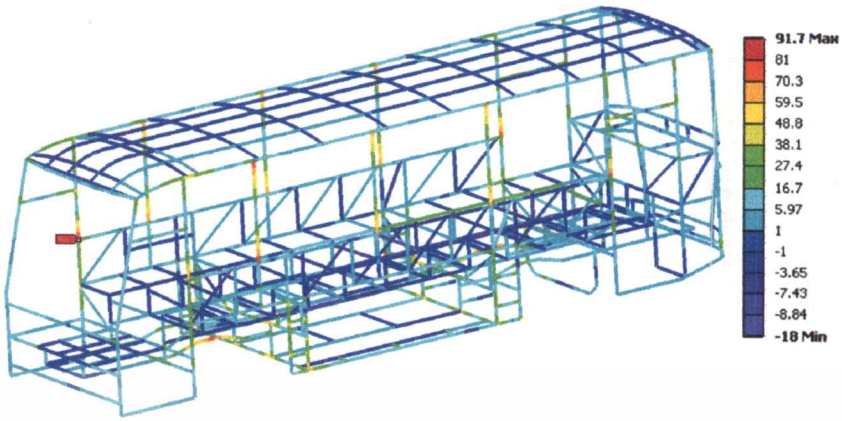

Figure 5.20 Stress distributions under torsional load

Figure 5.20 illustrates simulated stress distributions when a left front wheel was subjected to the vertical displacement of 200 mm. The critical stress of 91.7 MPa appeared at the column that forms a driver door that was on the right frame. It could be observed that considerable stress level was mainly displayed on both sides of the column members and front suspension.

5.2.5 Torsional Case (stiffness)

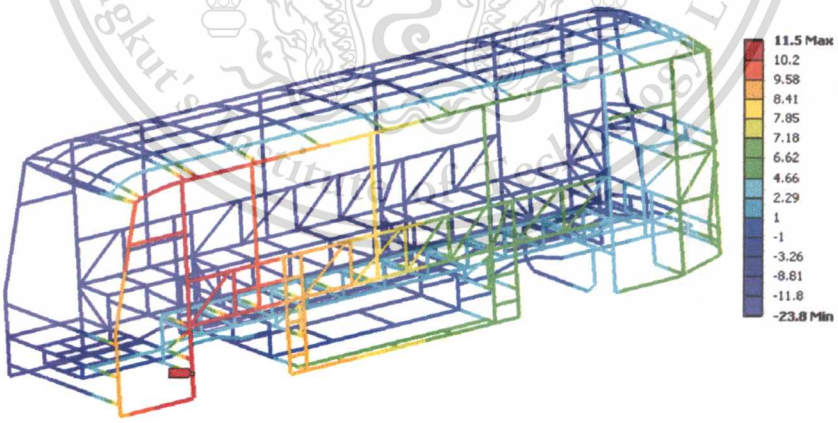

Figure 5.21 Vertical deformation under torsional load

It is generally accepted that the highest loading effect on the bus structure is from a torsional load. This load attempts to deform the structure along a longitudinal axis of the bus. In

This material is reserved for educational use only, not allowed for commercial use.
Forbidden to modify the content, and cite the document when use.

general, an assessment of a structural stiffness could be determined through a torsional stiffness. Figure 5.21 shows vertical deformation when the opposite vertical forces were applied at each location of front air bellows. The maximum deformation of 11.5 mm was predicted at the front door frame. The resulting numerical solutions could then be used to assess the torsional stiffness of the employed bus structure as shown in Figure 5.22.

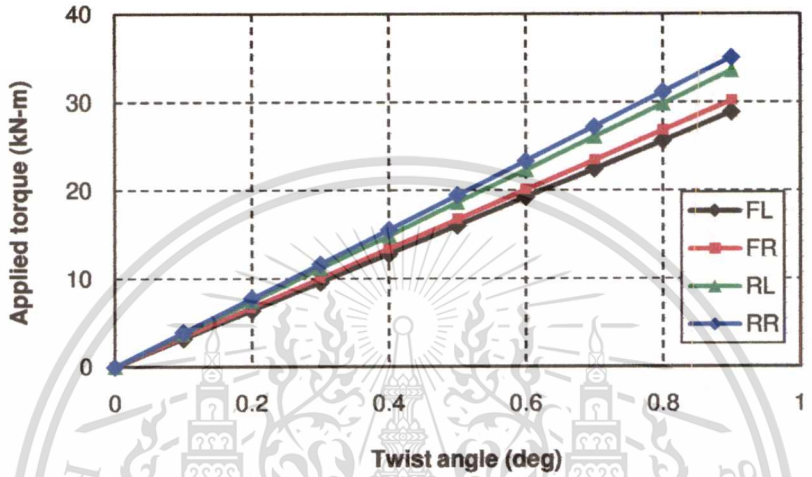

Figure 5.22 Comparison of torsional stiffness under different load cases

Figure 5.22 shows torsional stiffness under 4 different load conditions. For example, FL indicated when the front left wheel was lifted off the ground by the force increment while other 3 wheels were still attached the ground. Consequently, the reaction forces and structural twist angle were plotted. The torsional stiffness could be determined by a slope between the applied torque and the twist angle. In this case, the torsional stiffness were calculated to be 32,095, 33,548, 37,320, and 38,974 N-m/degree for front left (FL), front right (FR), rear left (RL), and rear right (RR) condition respectively.

5.3 Structural Strength of Original Bus Structure

From previous sections, several numerical solutions obtained under normal and severe loading conditions were illustrated. In order to conclude strength and a stiffness of an original electric bus structure, all resulting stresses, deflections, and stiffness are compared and presented in this section.

This material is reserved for educational use only, not allowed for commercial use.
Forbidden to modify the content, and cite the document when use.

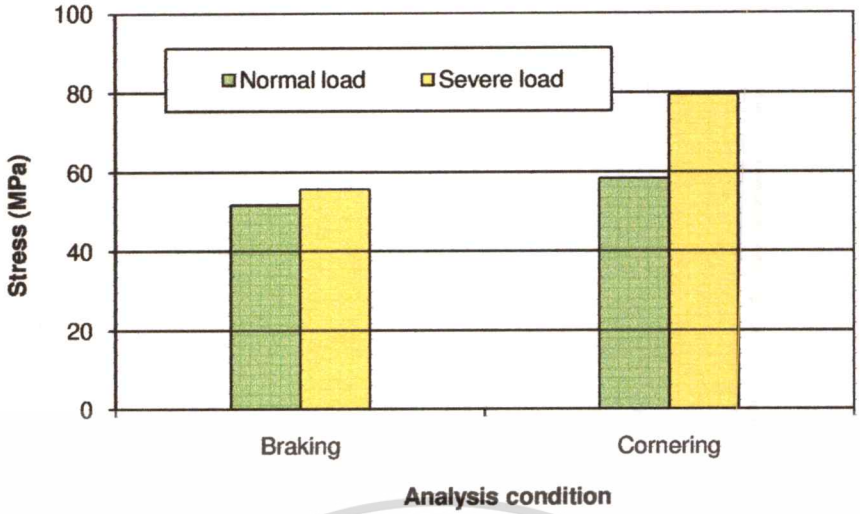

Figure 5.23 Stress comparison between normal and severe loads

In Figure 5.23, the maximum stress of 51.7 MPa and 55.7 MPa were determined in normal and severe braking cases respectively. In addition, the maximum translational stress under normal and severe load in cornering case was 58.4 MPa and 79.5 MPa respectively. The stress variation was calculated to be 7.44% and 30.6% in braking and cornering conditions. Moreover, the additional numerical solutions from bending and torsional analysis are summarized in Table 5.2.

Table 5.2 Summary numerical simulation in bending and torsional cases

Test condition		Numerical solution	Unit
Bending	Deflection	4.42	mm
	Stress	84.9	MPa
Torsional stress		91.7	MPa
Torsional stiffness		32,095	N-m/deg

5.4 Optimization Results

According to structural strength and stiffness on the original bus structure presented in previous section, it could be seen that that the structure of electric bus prototype contained relatively high strength and stiffness with respected to a yield strength and standard sets. Consequently, structural mass could be reduced in order to achieve a better electricity

This material is reserved for educational use only, not allowed for commercial use.
Forbidden to modify the content, and cite the document when use.

consumption and vehicle performance. A structural optimization work is reported in this section. For the optimization parameters, the objective function was to minimize the structural mass and the constraint function was the torsional stiffness. The selected design variables were a group of members in central tubular body, the roof frame, the side and the central members of the battery supporting frame defined by T1, T2, T3, and T4 respectively. These optimization parameters were explained in Chapter 4.

5.4.1 Optimization Sensitivity

After the optimization process was carried out, the correlation among the objective, constraint, and design variables could be displayed as presented in Figure 5.24 and Figure 5.25.

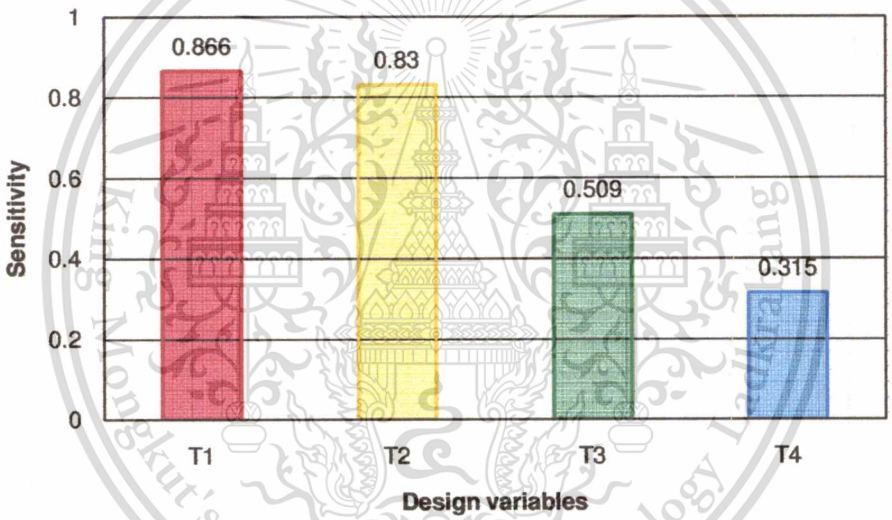

Figure 5.24 Sensitivities of structural mass

From Figure 5.24, it could be clearly seen how sensitive each design variables are to the structural mass under the same degree of design parameter, i.e. member cross-sectional thickness, and variation. It could be seen that the parameter T1 showed a sensitivity level of 0.866 which indicated the most sensitive parameter to the structural mass. The sensitivities of 0.83, 0.509, and 0.315 were illustrated for T2, T3, and T4 respectively.

This material is reserved for educational use only, not allowed for commercial use.
Forbidden to modify the content, and cite the document when use.

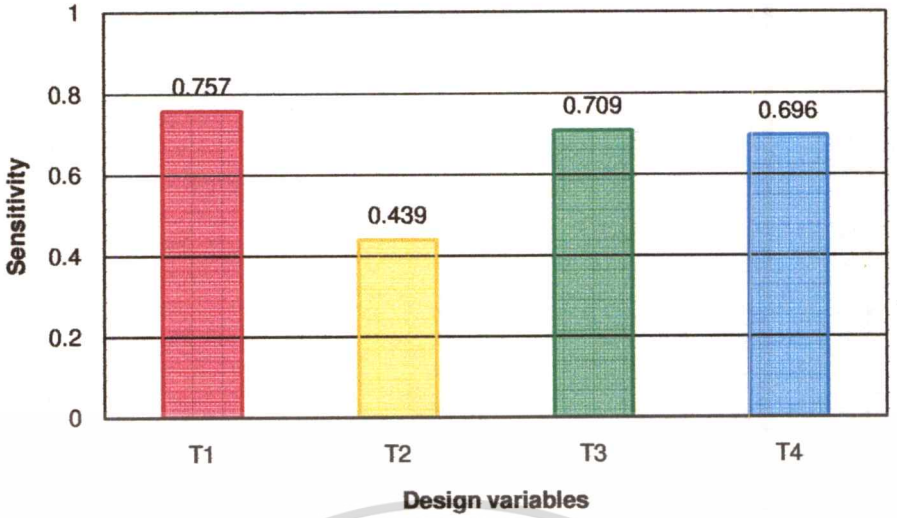

Figure 5.25 Sensitivities of torsional stiffness

From Figure 5.25, it was clear that most sensitive parameter could be ranged from T1, T3, T2, and T2 with respective sensitivity level of 0.757, 0.709, 0.696, and 0.439 respectively.

5.4.2 Cross-Sectional Feature Modification

In this section, the outputs obtained by the MOGA optimization including calculated variations between initial value and optimum values are listed in Table 3.

Table 5.3 Comparison between initial and optimized design

Optimized variables	Code	Initial	Allowable range	Optimum	Modification
Objective function	W (kg)	1962.5	-	1704.4	-13.15%
Constraint	TSF (N-m/deg)	32,095	22,000-32,095	22,028	-31.36%
Design variables	T1 (mm)	3.2	1.6-3.2	1.80	-43.75%
	T2 (mm)	3.2	1.6-3.2	1.94	-39.38%
	T3 (mm)	4.5	2.6-4.5	4.36	-3.11%
	T4 (mm)	6	3-6	4.83	-19.50%

This material is reserved for educational use only, not allowed for commercial use.
Forbidden to modify the content, and cite the document when use.

In summary of optimization results, it contained optimum values which were determined after optimization process. It was suggested that, under the employed design constraints and variables, the structural mass could be moderately reduced by 13.15% or 258.1 kg together with a decrease in torsional stiffness by 31.36%. This optimized stiffness of 22,028 N-m/deg was still within the range of structural requirement [52]. The modified cross-sectional thickness of design variables exhibited a reduction in cross-sectional thickness by 43.75%, 39.38%, 3.11%, and 19.50% for T1, T2, T3, and T4 respectively.

This material is reserved for educational use only, not allowed for commercial use.
Forbidden to modify the content, and cite the document when use.

CHAPTER 6

DISCUSSIONS

6.1 Finite Element Model Validation

In previous chapter, two FE bus models defined as "with" and "without" suspension were calculated using static and dynamic analysis while only the model without suspension was analyzed by static finite element procedures. The experimental data measured from braking, cornering, and double lane change maneuvers were then compared to those obtained by the FEA. In this section, the deviations of computational results from experimental results at 8 locations corresponding to strain gage attachment points are shown in Figure 6.1 - 6.3.

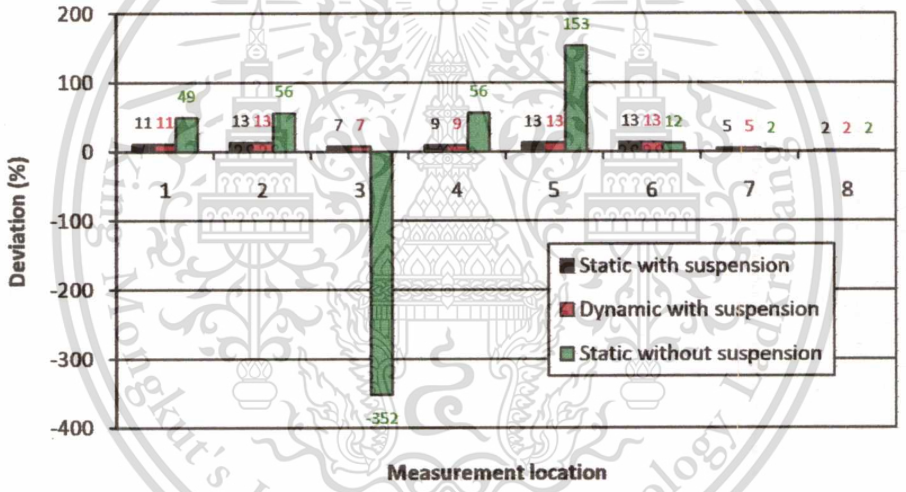

Figure 6.1 Comparison of deviations between computational models with and without spring suspension in braking case

This material is reserved for educational use only, not allowed for commercial use.
Forbidden to modify the content, and cite the document when use.

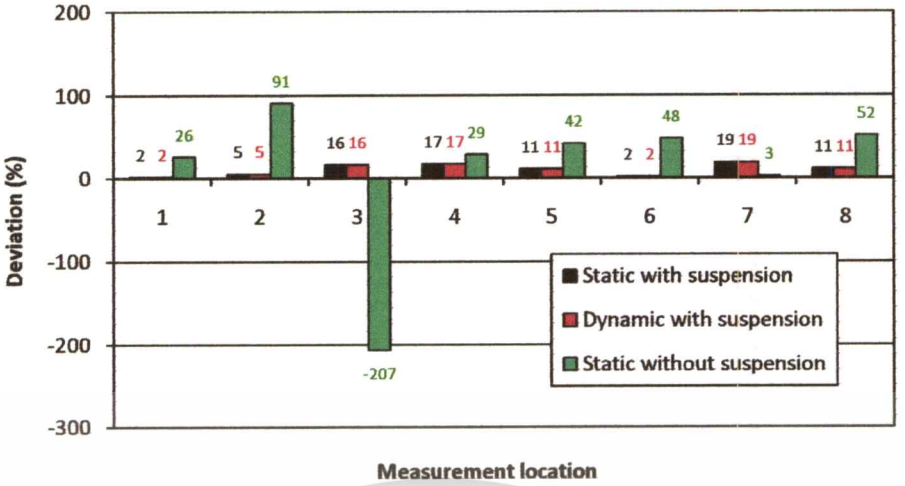

Figure 6.2 Comparison of deviations between computational models with and without spring suspension in cornering case

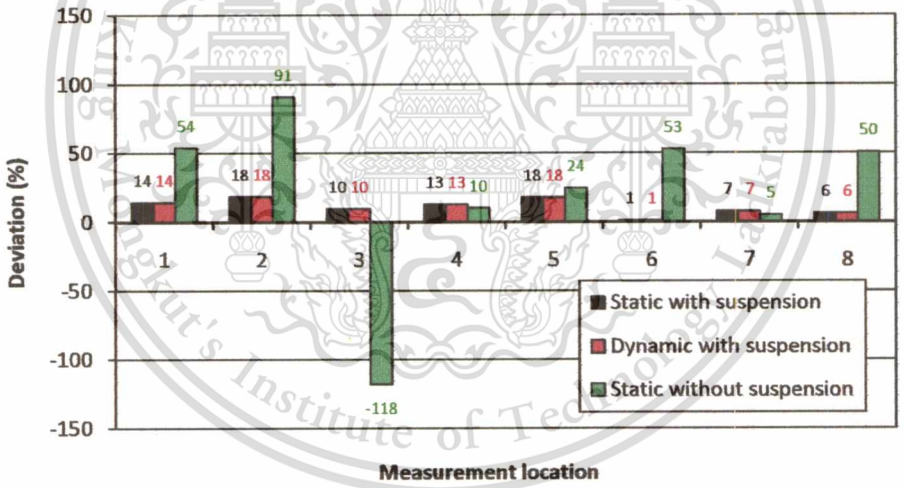

Figure 6.3 Comparison of deviations between computational models with and without spring suspension in double lane change case

In general, Figure 6.1-6.3 shows minute deviations in both static and dynamic cases on the bus model with suspension. However, significant variations were mainly found in the static analysis on the model without suspension. Thus, it could be said that the analysis of the FE model included with suspension could improve a solution accuracy compared to that computed by the

This material is reserved for educational use only, not allowed for commercial use.
Forbidden to modify the content, and cite the document when use.

model without suspension at all monitoring points under braking, cornering, and double lane change conditions. It was believed that a presence of spring elements, employed to represent simplified bus suspensions in this study, could reduce structural deformations when the external loads were applied on the structures. This could result in lower corresponding stresses in the simulations. It could be seen from Figure 6.1-6.3 that the maximum differences between experimental and analytical results for the model with suspension were 13% at locations S2, S5, and S6 in braking case, 19% at locations S7 in cornering case, and 18% occurred at locations S2, S4 in double lane change case. The errors might be due to a complexity of the bus model and a perfectly welding joint assumption such that they could affect the effective structural stiffness. Nonetheless, the static and dynamic analytical results from the models with suspension were in good agreement with those obtained from experiments in term of stress comparison. Thus, the FE bus model included with spring elements on both front and rear suspensions were acceptable for use in further structural analyses.

Moreover, for the model without suspension, the maximum deviations were 352%, 207%, and 118% in braking, cornering, and double lane change case respectively. It could be clearly noticed at the location S3 for all maneuver cases considered that there were another distinct set of deviations such that large amount of deviations as well as reverse in stress direction were calculated compared to the experimental data. The possible reason for such significant variations at this particular location might be explained by the deformation results shown in Figure 6.4 and Figure 6.5.

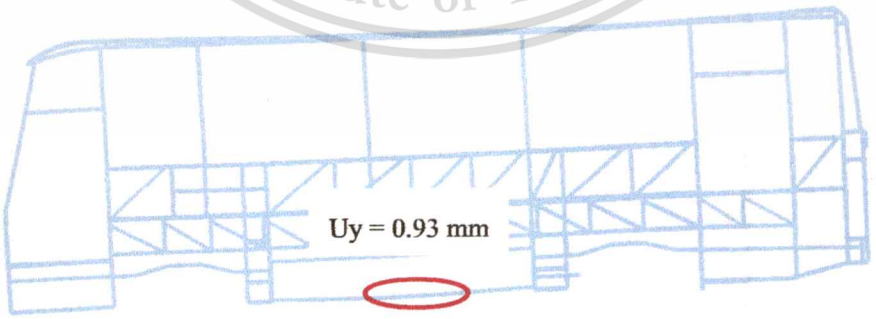

Figure 6.4 Deformed shape during deceleration with suspension with resulting deflection value at location S3

This material is reserved for educational use only, not allowed for commercial use.
Forbidden to modify the content, and cite the document when use.

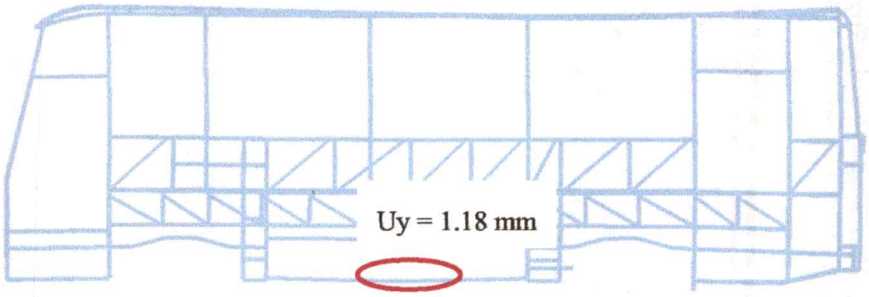

Figure 6.5 Deformed shape during deceleration without suspension with resulting deflection value at location S3

A braking condition was considered for this explanation. According to the computational steps during a braking case, the bus was subjected to a gravitational acceleration of 9.81 m/s^2 in the first step before the deceleration was then applied in the second step. In the first step, after both structures were subjected to the gravitational acceleration, small deflections at location S3 of the structure with and without suspension was observed as 0.97 mm and 0.98 mm respectively. It could be seen that the deflection of the structure with suspension was slightly lower than that without suspension. This might be because the spring elements could allow a vertical movement after absorbing the reaction forces transmitted to-and-from the ground at both front and rear suspension areas.

In the second step, the deceleration was applied and the deflection of the structure with suspension was reduced from 0.97 mm to 0.93 mm. As suggested in Figure 6.4, the structure with suspension was calculated to be in an inclined position during the deceleration with the front spring suspensions being considerably more compressed than the rear spring suspensions. It was believed to be due to the effect of the lumped masses on the bus structure attempted to move the structure forward. Hence, this forward-movement effort of the masses together with the structure inclination could result in a reduction of the deflection at location S3.

On the other hand, the deflection of the structure without suspension was increased from 0.98 mm to 1.18 mm with the corresponding deformed shape shown in Figure 6.5. One possible explanation was that the effect of lumped masses on the bus was more pronounced in a downward direction rather than a forward direction due to unallowable horizontal and vertical translations by the simply supported constraints at both front and rear suspensions. Generally, it could be said that the reversed stresses observed between the structure with and without suspension might come

This material is reserved for educational use only, not allowed for commercial use.
Forbidden to modify the content, and cite the document when use.

from the difference in a structural behavior around the area of the battery compartment during the deceleration depending on a nature of the constraint being applied on the computational model.

6.2 Comparison of Computational Efficiency between Static and Dynamic Analysis

To effectively solve engineering problems through finite element analysis, the computational time and accuracy of the solutions must be cooperative. In this section, comparison of computational efficiency between static and dynamic analysis performed in this study are considered. In analysis, steps for the calculation were divided into several small parts according to the boundary condition response. Multiple steps are useful if new loads are introduced at different times such as applied acceleration response. Therefore, it is necessary to use a small time step size that could perfectly represent the acceleration response collected from the experiment to achieve good quality results. Different applied time steps corresponding to the boundary conditions used in all analyses in this study are listed in Table 6.1.

Table 6.1 Steps controls for static and dynamic analysis

Model	Number of step
Braking	111
Cornering	132
Double Lane Change	136

Table 6.2 Computer specifications used for FEA simulation

Item	Specifications
CPU (4 cores)	Intel Xeon (X5472) 3.00GHz
Physical memory (RAM)	16.0 GB
Graphic card	NVIDIA Quadro FX 4600
Operating system	Windows Vista x64
Commercial FEA software	ANSYS 12.1

Table 6.2 reveals the specifications of workstation computer used for obtaining FEA outputs in this work. Two key factors could be used in implementing the computational

This material is reserved for educational use only, not allowed for commercial use.
Forbidden to modify the content, and cite the document when use.

efficiency. First, the floating-point operations (FLOPS) were employed to consider the computational resources. Another parameter was the CPU time, which could be directly related to the speed of the computational process. In this study, the static and dynamic analyses with suspension were implemented. The corresponding FLOPS and the CPU time are shown in Figure 6.6 and Figure 6.7.

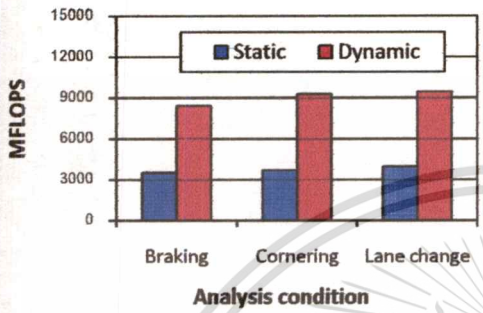

Figure 6.6 FLOPS comparison

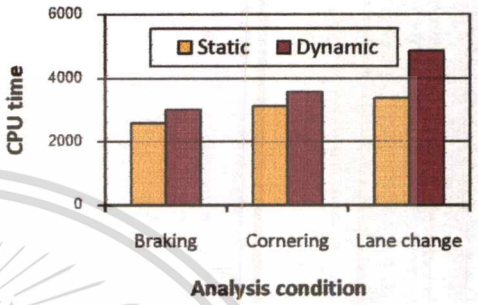

Figure 6.7 CPU time comparison

From a comparison of FLOPS for both static and dynamic analysis in Figure 6.6, it was clearly indicated that the dynamic analysis required more computational resources in all cases considered. The maximum difference was the cornering case at 85.78% while the minimum difference of 81.92% was found at the braking condition. Furthermore, the CPU time comparison in Figure 6.7 showed that the largest time for obtaining the solution was in the dynamic lane change case with the CPU time of 2919 seconds. In contrast, the quickest was on the braking case with 2578.2 seconds. The maximum difference in CPU time was calculated to be 36% in the lane change case. Theoretically, when a damper effect was included into finite element simulations, it could cause the computational time to increase. This was believed to be the main reason that the FLOPS and the CPU time were increased in cases of dynamic simulations. Thus, it could be concluded that by using the static analysis in bus structure simulations with suspensions included, similar computational solution accuracy could be obtained in comparison to those with dynamic analysis with a slightly reduction in the computational time and a significantly decrease in the computational resources.

This material is reserved for educational use only, not allowed for commercial use.
Forbidden to modify the content, and cite the document when use.

6.3 Comparison of Structural Strength between Original Structure and Optimized Structure

In Chapter 5, several boundary conditions of both normal and severe loading cases were employed to determine structural strength of original bus structure. After the calculated results indicated various locations of minute stresses and stiffness among the structural members, the structural optimization was utilized to minimize the structural mass in order to obtain a guideline on a lightweight bus model. As a result, the improved optimization parameters were obtained. In this section, the structural strength and torsional stiffness of the optimized bus structure was assessed via severe loading conditions. Stress comparison between original and optimized bus structure analysed under braking, cornering, bending, and torsional conditions are demonstrated in Figure 6.8 – Figure 6.11.

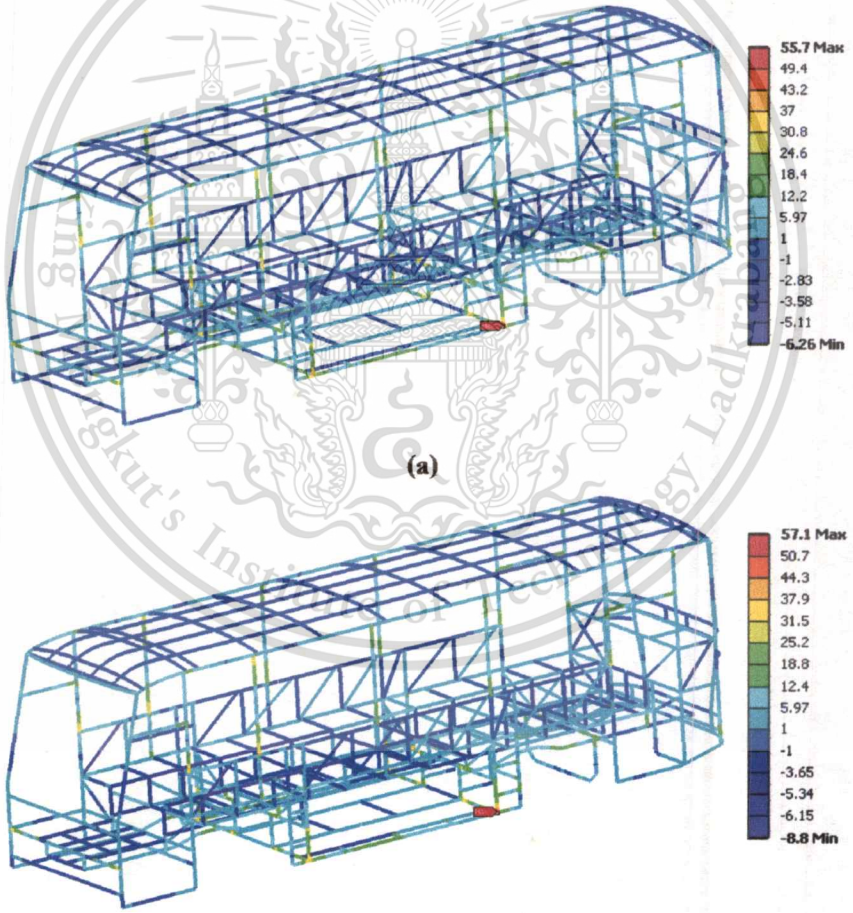

Figure 6.8 Resulting stress comparison under severe braking case: (a) original structure (b) optimized structure

This material is reserved for educational use only, not allowed for commercial use.
Forbidden to modify the content, and cite the document when use.

Figure 6.8 shows a comparison of resulting stress distribution between original and optimized structure calculated by severe braking case. It was found that the critical points occurred on both structures at the same location i.e. at the T-joint connection located at the left side of battery compartment. It could come from the weight of the battery packs. A maximum stress of the original and optimized structures was 55.7 MPa and 57.1 MPa respectively. In addition, stress distributions on both structures displayed a similar trend despite slightly differences in magnitude. The significant stress levels exhibited at the top of the column members, rear suspension, and battery compartment on both sides of the structures. On the other hand, insignificant stress levels were observed on the roof frame and the central tubular body even though wall thicknesses of the optimized structure were reduced by 43.75% and 39.38% on the central body and the roof members respectively. This might have come from the fact that the optimization only reduced the defined wall thicknesses without reducing the number of structural members. It could be said that the overall strength of the optimized structure was still high enough to resist a severe longitudinal load, which might be received during a suddenly braking condition.

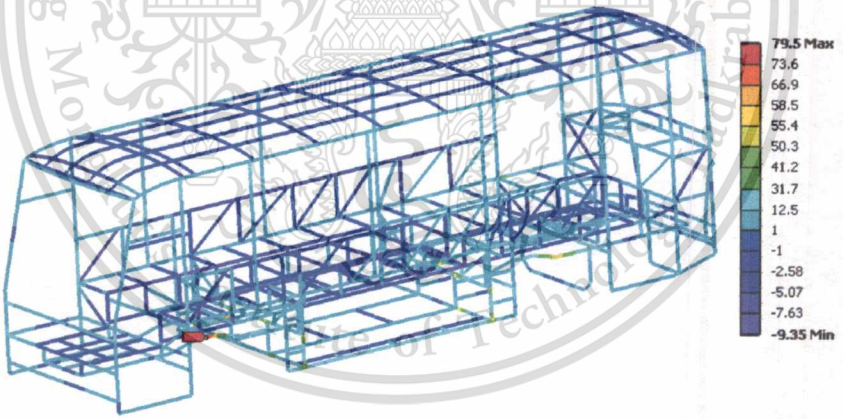

(a)

This material is reserved for educational use only, not allowed for commercial use.
Forbidden to modify the content, and cite the document when use.

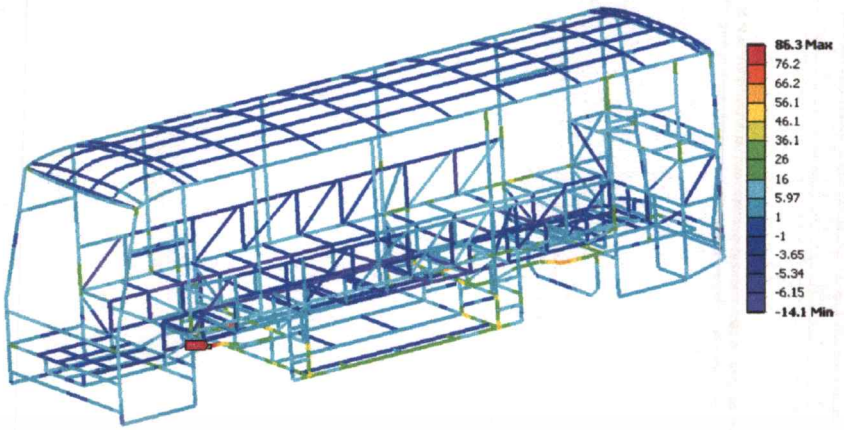

(b)

Figure 6.9 Resulting stress comparison under severe cornering case: (a) original structure (b) optimized structure

Stress distributions obtained from a right cornering condition are shown in Figure 6.9. It was observed that strength of the optimized structure was reduced in relation to structural thicknesses reduction. Consequently, the calculated stress in the optimized structure increased from 79.5 MPa to 86.3 MPa on the left side of front suspension where the air bellows was installed. It could also be seen that stress level throughout the structures exhibited a small change from original case. However, noticeable stresses were found in some areas such as left side of the rear suspension where the air bellows were located, the frame of the battery compartment, and the column members. The reason was that during the right turn, the structural load moved to the left side of frame such that the left side frame could be subjected to considerable effects.

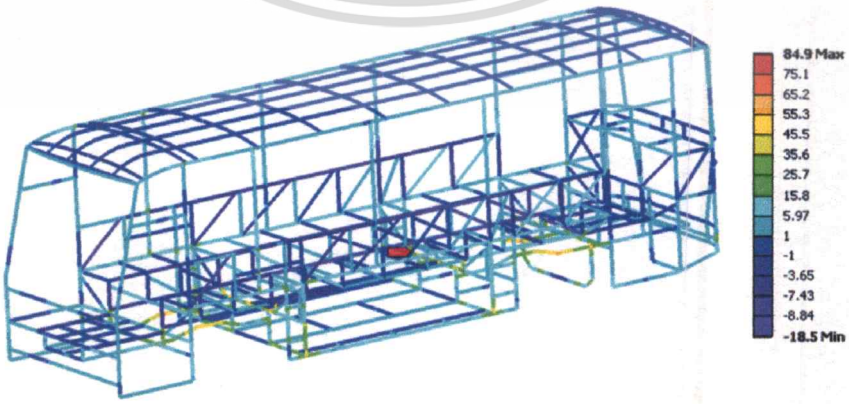

(a)

This material is reserved for educational use only, not allowed for commercial use.
Forbidden to modify the content, and cite the document when use.

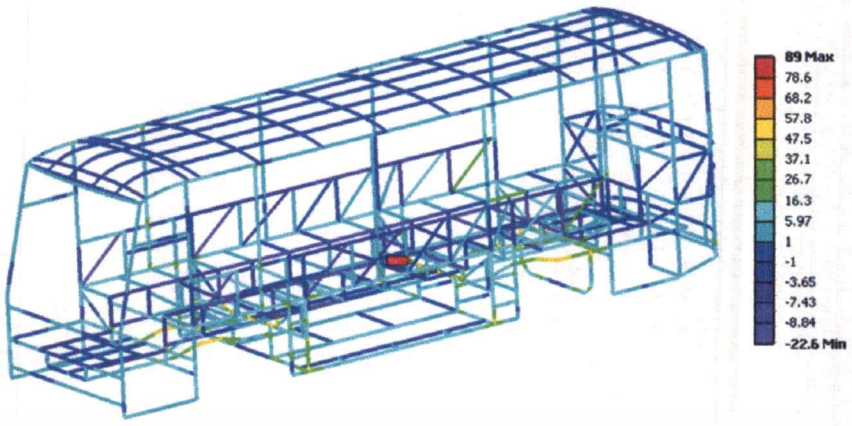

(b)

Figure 6.10 Resulting stress comparison under bending case: (a) original structure (b) optimized structure

In bending case, the objective was to determine a static characteristic of the bus structure i.e. bus floor deflection and permanent structural deformation. From the analysis, the chassis structures around the front and the rear suspension showed a noticeable stress level as shown in Figure 6.10. The critical areas on both structures are exhibited stress at the same locations i.e. the connecting members between the battery compartment frame and the floor member. The reason might come from lack of stiffness due to a few cross-sectional members and the passenger's weight placed on the floor. In general, highest tensile stress distribution was calculated to be 84.9 MPa and 89 MPa for original and optimized structure respectively. This little difference might have come from cross-sectional area reduction of the central tubular members after the optimization. On the other hand, both sides of longitudinal waist members displayed a maximum compressive stress of 18.5 MPa and 22.6 MPa for the original and optimized structure respectively. This could be an effect of the passenger weight attempted to bend the overall bus structure. However, the main focus in this case was directed to the roof frame and several members at the center of the optimized structure. These areas displayed relatively low stress level even though the cross sections were considerably reduced.

This material is reserved for educational use only, not allowed for commercial use.
Forbidden to modify the content, and cite the document when use.

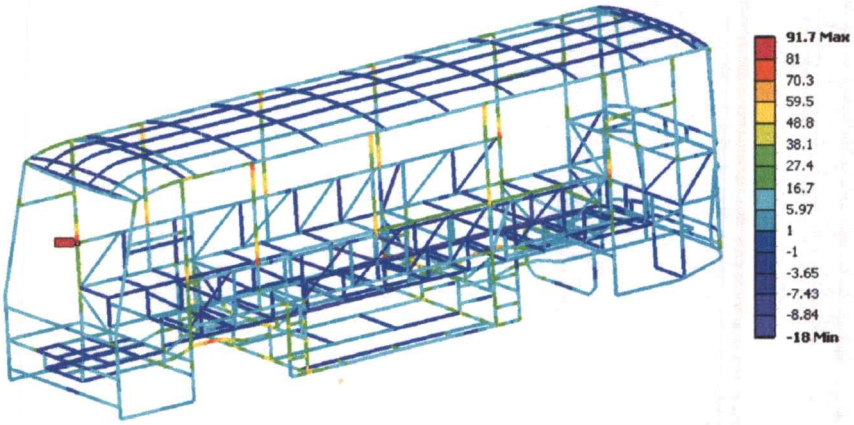

(a)

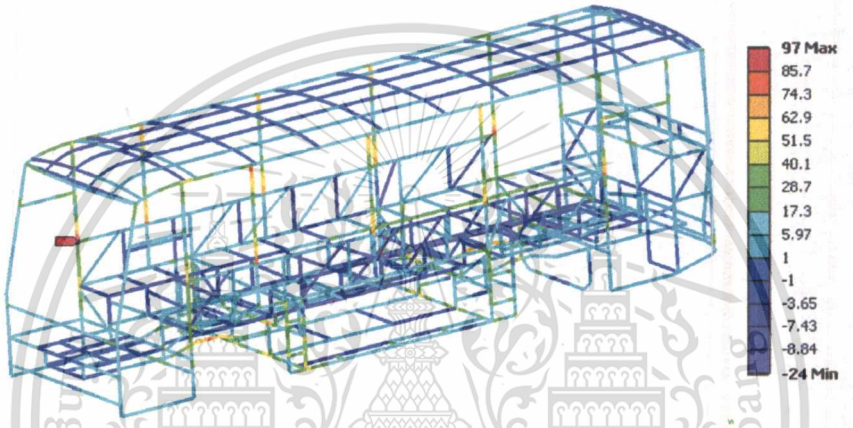

(b)

Figure 6.11 Resulting stress comparison under severe torsional case: (a) original structure (b) optimized structure

In Figure 6.11, the vertical displacement was used to induce a torsional load on the structure. The simulated solutions showed that maximum stress of 91.7 MPa and 97 MPa were generated at the front columns close to the driver's position on the original and optimized structure respectively. The critical points happened when the left front wheel was lifted off the ground by 200 mm. The noticeable stress was also observed at both top and bottom ends of the columns. The reason was that lack of reinforcement on the columns resulted in a weak characteristic to resist the torsional load compared to the central body. Another area was the front suspensions that received high reaction forces to create a torsional deformation. Stress distribution seemed to be low at the central body and the roof frame. It could then be concluded

This material is reserved for educational use only, not allowed for commercial use.
Forbidden to modify the content, and cite the document when use.

that the main members to receive the torsional load were the columns on both sides of the structures.

Table 6.3 Structural strength and stiffness verification of the optimized structure

Load condition		Numerical solution	Strength requirement
Braking		FOS = 6.86	FOS ≥ 3
Cornering		FOS = 4.06	FOS ≥ 3
Bending		δ_{max} = 4.61 mm	-
		σ_{max} = 88.9 MPa	*$\sigma_{max} < \sigma_{yield}$
Torsion	(Stress)	FOS = 3.6	FOS ≥ 3
	(Stiffness)	22,028 N-m/deg	18,000-40,000

*Requirement of permanent deflection (δ_{max} < 5 mm after unloading)

In order to verify the strength and stiffness of the optimized bus structure, Table 6.3 lists the numerical solutions obtained in this study in comparison to the defined values referred to the Urban Bus Specifications-II [52]. It was clear that strength and stiffness of the optimized structure were satisfactory at all load conditions considered in this study. In general, the safety factor higher than 3 was required for typical structural strength. In addition, the requirement stated that a maximum permanent defection must be lower than 5 mm in bending case. Consequently, a maximum calculated stress obtained from the FEA was considered in comparison with the yield strength of the material. In analysis, the yield strength was 350 MPa and the maximum calculated stress was 88.9 MPa. Therefore, the permanent deflection could not be observed because the stress was not reached the yield limit.

6.4 Optimization Response

When the optimization analysis was terminated, the output parameters that were recorded during the calculation could be plotted to visualize the development of the optimization process parameters. The optimization history carried out in this study is shown in Figure 6.12.

This material is reserved for educational use only, not allowed for commercial use.
Forbidden to modify the content, and cite the document when use.

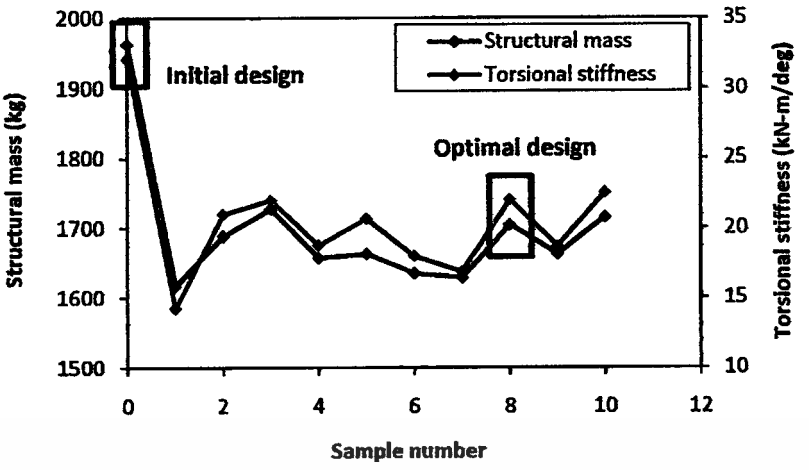

Figure 6.12 Optimization history regarding structural mass and torsional stiffness

Figure 6.12 illustrates the history of the mass and torsional stiffness changed during the optimization process. Before the optimization, both mass and stiffness was 1962.5 kg and 32,095 N-m/degree respectively. After the first calculation, both mass and stiffness were dramatically reduced. This was a first change searching for the targets according to the objective and constraint functions. After the values dropped to the lowest positions at sample 1, they were raised to approximately 1680 kg for mass and 21,000 N-m/degree for torsional stiffness. It could be seen that both optimized parameters were still attempted to achieve the targets. Hence, the optimization process was continuously executed. The variation of the sample numbers was then observed until sample 10. When the optimization was terminated, three optimum candidates were automatically promoted. In this stage, sample 3, 8, and 10 were identified. To make the decision what would be the optimal design, the final values of mass and torsional stiffness in each sample were compared. As a result, sample 8 was manually chosen to be the optimal design. Although the stiffness on this sample located at the middle level compared to the others, it showed the lowest amount of structural mass. Therefore, the optimized structural mass of 1704.4 kg and the torsional stiffness of 22,028 N-m/degree were proposed. In conclusion, the final structural mass and final torsional stiffness were calculated to be 13.16% reduction and 31.31% decrease from initial values respectively.

This material is reserved for educational use only, not allowed for commercial use.
Forbidden to modify the content, and cite the document when use.

6.5 Conclusions

The concept of selecting the bus model was to contain a lightweight structure with maintaining the structural strength and stiffness. In previous section, the original bus was analysed before a structural optimization was utilized to minimize the structural mass. At the end of the optimization process, various thicknesses on the central tubular body, the roof frame and the members underneath the battery packs were reduced. The optimized structure was simulated again under severe load cases in order to ensure the strength and torsional stiffness. The proposed bus model was confirmed to be able to sustain the severe load conditions such as a sudden braking, cornering at high vehicle speed, overloading by many passengers, and twisting from severe torsional load. Finally, the proposed optimized bus model could give a handling enhancement, electricity economy, high structural durability as well as production cost reduction by a reduced structural mass.

King Mongkut's Institute of Technology Ladkrabang

This material is reserved for educational use only, not allowed for commercial use.
Forbidden to modify the content, and cite the document when use.

CHAPTER 7

CONCLUSIONS AND SUGGESIONS

7.1 Conclusions

This research focussed on analyzing a bus structure in term of stress and stiffness and improving the structural weight. A medium-sized electric bus prototype was employed in this study. The novel approach of creating an appropriate finite element (FE) bus model was proposed by including linear spring elements into bus suspensions. The proposed FE model was investigated through both numerical simulation and experimental measurement. The investigations were carried out on several driving conditions such as braking, cornering, and double lane change. After the FE bus was verified, additional bending and torsional conditions were included in order to study vertical and twisting deformations of the bus structure. In order to determine relevant structural strength of the bus prototype, severe loading cases were then considered to obtain the resulting stress distributions. Moreover, the torsional stiffness of existing bus prototype was assessed. The computational results indicated that, under the studied conditions, the current bus structures were more than adequate in terms of both strength and stiffness. Thus, a structural optimization was carried out to minimize the structural mass with a constraint of maintaining the torsional stiffness. The optimized structure showed considerable improvement in mass reduction. Furthermore, the optimized structure was analyzed under the severe loads in order to compare between original and optimized structures. The main conclusions of this study were as followed:

- The proposed FE bus model illustrated the maximum deviation of 19% for stresses occurred at the middle of the side waist member during a cornering maneuver. In contrast, the FE model excluding the spring suspensions displayed much higher deviation or reversed stress direction than those calculated by including the spring suspensions. This relatively poor solution accuracy could be found in all investigated conditions and with majority of chosen measurement locations.
- The comparison between static and dynamic analysis showed a maximum reduction of 85.78% for the Floating Point Operations (FLOPS) and of 36% for the CPU time with the FE analyzes under the static procedure.

This material is reserved for educational use only, not allowed for commercial use.
Forbidden to modify the content, and cite the document when use.

- Structural mass of the original bus structure was reduced by means of the Multi Objective Genetic Algorithm (MOGA) optimization provided by ANSYS. After the optimization, it was suggested that the wall thickness of members at the central tubular body could be reduced by 43.75% with a decrease in the structural stiffness by 31.36%. Consequently, overall structural mass could be reduced by 13.15% or 258.1 kg.
- Structural strength and stiffness of the optimized bus structure was ensured to withstand the certain severe driving conditions such as braking, cornering, bending, and torsion by corresponding safety factor of 6.86, 4.06, 4.16, and 3.6 respectively. In addition, bending case showed the maximum deflection of 4.42 mm occurred at the rear end of the bus chassis.

Therefore, it was clearly shown in this work that the bus structure model consisted of the spring suspensions coupled with a static analysis offered an improved accuracy of the predicted solution as well as reducing the computational time. Thus, the results of the present study could be useful practical guideline for the bus analysis. Finally, the optimized bus structure was satisfied by reducing the structural mass while maintaining the structural safety.

7.2 Suggestions for Further Research

The suggestions for further research are listed as followed:

7.2.1 Experimental Measurement

In this study, several normal driving conditions were carried out by dynamic tests. In order to ensure the strength of the bus structure in the critical condition, a rollover test is suggested because it is considered in the ECE-R66 regulation as a critically severe condition for the bus structures. In experiment, the use of a structural bay to roll would allow for deformation measurement.

7.2.2 Finite Element Analysis

The rollover test was suggested for implementing a physical experiment. However, the computational simulation could be carried out due to a local area consideration of the deformed shape. Moreover, this FEA study could be used to execute a local area optimization that can improve the bus structure especially to withstand a rollover situation.

This material is reserved for educational use only, not allowed for commercial use.
Forbidden to modify the content, and cite the document when use.

7.2.3 Structural Optimization

It is suggested that before selecting the wall thickness as a design variable for optimization, reduction of less significant members should be considered via simulation results. The reason is that eliminated members will not be taken into account in the bus structure even during the optimization. As a result, the overall mass of the optimized structure could be lower than that without removing the parts.

This material is reserved for educational use only, not allowed for commercial use.
Forbidden to modify the content, and cite the document when use.

REFERENCES

[1] Chinnaraj K., Sathya Prasad M., and C. Lakshmana R. 2008. "Experimental Analysis and Quasi-Static Numerical Idealization of Dynamic Stresses on a Heavy Truck Chassis Frame Assembly." **Applied Mechanics and Materials.** vol.13-14 : 271-280.

[2] Thacker J.G., Reagan S.W., Pellettiere J.A., Pilkey W.D., and Crandall J.R. 1998. "Experiences during development of a dynamic crash response automobile model." **Finite Elements in Analysis and Design.** vol.30 : 279-295.

[3] Richard G. Budynas, and J. Keith N. 2011. **Shigley's Mechanical Engineering Design.** 9th Edition, Published by McGraw-Hill.

[4] **ANSYS 12.0**, User Manual.

[5] Mundoa D., Hadjitb R., Dondersb S., Brughmansb M., Masb P., and Desmetc W. 2009. "Simplified modeling of joints and beam-like structures for BIW optimization in a concept phase of the vehicle design process." **Finite Elements in Analysis and Design.** vol.45 : 456-462.

[6] How Strain Gage Work, **KYOWA**, 1999

[7] Dusan M. and Momir L. 2010. "The Strength of the Bus Structure with the Determination of Critical Points." **Journal of Mechanical Engineering.** vol.56(9) : 544-550.

[8] Ilankamban R., Perumalswami P.R., and Page A.J. "Back Load Calculation-A Method of Measuring Component Loads without Load Cells." **Technical Report.** Ford Motor Company.

[9] Emmanuel F., Gerry H., and Stacy H. 2007. "Truck Instrumentation for Dynamic Load Measurement." **Technical Report.** Documentation 0-4863-1.

[10] Acceleration Transducers, **KYOWA**, 2005.

[11] Mitsutaka K. 2005. "Miniature Damped Accelerometer Series offers Wide Range of Applications." **Kyowa Electronic Instruments**, Presentation at Automotive Testing Expo 2005 Europe.

[12] Mujahid A. 2006. "On the Dynamics of Automobile Drifting." **SAE Technical Paper**, 2006-01-1019.

[13] Timothy J.G. and Zevi B. 2007. "Vibration Transmission from Road Surface Features-Vehicle Measurement and Detection." **Technical Report.**

This material is reserved for educational use only, not allowed for commercial use.

Forbidden to modify the content, and cite the document when use.

REFERENCES (CONT.)

[14] **National Instruments,** Documentation

[15] Jeremy D. and John D. 2006. "Accelerometers: One size does not fit all." **20th Annual IATAI Conference.**

[16] Nunney M.J. 2007. **Light and Heavy Vehicle Technology.** 4th Edition, Published by Elsevier Ltd.

[17] Edited by Julian H.S. 2002. **An Introduction to Modern Vehicle Design.** First Published, Reed Education and Professional Publishing Ltd.

[18] Thomas D. Larson. 2013. Pennsylvania Transportation Institute, **Bus Testing and Research Center.** STURAA TEST PTI-BT-R1213.

[19] Steven T., Ebrahim E., and Ahmad B. 2011. "Methods to Determine Torsion Stiffness in an Automotive Chassis." **Computer-Aided Design & Applications.** vol.(1) : 67-75.

[20] B.L. Boada, A. Gauchia, M.J.L. Boada, and Diaz V. 2007. "A Genetic-Based Optimization of a Bus Structure as a Design Methodology." **12th IFToMM World Congress.** Besancon.

[21] John S. and Terblanche E. 2007. "Report on Torsional Stiffness Determination on a CAV GT Chassis." **Technical Report.**

[22] Lonny L. Thompson, Jon K. L., and E. Harry L. 1998. "Design of a Twist Fixture to Measure the Torsional Stiffness of a Winston Cup Chassis." **SAE Technical Paper.** 983054.

[23] Belegundu Ashok D. and Chandrupatla Tirupathi R. 2011. **Optimization Concepts and Applications in Engineering.** ,Cambridge University Press.

[24] Kim H. S., Hwang Y. S., and Yoon H. S. 2000. "Dynamic Stress Analysis of a Bus Systems." **Proceedings of 2nd MSC Worldwide Automotive Conference.**

[25] Zhang D., Zhang T., Zhang G., and Zhao W. 2009. "Structural Reliability Analysis of Bus Body in Consideration to the Correlation of Working Conditions." **International Conference on Measuring Technology and Mechatronics Automation.** China.

[26] Jin Y.M. 2000. "Analysis and Evaluation of Minivan Body Structure." **Proceedings of 2nd MSC worldwide automotive conference.**

[27] Chandna P., Bhushan G., V.P. Singh., Kumar D., and Kumar A. "Finite Element Analysis of a Bus Body Structure using CAE Tools." **Driving Innovation With Enterprise Simulation.**

This material is reserved for educational use only, not allowed for commercial use.
Forbidden to modify the content, and cite the document when use.

REFERENCES (CONT.)

[28] Dario C., Massimiliano D.A., and Nicolo V. 2011. "Structural Analysis of an Articulated Urban Bus Chassis via FEM: a Methodology Applied to a Case Study." **Journal of Mechanical Engineering.** vol.57(11) : 799-809.

[29] Review and Revision of UN-ECE R66. 2003. **Regulation No. 66 of the Economic Commission for Europe of the United Nations.** Uniform Technical Prescriptions.

[30] Yu-Cheng Lin and Hong-Chi N. 2005. "Structural Design Optimization of the Body Section Using Finite Element Method." **SAE Technical Paper.** 2006-01-0954.

[31] Lan F., Chen J., and Lin J. 2004. "Comparative analysis for bus side structures and lightweight optimization." **Journal of Automobile Engineering.** vol.218 : 1067-1075.

[32] Zhang X. and Tao Z. 2009. "A Study Shape Optimization of Bus Body Structure Based on Stiffness Sensitivity Analysis." **IEEE Journal.** China : 1225-1229.

[33] Butdee S. and Vignat F. 2008. "TRIZ Method for Light Weight Bus Body Structure Design." **Journal of Achievements in Materials and Manufacturing Engineering.** vol.31(2) : 456-462.

[34] Kim M.H., Suh M.W., and Bae D.H. 2000. "Development of an Optimum Design Technique for the Bus Window Pillar Member." **Journal of Automobile Engineering.** vol.215 : 11-19.

[35] Zhang Y., Zhu P., and Chen G. 2007. "Lightweight Design of Automotive Front Side Rail Based on Robust Optimization." **Thin-Walled Structures.** vol.45 : 670-676.

[36] Manokruang S. and Butdee S. 2009. "Methodology of Bus-Body Structural Redesign for Lightweight Productivity Improvement." **AIJSTPME.** vol.2(2) : 79-87.

[37] Osvaldo R., Edgar I., Victor. H., Rafael. S., and Armando O. 2012. "Efficient Optimization of the Structure of a Passenger Bus by Iterative Finite Element Models with Increasing Degrees of Complexity." **3rd International Conference on Engineering Optimization.** Rio de Janeiro, Brazil.

[38] Gauchia A., Diaz V., Boada M.J.L., and Boada B.L. 2010. "Torsional Stiffness and Weight Optimization of a Real Bus Structure." **International Journal of Automotive Technology.** vol.11(1) : 41-47.

This material is reserved for educational use only, not allowed for commercial use.
Forbidden to modify the content, and cite the document when use.

REFERENCES (CONT.)

[39] Asnafi N., Langstedt G., Andersson C., Stergren N., and Hakansson T. 2000. "A New Lightweight Metal-Composite-Metal Panel for Applications in the Automotive and Other Industries." **Thin-Walled Structures.** vol.36 : 289-310.

[40] Cruz M.G.H. and Viecelli A. 2008. "A Methodology for Replacement of Conventional Steel by Microalloyed Steel in Bus Tubular Structures." **Materials and Design.** vol.29 : 539-545.

[41] Belure S.B., Kadam S.S., and Wadkar S.B. 2005. "Criticality Analysis of Passenger Bus Body Structural Design Using Finite Element Method." **National Conference on Computational Methods in Mechanical Engineering.** : 59-64.

[42] Antero K., Martti V., and Hannu H. 2000. "Use of Stainless Steels in Bus Coach Structures." **Journal of Materials Engineering and Performance.** vol.9(6) : 669-677.

[43] Haibin N., Selvum P., and Uday K.V. 2009. "Design and Development of Thermoplastic Composite Roof Door for Mass Transit Bus." **Materials and Design.** vol.30 : 983-991.

[44] **TML Strain Gauges.** Tokyo Sokki Kenkyujo Co., Ltd., TML Pam E-101S.

[45] Jacob F. and Ted B. 2007. **A First Course in Finite Elements.** John Wiley & Sons Ltd.

[46] MabWeb Online, **AISI 6150 Steel.** Mechanical Properties, www.matweb.com

[47] Gillispie T. 1992. **Fundamental of Vehicle Dynamics.** Warrendale, PA, Society of Automotive Engineers.

[48] Firestone Industrial Products Company, **Engineering Manual and Design Guide 2007.**

[49] MatWeb Online, **AISI 1020 Steel.** Mechanical Properties, www.matweb.com

[50] ISO8855. 1991. Road Vehicles-Vehicle Dynamics and Road-Holding Ability, **International Organization for Standardization.** Geneva.

[51] Riley W.B. and George A.R. 2002. "Design, Analysis and Testing of Formula SAE Race Car Chassis." **SAE Technical Paper,** 2002-01-3300.

[52] **Urban Bus Specifications-II.** Ministry of Urban Development, Government of India.

This material is reserved for educational use only, not allowed for commercial use.
Forbidden to modify the content, and cite the document when use.

APPENDIX A

LABVIEW BLOCK DIAGRAM FOR STRAIN-ACCELERATION MEASUREMENT

This material is reserved for educational use only, not allowed for commercial use.
Forbidden to modify the content, and cite the document when use.

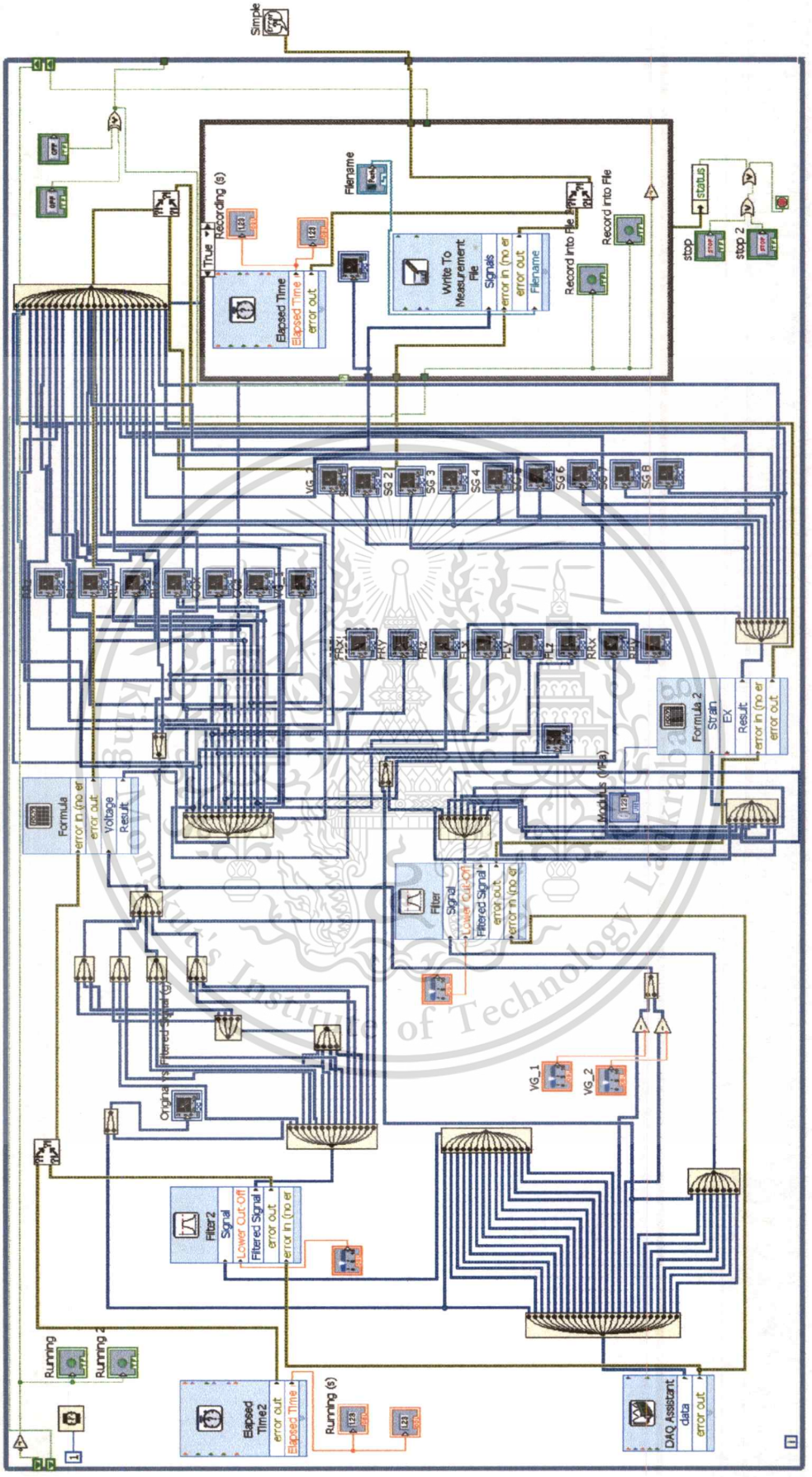

This material is reserved for educational use only, not allowed for commercial use.
Forbidden to modify the content, and cite the document when use.

APPENDIX B

STRAIN GAGE SPECIFICATIONS AND BONDING PROCEDURES

King Mongkut's Institute of Technology Ladkrabang

This material is reserved for educational use only, not allowed for commercial use.
Forbidden to modify the content, and cite the document when use.

TML STRAIN GAUGE TEST DATA

GAUGE TYPE	: UFLA-5-11-3LT	TESTED ON	: SS 400
LOT NO.	: A510611	COEFFICIENT OF THERMAL EXPANSION	: 11.8 $\times 10^{-6}$/℃
GAUGE FACTOR	: 2.12 ±1%	TEMPERATURE COEFFICIENT OF G.F.	: +0.08±0.05 %/10℃
ADHESIVE	: NP-50	DATA NO.	: U0049

THERMAL OUTPUT (εapp : APPARENT STRAIN)

$\varepsilon app = -6.29\times10^{-1}+2.93\times10^{-1}\times T^{1}-1.28\times10^{-2}\times T^{2}-2.22\times10^{-5}\times T^{3}+5.14\times10^{-7}\times T^{4}$ (μm/m)

TOLERANCE : ±0.85 [(μm/m)/℃] , T : TEMPERATURE

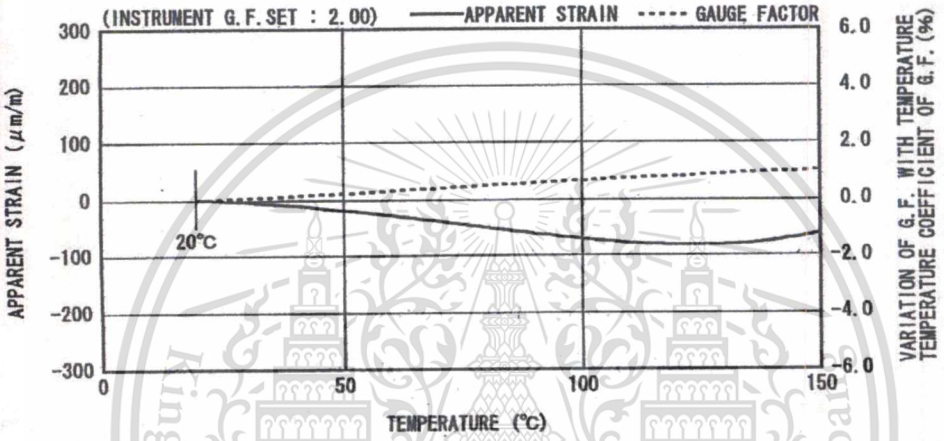

ひずみゲージ取扱いの注意事項

- ●上記の特性データは、リード線の取付けによる影響を含んでおりません。裏面記載のリード線の測定値への影響に従って補正してください。
- ●ゲージの使用温度は、接着剤の耐熱温度などにより変わります。
- ●絶縁抵抗などの点検は、印加電圧を50V以下にしてください。
- ●ゲージリード線に無理な力を加えないでください。
- ●ゲージ裏面に接着剤を塗布して接着してください。
- ●ひずみゲージの裏面は脱脂洗浄してありますので、汚さないように取扱いしてください。
- ●ゲージの包装を開封後は、乾燥した場所で保管してください。
- ●ご使用に際してご不明な点などがございましたら、当社までお問い合わせください。

CAUTIONS ON HANDLING STRAIN GAUGES

- ● The above characteristic data do not include influence due to lead wires. Correct the data in accordance with the influence of lead wires on measured values described overleaf.
- ● The service temperature of strain gauge depends on the operating temperature of adhesive, etc.
- ● Check of insulation resistance, etc. should be made at a voltage of less than 50V.
- ● Do not apply an excessive force to the gauge leads.
- ● Apply an adhesive to the back of a strain gauge and stick the gauge to a specimen.
- ● As the back of strain gauge has been degreased and washed, do not contaminate it.
- ● After unpacking, store strain gauges in a dry place.
- ● If you have any questions on strain gauges or installation, contact TML or your local agent.

Made in Japan

TML 株式會社 東京測器研究所

〒140-8560 東京都品川区南大井 6 - 8 - 2
TEL 03 - 3763 - 5611
FAX 03 - 3763 - 6128

Tokyo Sokki Kenkyujo Co., Ltd.

8 - 2, Minami - Ohi 6 - Chome
Shinagawa - ku, Tokyo 140-8560

This material is reserved for educational use only, not allowed for commercial use.
Forbidden to modify the content, and cite the document when use.

PRIMARY INSTALLATIONS

When bonding the strain gauges, the most suitable adhesive should be selected for each application. A typical installation procedure is described below using the fast-curing adhesive CN.

1. Preparation

The following items are required for bonding and lead wire connection:Strain gauges, bonding adhesive, connecting terminals, test specimen, solvent, cleaning tissue for industrial use, soldering iron, solder, abrasive paper (120 - 320 grit), marking pencil, scale, tweezers, extension lead wire, polyethylene sheet, nippers.

2. Positioning

Roughly determine the location on the test specimen where the strain gauge is to be bonded.

3. Surface preparation

Before bonding, remove all grease, rust, paint, etc., from the bonding area. Sand an area somewhat larger than the bonding area uniformly and finely with abrasive paper. Finish the surface with #120 to 180 abrasive paper for steel, or #240 to 320 for aluminium.

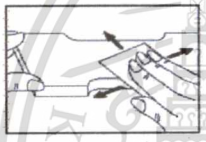

4. Fine cleaning

Clean the bonding area with industrial tissue paper or cloth soaked in a small quantity of chemical solvent such as acetone. Continue cleaning until a new tissue or cloth comes away completely free of contamination. Following the surface preparation, be sure to attach the gauge before the surface becomes covered with an oxidizing membrane or becomes newly contaminated.

5. Applying bonding adhesive

Drop the proper amount of adhesive onto the back of the gauge base. Usually one drop of adhesive will suffice, but you may increase the number of drops according to the size of the gauge. Use the adhesive nozzle to spread the adhesive over the back surface thinly and uniformly.

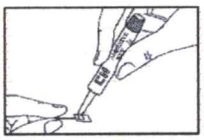

6. Curing and pressing

Place the gauge on the guide mark, place a polyethylene sheet onto it and press down on the gauge constantly using your thumb or a gauge pressing device. This should be done quickly as the curing process is completed very fast. The curing time varies depending on the gauge, test specimen, temperature, humidity and pressing force. The curing time under normal conditions is 20 - 60 seconds.

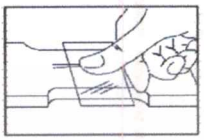

7. Raising the gauge leads

After curing completely, remove the polyethylene sheet, and raise the gauge leads with a pair of tweezers.

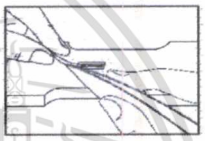

8. Bonding connecting terminals

Position the proper size connecting terminals adjacent to the bonded gauge. A distance of 3 - 5mm generally allows for easier wiring later.

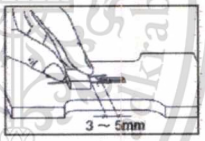

9. Soldering the gauge leads

Wrap the gauge leads around the connecting terminal wires. Solder the junction area with a little slack in the gauge leads, taking care to prevent excessive tension during measurement.

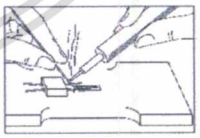

10. Soldering extension lead wires

Solder an extension lead wire to the terminal wires on the opposite side of the connecting terminals. Clip off any excess extension lead wire with a pair of pliers or wire cutters.

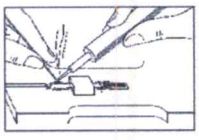

This material is reserved for educational use only, not allowed for commercial use.
Forbidden to modify the content, and cite the document when use.

APPENDIX C

ACCELERATION SPECIFICATIONS

This material is reserved for educational use only, not allowed for commercial use.
Forbidden to modify the content, and cite the document when use.

ANALOG DEVICES

Small, Low Power, 3-Axis ±3 *g* Accelerometer

ADXL335

SPECIFICATIONS

T_A = 25°C, V_S = 3 V, C_X = C_Y = C_Z = 0.1 µF, acceleration = 0 *g*, unless otherwise noted. All minimum and maximum specifications are guaranteed. Typical specifications are not guaranteed.

Table 1.

Parameter	Conditions	Min	Typ	Max	Unit
SENSOR INPUT	Each axis				
Measurement Range		±3	±3.6		*g*
Nonlinearity	% of full scale		±0.3		%
Package Alignment Error			±1		Degrees
Interaxis Alignment Error			±0.1		Degrees
Cross-Axis Sensitivity[1]			±1		%
SENSITIVITY (RATIOMETRIC)[2]	Each axis				
Sensitivity at X_{OUT}, Y_{OUT}, Z_{OUT}	V_S = 3 V	270	300	330	mV/*g*
Sensitivity Change Due to Temperature	V_S = 3 V		±0.01		%/°C
ZERO *g* BIAS LEVEL (RATIOMETRIC)					
0 *g* Voltage at X_{OUT}, Y_{OUT}	V_S = 3 V	1.35	1.5	1.65	V
0 *g* Voltage at Z_{OUT}	V_S = 3 V	1.2	1.5	1.8	V
0 *g* Offset vs. Temperature			±1		mg/°C
NOISE PERFORMANCE					
Noise Density X_{OUT}, Y_{OUT}			150		µg/√Hz rms
Noise Density Z_{OUT}			300		µg/√Hz rms
FREQUENCY RESPONSE[4]					
Bandwidth X_{OUT}, Y_{OUT}[5]	No external filter		1600		Hz
Bandwidth Z_{OUT}[5]	No external filter		550		Hz
R_{FILT} Tolerance			32 ± 15%		kΩ
Sensor Resonant Frequency			5.5		kHz
SELF-TEST[6]					
Logic Input Low			+0.6		V
Logic Input High			+2.4		V
ST Actuation Current			+60		µA
Output Change at X_{OUT}	Self-Test 0 to Self-Test 1	−150	−325	−600	mV
Output Change at Y_{OUT}	Self-Test 0 to Self-Test 1	+150	+325	+600	mV
Output Change at Z_{OUT}	Self-Test 0 to Self-Test 1	+150	+550	+1000	mV
OUTPUT AMPLIFIER					
Output Swing Low	No load		0.1		V
Output Swing High	No load		2.8		V
POWER SUPPLY					
Operating Voltage Range		1.8		3.6	V
Supply Current	V_S = 3 V		350		µA
Turn-On Time[7]	No external filter		1		ms
TEMPERATURE					
Operating Temperature Range		−40		+85	°C

This material is reserved for educational use only, not allowed for commercial use.
Forbidden to modify the content, and cite the document when use.

APPENDIX D

DATA ACQUISITION SPECIFICATIONS

- **CHASSIS MODULE - cDAQ 9172**
- **STRAIN GAGE MODULE - NI 9235**
- **ACCELEROMETER MODULE - NI 9205**

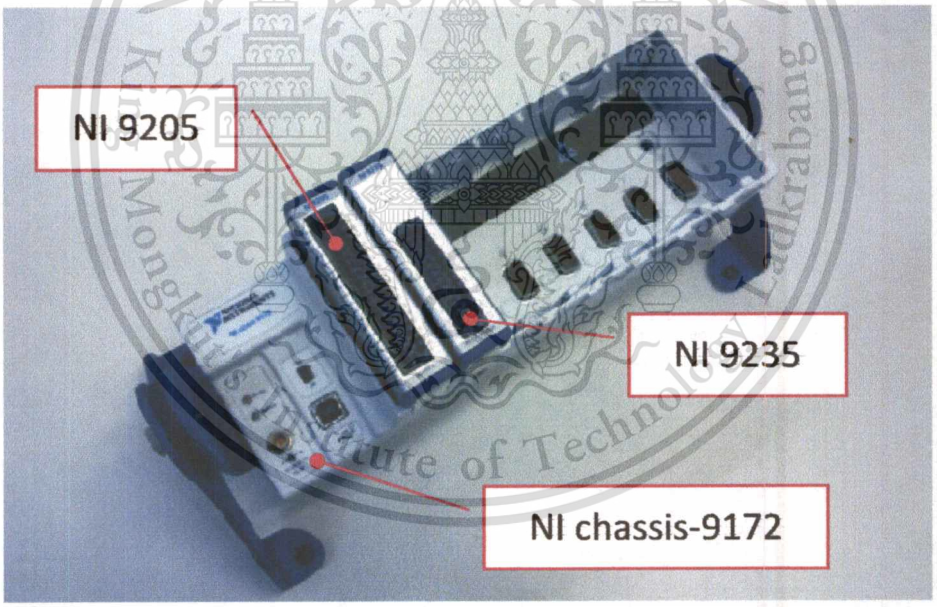

This material is reserved for educational use only, not allowed for commercial use.
Forbidden to modify the content, and cite the document when use.

NI cDAQ-9172

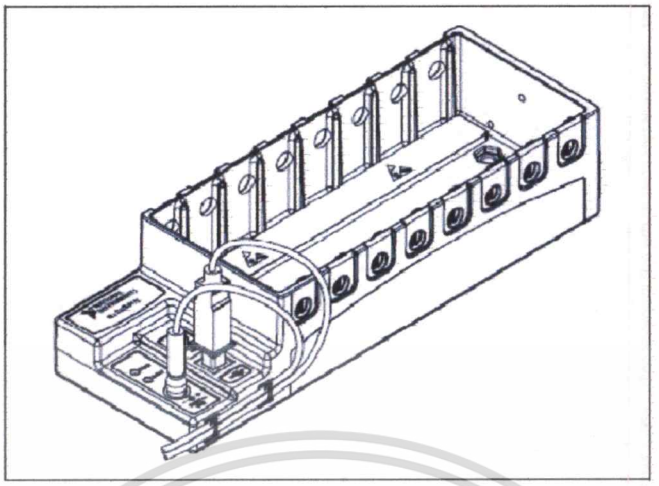

Analog Input

Input FIFO size	2,047 samples
Sample rate[1]	
Maximum	3.2 MS/s (multi-channel, aggregate)
Minimum	0 S/s
Timing accuracy[2]	50 ppm of sample rate
Timing resolution[2]	50 ns
Number of channels supported	Determined by the C Series I/O modules

Analog Output

Numbers of channels supported	
In hardware-timed task	16
In non-hardware-timed task	Determined by the C Series I/O modules
Maximum update rate	1.6 MS/s (multi-channel, aggregate)
Timing accuracy	50 ppm of sample rate
Timing resolution	50 ns
Output FIFO size	8,191 samples shared among channels used

Bus Interface

USB specification	USB 2.0 Hi-Speed
Power from USB	
4.10 to 5.25 V	500 µA maximum

This material is reserved for educational use only, not allowed for commercial use.
Forbidden to modify the content, and cite the document when use.

NI 9235

8-Channel, 24-Bit Quarter-Bridge Analog Input Module

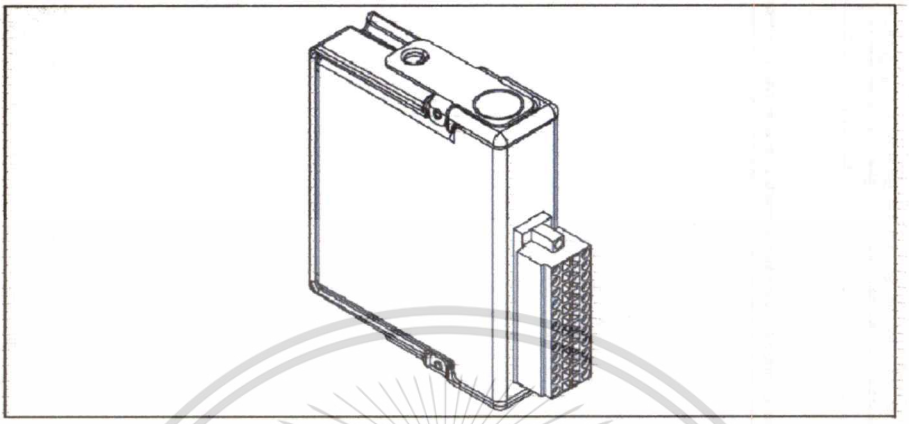

Input Characteristics

Number of channels ..... 8 analog input channels

Quarter-bridge completion

- NI 9235 ..... 120 Ω, 10 ppm/°C max
- NI 9236 ..... 350 Ω, 10 ppm/°C max

ADC resolution ..... 24 bits

Type of ADC ..... Delta-Sigma (with analog prefiltering)

Sampling mode ..... Simultaneous

Internal master timebase (f_M)

- Frequency ..... 12.8 MHz
- Accuracy ..... ±100 ppm max

Data rate range (f_s) using internal master timebase

- Minimum ..... 794 S/s
- Maximum ..... 10 kS/s

Data rate range (f_s) using external master timebase

- Minimum ..... 195.3125 S/s
- Maximum ..... 10.547 kS/s

Data rates[1] (f_s) ..... $\frac{f_M \div 256}{n}$, $n = \{2; 4, 5, ..., 63\}$

Full-scale range ..... ±29.4 mV/V (+62,500 με/–55,500 με)

This material is reserved for educational use only, not allowed for commercial use.
Forbidden to modify the content, and cite the document when use.

NI 9205

32-Channel, ±200 mV to ±10 V, 16-Bit Analog Input Module

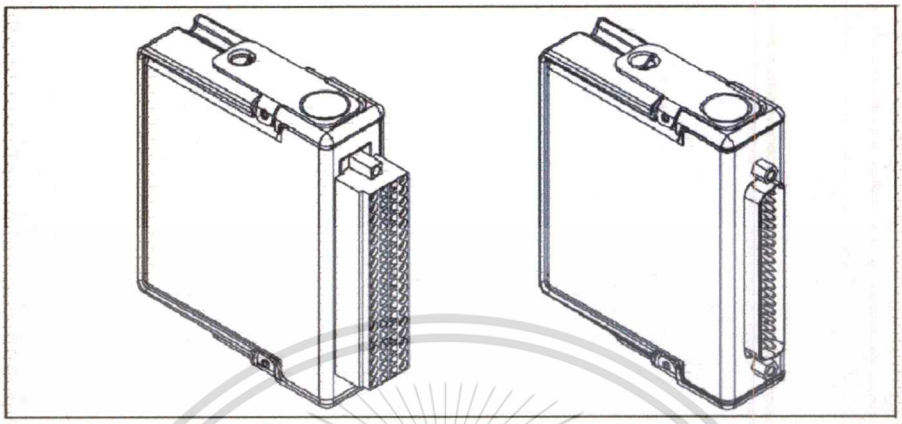

Analog Input Characteristics

Number of channels ..... 32 single-ended or 16 differential analog input channels, 1 digital input channel, and 1 digital output channel

ADC resolution ..... 16 bits

DNL ..... No missing codes guaranteed

INL ..... Refer to the *AI Absolute Accuracy Tables and Formulas*

MTBF ..... 775,832 hours at 25 °C; Bellcore Issue 6, Method 1, Case 3, Limited Part Stress Method

Conversion time

R Series Expansion chassis ..... 4.50 µs (222 kS/s)

All other chassis ..... 4.00 µs (250 kS/s)

Input coupling ..... DC

Nominal input ranges ..... ±10 V, ±5 V, ±1 V, ±0.2 V

Minimum overrange (for 10 V range) 4%

Maximum working voltage for analog inputs (signal + common mode) ..... Each channel must remain within ±10.4 V of common

This material is reserved for educational use only, not allowed for commercial use.
Forbidden to modify the content, and cite the document when use.

APPENDIX E

PROCEEDINGS

- **Appendix E-1:** Comparative Analysis of an Electric Bus Body Structure for Lightweight Design

- **Appendix E-2:** A Numerical and Experimental Measurement in a Dynamic Strain Response of an Electric Bus Body Structure

- **Appendix E-3:** Finite Element Analysis of an Electric Bus Body Structure in Real Driving Conditions

King Mongkut's Institute of Technology Ladkrabang

This material is reserved for educational use only, not allowed for commercial use.
Forbidden to modify the content, and cite the document when use.

Appendix E-1: Comparative Analysis of an Electric Bus Body Structure for Lightweight Design

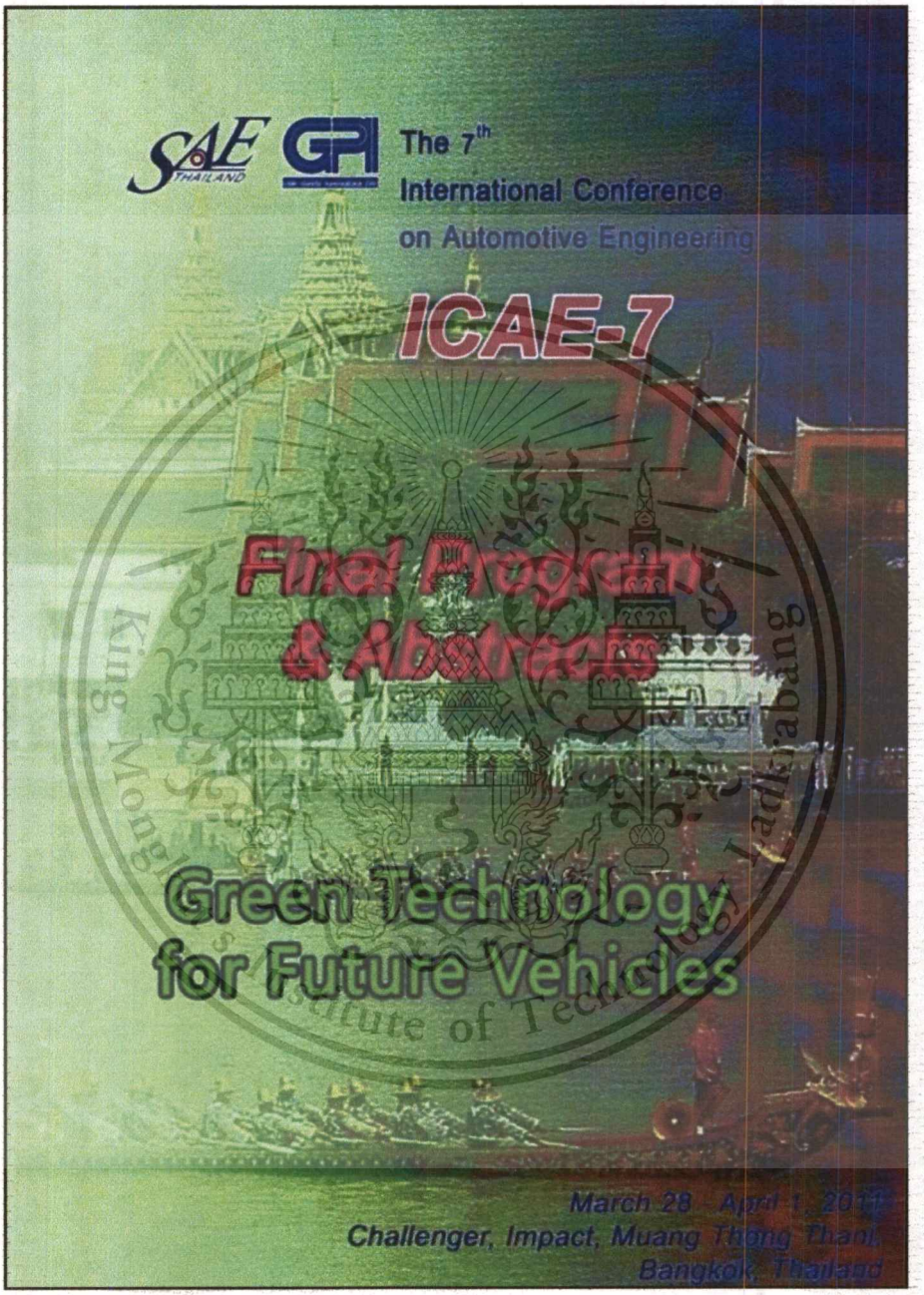

This material is reserved for educational use only, not allowed for commercial use.
Forbidden to modify the content, and cite the document when use.

The 7th International Conference on Automotive Engineering (ICAE-7)
March 28 – April 1, 2011, Challenger, Impact, Muang Thong Thani, Bangkok, Thailand

Comparative Analysis of an Electric Bus Body Structure for Lightweight Design

Dittapoom Shinabuth
TAIST-Tokyo Tech, Automotive Engineering

Chi-na Benyajati, Anek Phuchamnong
Automotive Laboratory, National Metal and Materials Technology Center

Monsak Pimsarn
Department of Mechanical Engineering, King Mongkut's Institute of Technology Ladkrabang

Masaaki Okuma
Department of Mechanical and Aerospace Engineering, Tokyo Institute of Technology

ABSTRACT

In this work, strength of an electric bus body structure was analyzed by using finite element analysis (FEA) in order to study an appropriate approach for a lightweight design of a medium-sized bus. Before a lightweight redesign could be carried out, both computational and experiment were needed for validation of model. In an experimental part, an existing EV bus prototype model was tested to collect a strain response of chassis structure from the actual driving conditions by using strain gauges at 4 different locations. Furthermore, geometric locations which exhibited a relatively higher risk of failure were identified via analysis, leading to a possible improvement on electric bus body design focusing on lightweight aspect.

INTRODUCTION

Nowadays, using a bus as means of transportation is still a popular trend in Thailand especially in a city and also tourist industries. In fact, 80% of buses are locally manufactured based on the skill and experience of local mechanics while another 20% are imported from other countries. In general, most of buses are operated with a combustion engine while only few are operated by electricity from batteries system. In the order to tackle energy crisis and environmental problems, an interest in electric vehicles (EV) has rapidly increased in the last few years within the research centers and among car manufacturers. Additionally, many buses which are now operating on the road might not have been fully inspected. As the result, these could be accompanied by various problems such as damage, unbalance weight of structure which could affect to tire wear and, high fuel consumption due to excessive structural weight.

METHODOLOGY

POSITIONING OF STRAIN GUAGES

Normal strain in any given direction on the surface of a material can be determined by measuring the length along a direction of interest. The normal strain is equal to a change in a length of longitudinal direction of a body divided by the original length. However, for more accurate results throughout static loading, an electrical resistance "Strain Gauge" should be used to measure surface strain. Strain gauge can be installed in many different ways depending on the purpose of measurement as shown in Figure 1.

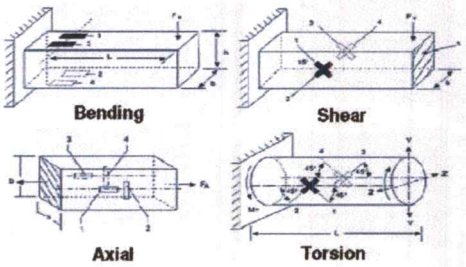

Figure 1. Typical Strain Gauge Installation for various loading applications

This material is reserved for educational use only, not allowed for commercial use.
Forbidden to modify the content, and cite the document when use.

The 7th International Conference on Automotive Engineering (ICAE-7)
March 28 – April 1, 2011, Challenger, Impact, Muang Thong Thani, Bangkok, Thailand

EXPERIMENTAL SETUP

Typical load situations encountered by buses while running on smooth-road and rough-road or heavy operating conditions can be categorized into bending, torsion, braking, cornering and acceleration [1,2]. Among these loading conditions, bending and torsion are static in nature, while other conditions such as braking and cornering need to be considered as dynamic determination.

Figure 2. (a) Electric Bus Prototype by MTEC (NSTDA)
(b) Bus General Dimensions

In present work, experimental strain measurements during bumping test was carried out to study a structure behavior of an EV bus prototype displayed in Figure 2. Generally, failure of a bus structure will occur on the chassis around areas of welding joint between chassis and body structure, which results in high stress concentration [3]. For strain measurements, strain gauges were attached onto a chassis structure at four different locations as shown in Figure 3. A half bridge of strain gauge configuration was used to balance the Wheatstone circuit properly collecting the bending strain at all measurement locations [4].

Furthermore, since magnitude of measured strain could be very small, in order of micro-strain, a signal conditioner (Figure 4) was also used to amplify the measured strain signal during data acquisition process.

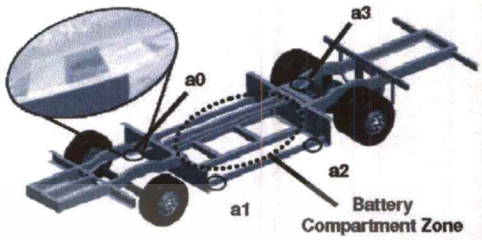

Figure 3. Experimental Strain Gauge Measurement Locations

Figure 4. Data Acquisition (DAQ) tool NI USB-9219

FINITE ELEMENT MODELING

The numerical simulation based on a finite element (FE) method was performed to study physical behavior of EV bus structure. A FE model was generated as shown in Figure 5a. All members of the body structure and chassis were comprised of 20,145 beam and 42,635 shell elements respectively, and operating within a global element size of 7 mm.

A shell element was chosen for the chassis structure because the component thickness was very small compared to other geometries. Additionally, shell element was performed using plane stress system. On the other hand, a beam element was selected for the body structure since a length of a beam was large compared to its cross-sectional dimensions.

For suspension systems, linear springs were used to represent a stiffness provided by an air bag suspension and a leaf spring. The configuration of linear spring in the analysis is shown in Figure 5b.

In order to create connection between beam and shell elements, Multi-Point Connections

This material is reserved for educational use only, not allowed for commercial use.
Forbidden to modify the content, and cite the document when use.

The 7th International Conference on Automotive Engineering (ICAE-7)
March 28 – April 1, 2011, Challenger, Impact, Muang Thong Thani, Bangkok, Thailand

(MPC) was employed to create special elements to bond those surfaces and points of a beam together. Additionally, in order to simplify all suspension of EV components and to reduce a computational time, front and rear axles were assigned as rigid elements to represent the actual parts of an EV bus [1,5].

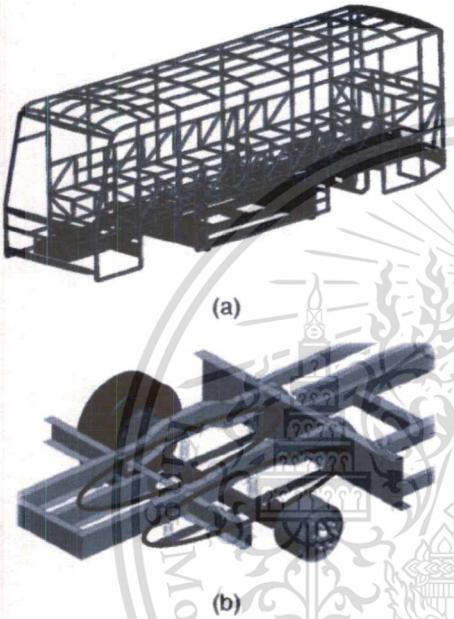

Figure 5. Finite element model of EV bus structure (a) FE model of body and chassis (b) Front suspension with linear spring set up

BOUNDARY CONDITIONS FOR SIMULATION

In order to evaluate the bending strain of the chassis structure, specified structural boundary conditions were as follow:

- Material properties of all components were common steel with mechanical properties from testing as 195 GPa for Young's modulus, 245 MPa for Tensile Yield Strength and 0.29 for Poisson's Ratio.
- For loading, a battery loading of 2,000 kg was directly assigned to a central chassis structure around the battery compartment zone (Figure 3). An external loading by moving mass of 1,300 kg, consisted of bus floor, seats, and other electronic components, was assigned as a remote lump mass located at a position of the Center of Gravity (CG).
- For bumping drive conditions, a displacement was applied separately to a front and a rear suspension at both ends of each axle. Front axle was raised up first along vertical direction by 70 mm, and then the same amount was applied separately afterwards on rear axle.
- For realistic suspension parts, longitudinal stiffness of 800 kN/m and 200 kN/m was used for each air bag suspension and leaf spring respectively [6]. In addition, during simulating a FE model all translation and rotation movements of front and rear axles were fixed because the end points of each axle were supported by the wheels.

RESULTS AND DISSCUSSIONS

SIMULATION

For analytical results of static analysis shown in Figure 6, principal strains occurred at the strain gauge attachment locations (Figure 3) were calculated based on the linear elastic computation.

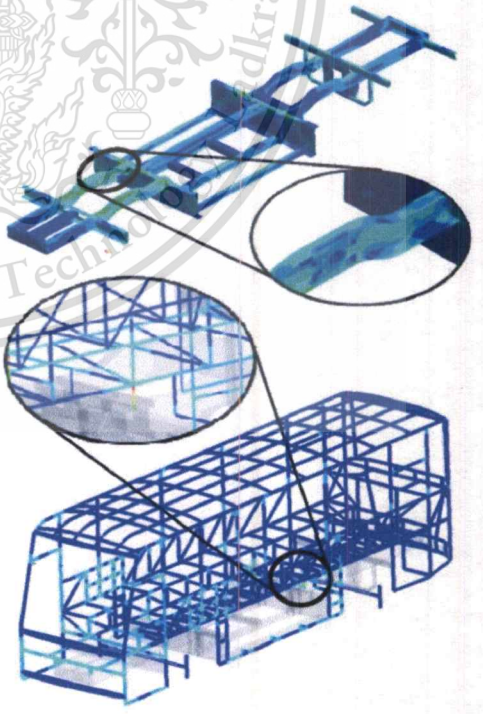

Figure 6. Analytical solutions of principal strain for EV bus Structure on bumping test

This material is reserved for educational use only, not allowed for commercial use.
Forbidden to modify the content, and cite the document when use.

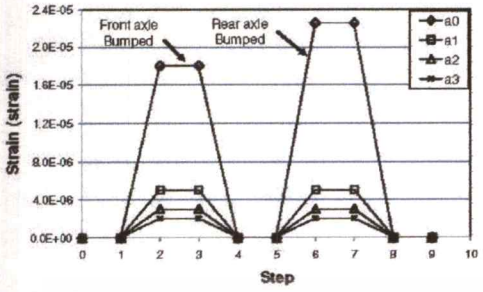

Figure 7. Results of calculated principal strain on the chassis at different locations

Comparison of principal strains obtained from analysis at different measurement locations is shown in Figure 7. During the bumping tests, the strain response at location "a0" was determined to be significantly higher compared to other locations. This could indicate that this particular area was relatively more vulnerable than others. This could be because the chassis components around location "a0" have no other supporting features apart from a body structure. Therefore, the design of the location "a0" should be studied further to obtain better load distribution on the chassis.

EXPERIMENT

In the experiment, the Hook's Law of linear material was employed to convert the strain value to stress under the linear elastic assumption. The result of strain measurements in various locations during the bumping test run is displayed in Figure 8. After conversion, the maximum stress was calculated to be 11 MPa.

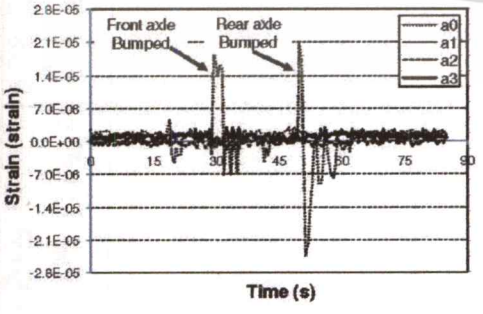

Figure 8. Results of Strain Measurement on Electric Bus Structure during a Test Run

The measurement results showed a similar trend to those of analytical solutions, with location "a0" exhibited two distinct strain responses compared to other locations. These peaks were corresponding to when the bus was running over a road bump at the front and rear axle respectively during test run. Furthermore, right after running over a road bump, negative strain responses were observed for both front and rear axles. By strain gauge set up, positive values indicated that the chassis was bending in a concave fashion whereas the opposite applied for the negative values. This could mean that after the rear axle went pass a road bump, the rear suspension allowed the rear part of the chassis to move down. As a result, the chassis would deform into a convex shape and hence the observed negative values.

RESULTS COMPARISON

The comparison of strain results between experiment and analysis at each strain gauge locations can be found in Figure 9 – 12.

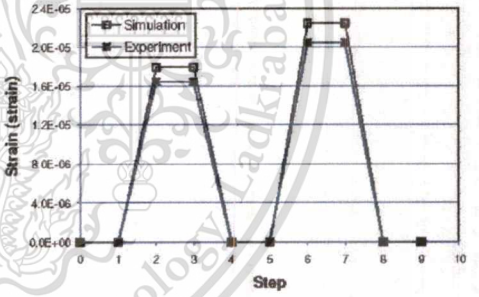

Figure 9. Resulting strain comparison between measurement and analysis at position "a0"

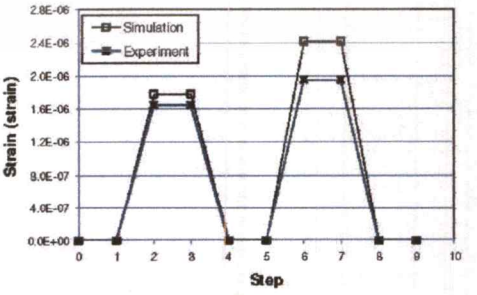

Figure 10. Resulting strain comparison between measurement and analysis at position "a1"

This material is reserved for educational use only, not allowed for commercial use.
Forbidden to modify the content, and cite the document when use.

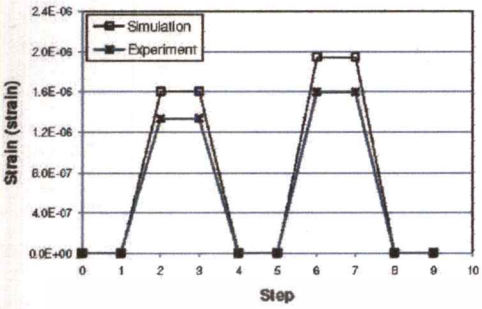

Figure 11. Resulting strain comparison between measurement and analysis at position "a2"

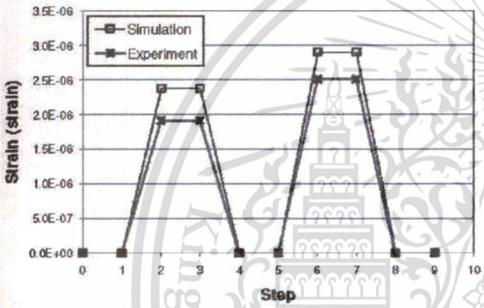

Figure 12. Resulting strain comparison between measurement and analysis at position "a3"

As can be seen from Figure 9-12, despite similarity in the strain response trend, all of simulation results were higher than those measured from experiments. The difference between two set of results were found to be approximately 5% and 18% for front axle and rear axle respectively. Such deviation could be reduced by performing a dynamic analysis including a damping parameter [7]. However, the resulting stresses calculated from strain values were much lower than the yield strength of the chassis material. This might suggested that further tests under more severe driving conditions should be carried out to study the structural behavior of the bus in more details.

CONCLUSION

The present work involved measurements and simulations to study the structural behavior of the chassis specifically designed for the medium-sized of an electric bus application. The weight of battery packs, located at the centre compartment of chassis, was taken into account for the simulation work. Strain gauges and commercial finite element software were employed on actual driving conditions for computational model validation. Following conclusions can be made:

- The deviations between both experimental and analytical results were small offset due to strain gauge attachments capability and boundary conditions applied to analytical model. Therefore, dynamic analysis should be carried out for an improved accuracy.
- On an EV bus structural design, location with high risk of failure could be indicated to be an area between frontal of chassis structure, close to location "a0", and the middle of chassis structure. However, the maximum stress reported from bumping test was diminutive and under the yield strength.

ACKNOWLEDGMENTS

The author would like to thank Automotive Laboratory, National Metal and Materials Technology Center (MTEC), Thailand for their support to this work.

REFERENCES

[1] **K. Chinnaraj, M. Sathya Prasad** and **C. Lakshmana Rao** "*Experimental Analysis and Quasi-static Numerical Idealization of Dynamic stresses on a Heavy Truck Chassis Frame Assembly*", IIT Madras, Chennai, India, Applied Mechanics and Materials Vols. 13-14(2008) Trans Tech Publications Switzerland

[2] **E. Fernando, G. Harrison, S. Hilbrich** *"Truck In-strumentation for Dynamic Load Measurement"* Texas Department of Transportation Research and Technology, Austin Texas (2007)

[3] **F Lan1, J Chen1** and **J Lin2** "*Comparative Analysis for Bus side Structures and Lightweight Optimization*", School of Automotive Engineering, Jilin University, China and Mechanical and Manufacturing Engineering, University of Birmingham UK, IMechE 2004

[4] **T. Pinkaew P. Asnachinda** "*Experimental study on the identification of dynamic axle*

This material is reserved for educational use only, not allowed for commercial use.
Forbidden to modify the content, and cite the document when use.

loads of moving vehicles from the bending moments of bridges" Department of Civil Engineering, Chulalongkorn University, Thailand. Engineering Structure, Science Direct. 29 (2007) 2282-2293

[5] **Nawar A, S. Abdullah A.K. Ariffin** *"Comparison between Experimental Road Data and Finite Element Analysis Data for the Automotive Lower Suspension Arm"* European Journal of Scientific Research Vol. 20 PP. 558-571

[6] **W. Harwood, J.TorbicReview, R.Richard** *"Review of Truck Characteristics as Factors of Roadway Design"* NCHRP (report 505) p.56, Washington D.C (2003)

[7] **Gyu Ha Kim, Kyu Zong Cho, In Bum Chyum, Gi Seob Choi** *"Dynamic Stress Analysis of Vehicle Frame using Nonlinear Finite Element Method"*, Department of Mechanical Engineering, Chonuam National University, vol. 17 (2003) KSME Korea

CONTACT

TAIST-Tokyo Tech, Automotive Engineering, King Mongkut's Institute of Technology Ladkrabang (KMITL), Thailand.
E-mail: dit_4@windowslive.com (D. Shinabuth)

This material is reserved for educational use only, not allowed for commercial use.
Forbidden to modify the content, and cite the document when use.

Appendix E-2: A Numerical and Experimental Measurement in a Dynamic Strain Response of an Electric Bus Body Structure

This material is reserved for educational use only, not allowed for commercial use.
Forbidden to modify the content, and cite the document when use.

CST10
The Second TSME International Conference on Mechanical Engineering
October 19-21, 2011, Krabi, Thailand

A Numerical and Experimental Measurement in a Dynamic Strain Response of an Electric Bus Body Structure

Dittapoom Shinabuth[1,*], Chi-na Benyajati[2], Anek Phuchamnong[2], Monsak Pimsarn[3] and Masaaki Okuma[4]

[1]TAIST-Tokyo Tech, Automotive Engineering, Bangkok, Thailand 12120

[2]Automotive Laboratory, National Metal and Materials Technology Center, National Science and Technology Development Agency, Bangkok, Thailand 12120

[3]Department of Mechanical Engineering, Faculty of Engineering, King Mongkut's Institute of Technology Ladkrabang, Bangkok, Thailand 10520

[4]Department of Mechanical and Aerospace Engineering, Graduate School of Science and Engineering, Tokyo Institute of Technology, Tokyo, Japan 152-8550

*Corresponding Author: E-mail dit_4@windowslive.com

Abstract

In this paper, a structural analysis of a medium-sized electric (EV) bus is proposed. Due to an increasing demand of bus transport in Thailand, a numerical technique called Computer-Aided Engineering (CAE) has now become a necessary tool in a bus analysis for verifying the strength of a structure and predicting any potential problems. Generally, computational modeling of a bus is often investigated via the use of finite element analysis in comparison with strain responses that are experimentally measured by strain gauges at various locations during a test run. In this study, a numerical analysis was carried out on both chassis and body structure of an 8m-bus prototype which was purely powered by electricity. A computational model of the bus structure was consisted of shell and beam elements for chassis and body structure respectively. Linear springs were applied on the chassis model to represent actual suspension components such as leaf spring and air bellows in order to give the computational model a dynamic response in various driving conditions. A bumping test where the bus was driving pass a single speed bump with a front axle followed by a rear axle was considered in this study. A maximum stress of 10.97 MPa and a maximum deviation of 17.35% compared to experimental results were calculated to occur at a front section of the chassis where front chassis side-rail members and battery compartment were connected. Furthermore, the results from this study could be used as a guideline to an EV bus design in Thailand by giving approximated solutions to examine strength of the bus body structure.

Keywords: Electric bus, Computer-Aided Engineering, Linear spring, Dynamic response, Speed bump

This material is reserved for educational use only, not allowed for commercial use.
Forbidden to modify the content, and cite the document when use.

TSME - ICOME

CST10
The Second TSME International Conference on Mechanical Engineering
October 19-21, 2011, Krabi, Thailand

1. Introduction

Nowadays, bus is still a popular road transportation mode in Thailand in both short and long-range applications such as in cities, or tourism and inter-state routes. Most buses are constructed by local mechanics while only few are imported from other countries. In a fabrication of local buses, a main concern is usually given to an overall stiffness of a bus with little focus on resulting structural weight. This could have detrimental effect on various issues such as structural durability, unbalance of a vehicle weight, fuel consumption, and driving performance. In recent times, Computer-Aided Engineering (CAE) has been increasingly accepted among major local bus manufacturers as an important tool to achieve an effective design within existing governing standards as well as production cost and time reduction.

There have been many studies in the literature focusing on a bus design and analysis using CAE. F Lan and J Chen [1] demonstrated a structural analysis of a bus frame side with/without supporting member before a structural optimization was performed. Cross sectional shape and component thickness were the design variables of interest. Manokruang S. and Butdee S. [2] proposed a bus body design using a wireframe modeling on Computer-Aided Design (CAD). It was found that wireframe of a bus structure modeling was suitable for a beam or frame analysis in CAD/CAE systems. K. Chinnaraj and M. Sathya Prasad [3] studied a dynamic strain response of a truck chassis under braking and cornering maneuver conditions. They reported that deviation of the results was possibly due to the unknown residual stress, which was contained during fabrication process. Moreover, the study concluded that the residual effect would not have affected strength of the frame rail but it would accelerate a fatigue failure.

From literature reviews, majority of work has been done on a vehicle operated with a combustion engine. However, in electric bus applications, a presence of battery packs results in an additional concentrated weight on the chassis such that it could directly affect the structural stiffness specifically during a drive. Therefore, the purpose of this study is to investigate strength of an electric bus body structure using a dynamic capability of a finite element analysis and experimental strain measurement of a strain gauge attachment.

2. Methodology

In order to investigate a bus body structure, a finite element analysis and an experimental strain measurement from a field test were carried out. An electric bus investigated in this study was an 8m 6-wheels bus prototype as displayed in Figure 1.

(a)

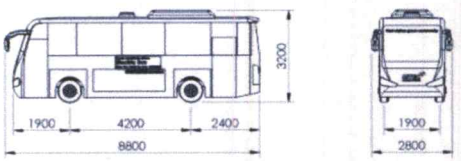

(b)

Fig. 1 (a) Electric bus prototype
(b) Bus general dimensions (in mm.)

This material is reserved for educational use only, not allowed for commercial use.
Forbidden to modify the content, and cite the document when use.

TSME - ICOME

CST10
The Second TSME International Conference on Mechanical Engineering
October 19-21, 2011, Krabi, Thailand

Strain responses of a bus structure usually come from contacts between wheels and the road before being transmitted to a chassis via suspension system. These responses vary continuously with time indicating a dynamic application. However, most studies from the literature have carried out a computational analysis in a static fashion i.e. without taking the effect of suspension system into account. Therefore, the aim of the current study was to perform a dynamic analysis on the electric bus prototype.

2.1 Computational modeling and analysis

In general, an overall bus body structure is integration between a primary chassis structure which is a frame configuration consisted of formed sheet metals, and a body structure which is a network of tubular members forming a bus body. An analysis of an electric bus might not be similar to that of a conventional bus because the main loading comes from a battery weight.

In order to simplify an analytical model of the bus structure, a simple line and surface bodies were used to represent the bus geometry. Apart from a physical geometry of the bus, a suspension system was also considered. Suspension of a bus typically contains leaf springs and dampers. Furthermore, an additional air bellows could be installed to improve a passenger comfort further. In a finite element modeling, a suspension system for each wheel containing leaf springs, dampers, and air bellows could be represented by linear springs and a damper model as presented in Figure 2 [4]. In this study, a stiffness of front and rear portion of leaf spring, a tire, and air bellows was 170 kN/m (K_{s1}) and 85 kN/m (K_{s2}), 900 kN/m (K_t), and 800 kN/m (K_{air}) respectively.

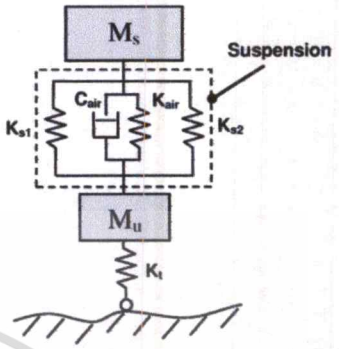

Fig. 2 Schematic of a suspension modeling

In addition, the air bellows was also assigned with a damping of 150 kN-s/m [5,6]. Furthermore, an unsprung mass (M_u) consisted of mass underneath a suspension system such as axle and wheel. On the other hand, a sprung mass (M_s) was comprised of the components supported by suspension system. Details of these external loading are listed in Table 1 [7].

Table. 1 External loadings for bus structural analysis

Battery	2000	kg
*Unsprung mass, M_u	400	kg
Electric motor	190	kg
Air conditioning	200	kg
Passengers and accessories	2300	kg
Electrical control system	300	kg
Total	5390	kg

* A quarter car modeling

In a finite element model of the bus structure, chassis and bus body was represented by shell and beam elements respectively. The completed model shown in Figure 3 was comprised of 56,746 shell elements and 35,887 beam elements with additional element mid-side nodes. Multi-Point

This material is reserved for educational use only, not allowed for commercial use.
Forbidden to modify the content, and cite the document when use.

Constraints (MPC) [8,9] was employed to connect a shell and beam elements. Material properties of conventional steel were applied with Young's modulus, yield strength, and Poisson's ratio of 195 GPa, 245 MPa, and 0.29 respectively.

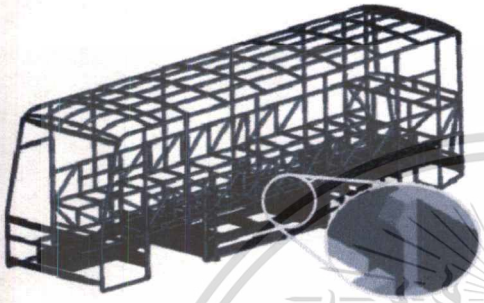

Fig. 3 Finite element model of electric bus

For an applied load, bumping situation displayed in Figure 4 was inspected in this study. A bus structure received a vertical loading effect when a vehicle travelled over a small bump. Hence, a boundary condition of a vertical displacement loading equal a height of speed bump in an actual test was sequentially applied to raise the front axle and rear axle.

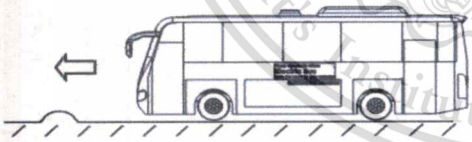

Fig. 4 Bumping situation test

2.2. Experimental strain measurement

In experiment, uniaxial strain gauges were employed to detect a minute of surface deformation of the bus structure during a test run as demonstrated in Figure 5. Eight strain gauges were attached at various locations on both chassis and body structure. Strain gauge attachment locations on the bus structure are shown in Figure 6. During the test, the bus was driven to a speed bump and then slowly climbed over it at a constant speed.

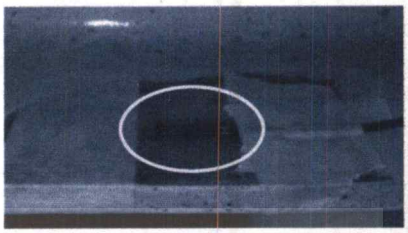

Fig. 5 Example of a uniaxial strain gauge attachment on the bus chassis

The tested speed bump had 70 mm height and 1100 mm length. The generated strains on the bus structure were recorded since front wheels came into contact until rear wheels subsequently preceded with a bump.

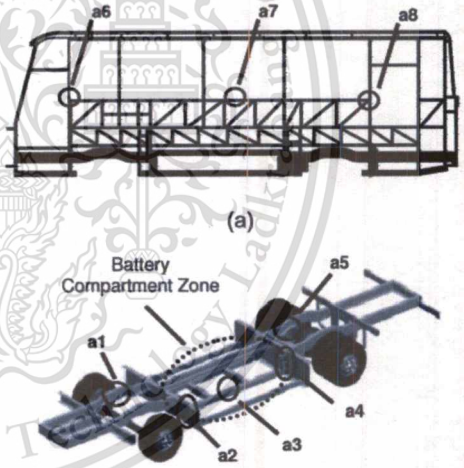

Fig. 6 Strain gauge attachment locations
(a) Right side of body frame (b) Chassis

3. Results and Discussion

3.1 Numerical simulation

Results of a bumping simulation were presented by contour of a strain distribution as shown in Figure 7. Calculated strain seemed to locally concentrate on sensitive areas especially at a front section of the bus chassis where there

This material is reserved for educational use only, not allowed for commercial use.
Forbidden to modify the content, and cite the document when use.

was no supporting feature apart from the welding lines between front chassis side rails and battery compartment plate.

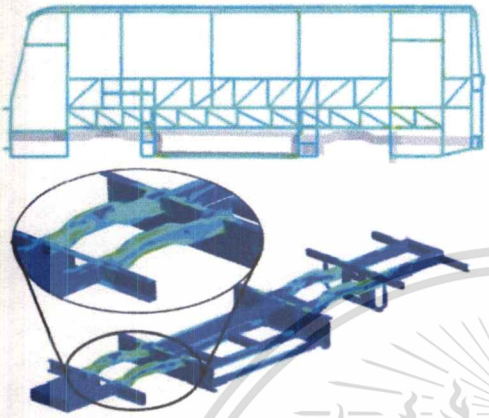

Fig. 7 Strain distribution on a bumping simulation

Furthermore, the calculated strain was monitored locally from 8 defined locations at approximately the same place as those displayed in Figure 6. A maximum strain of 6.23e-5 in compression was found at location "a1". Thus, it could be concluded from the bumping simulation that the area on the chassis subjected to risk of failure were around the connecting positions between chassis side rails and battery compartment by the welding process. Another area was on the chassis side rails where they were connected to a suspension system. Moreover, on the body structure, a relatively high strain was observed on the members close to the rear door.

3.2 Experimental measurement

A dynamic strain history of the bus was measured during an actual driving. An example of strain history at location "a1" is shown in Figure 8. It can be seen that the measured data had to be filtered first to allow an effective investigation of a specified area.

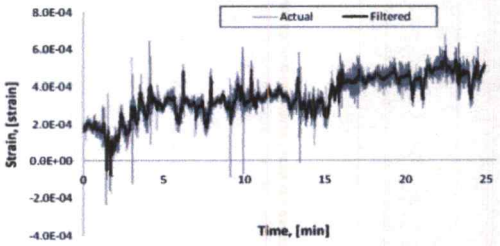

Fig. 8 Dynamic strain history on a normal test

The filtered strain history was then considered only during a period of bumping movement with the aim of a comparison both experimental and numerical data.

3.3 Simulation vs. Measurement

Figure 9 presents an investigation of dynamic strain at location "a1" under a bumping test. It can be seen that a numerical simulation displayed a similar trend to that of the experiment. At both sets of result, the highest strain magnitude at this location occurred when the front wheels were at the highest position of the speed bump i.e. "front-bumped". The maximum values were 5.63e-5 and 6.23e-5 for measured and analyzed strain respectively.

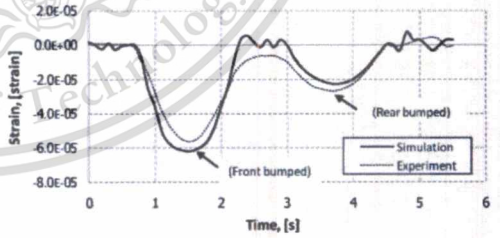

Fig. 9 Dynamic strain comparison at location "a1" during a bumping maneuver

Furthermore, a relatively much smaller strain peak response was observed at location "a1" in both measured and analyzed strain variation when the rear wheels went over the speed bump afterwards i.e. "rear-bumped". A deviation of the strain results during a bumping

This material is reserved for educational use only, not allowed for commercial use.
Forbidden to modify the content, and cite the document when use.

was calculated to be 10.65% and 17.35% for "front-bumped" peak and "rear-bumped" peak respectively.

In addition, investigation of the whole bus structure at all measurement locations was carried out in order to validate the computational model of the bus and the employed boundary conditions. Additionally, all strain data were converted to a corresponding stress in order to assess the resulting safety factor of the bus structure. A stress comparison between numerical simulations and experiments at all measurement locations is shown in Figure 10.

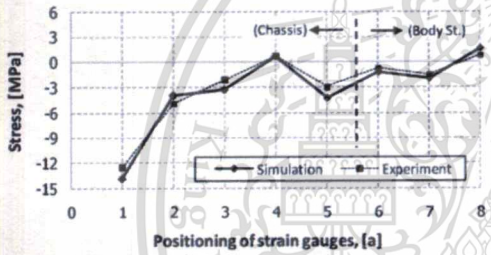

Fig. 10 Stress comparison of an entire structure on a bumping test

A stress comparison of both simulation and experiment at 8 strain gauge locations showed a similar trend with various degree of discrepancy at each point. Deviations on chassis structure locations were calculated to be 10.66% and 9.6% for maximum and minimum respectively while 23.12% and 11.03% for maximum and minimum were determined on the body structure locations. These deviations might come from a complexity of converting the actual bus structure into a CAD system, and an assumption of rigid connection for all the welding joints. Moreover, the corresponding stress that was found on the bus structure under the bumping test in this study would give a significantly higher safety factor than that required by the transportation regulation set.

4. Conclusion

In this study, the dynamic investigation of an electric bus was carried out on a bumping test using a dynamic analysis of a numerical calculation and strain measurement of a strain gauge setup. Computational model of chassis and body structure were combined and analyzed together. In order to acquire a strain history, strain gauges were attached at various locations over an entire structure. Results of this research can be summarized as followed:

- A maximum stress of 10.97 MPa was found at location "a1" on the front section of the chassis while a maximum deviation of 23.12% was found at location "a8" on the rear part of the body structure.
- A strain comparison at location "a1" showed a very similar trend despite an offset of the magnitudes ranging between 10-17%.
- The deviations between both numerical and experimental data could be due to a complexity of the body structure, and the welding joint assumption.
- Under the bumping test investigated, the area on the chassis subjected to risk of failure were around the connecting positions between the chassis and the battery compartment while another location was the body members close to the rear door.

The higher strain area especially members on the body structure would require an improvement by adding or changing some design features or material that would affect overall strength of the bus structure. However,

This material is reserved for educational use only, not allowed for commercial use.
Forbidden to modify the content, and cite the document when use.

this study was only conducted on a bumping test. A braking and cornering maneuver will be investigated in order to further validate the employed physical modeling and to obtain a lightweight optimization of the bus. Furthermore, the results from this study could be used as a guideline to an electric bus design by a finite element analysis.

5. Acknowledgements

The authors are very grateful to Automotive Laboratory, National Metal and Materials Technology Center (MTEC), Thailand for their supports to this work.

6. References

[1] F Lan, J Chan and J Lin, Comparative Analysis for Bus Side Structure and Lightweight Optimization, *Proc. Instn. Mech. Engrs.*, Part D: J. Automobile Engineering, 218, pp. 1067-1075.

[2] Manokruang S. and Butdee S., Methodology of Bus-Body Structural Redesign for Lightweight Productivity Improvement, *AIJSTPME*, (2009) 2(2), pp. 79-87.

[3] K. Chinnaraj, M. Sathya Prasad and C. Lakshmana Rao, Experimental Analysis and Quasi-Static Numerical Idealization of Dynamic Stresses on a Heavy Truck Chassis Frame Assembly, *Applied Mechanics and Materials*, Vols. 13-14 (2008), pp. 271-280.

[4] M.M.M. Salem and Ayman A. Aly, Fuzzy Control of a Quarter-Car Suspension System, *World Academy of Science, Engineering and Technology*, 53 (2009), pp. 258-263.

[5] T.-T. Fu and D. Cebon, Analysis of a Truck suspension Database, International *Journal of Vehicle Design, Heavy Vehicle Systems*, March (2002).

[6] NCHRP (report 505), Review of Truck Characteristics as Factors in Roadway Design, ISBN:0-309-08779-1, Washington D.C. (2003).

[7] S. Butdee and F. Vignat, TRIZ Method for Lightweight Bus Body Structure Design, *Journal of Achievements in Materials and Manufacturing Engineering*, Vols. 31, Issue 2, December (2008), pp. 456-462.

[8] T.H.T. Chan, Y.Yu, K.Y.Wong and Z.X.Li, Condition-Assessment-Based Finite Element Modeling of Long-span Bridge by Coupling Method, *National Natural Science Foundation of China*, (No. 50278017).

[9] V. Adams and A. Askenazi. *Building Better Products with Finite Element Analysis*, 1st edition, ISBN: 978-1566901604, On Word Press (1999).

This material is reserved for educational use only, not allowed for commercial use.
Forbidden to modify the content, and cite the document when use.

Appendix E-3: Finite Element Analysis of an Electric Bus Body Structure in Real Driving Conditions

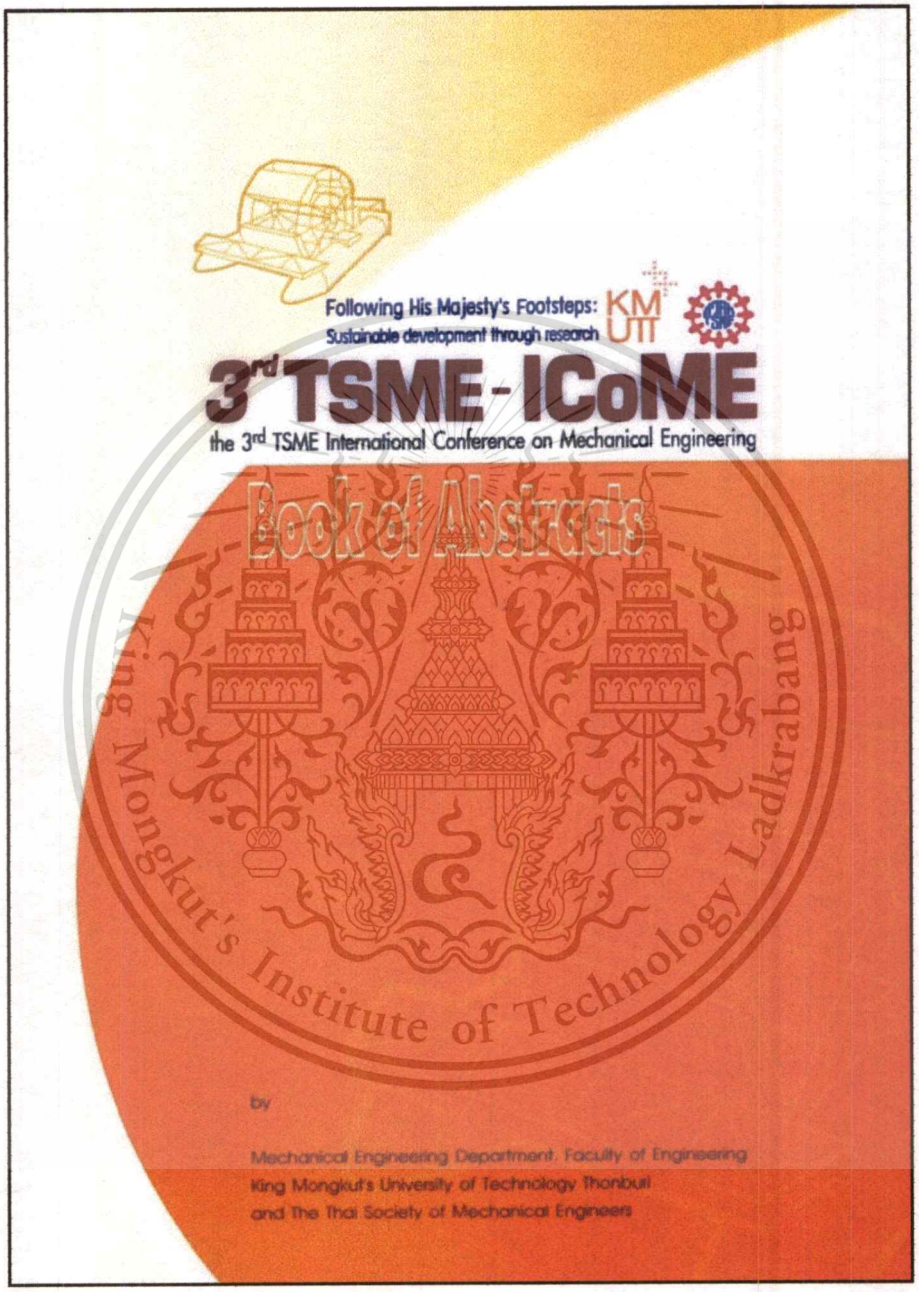

This material is reserved for educational use only, not allowed for commercial use.
Forbidden to modify the content, and cite the document when use.

Paper ID
CST 1020

The 3rd TSME International Conference on Mechanical Engineering
October 2012, Chiang Rai

Finite Element Analysis of an Electric Bus Body Structure in Real Driving Conditions

Dittapoom Shinabuth[1,*], Chi-na Benyajati[2], Sittikorn Lapapong[2], Monsak Pimsarn[3] and Masaaki Okuma[4]

[1]TAIST-Tokyo Tech, Automotive Engineering, Bangkok, Thailand 12120
[2]Automotive Laboratory, National Metal and Materials Technology Center, National Science and Technology Development Agency, Bangkok, Thailand 12120
[3]Department of Mechanical Engineering, Faculty of Engineering, King Mongkut's Institute of Technology Ladkrabang, Bangkok, Thailand 10520
[4]Department of Mechanical and Aerospace Engineering, Graduate School of Science and Engineering, Tokyo Institute of Technology, Tokyo, Japan 152-8550
*Corresponding Author: E-mail dit_4@windowslive.com

Abstract

In order to evaluate structural strength of a bus body, it could involve a lot of materials cost and time by using an experimental approach. This research proposed procedures for reducing such drawbacks by a transient response study using finite element analysis. In this work, a computational model was created to replicate a chassis and body framework of an electric bus prototype. In analysis, four driving conditions were studied to obtain the dynamic responses. It was found that the maximum stress of 57.21 MPa, 93.41 MPa, 154.64 MPa, and 141.94 MPa were generated in bumping, braking, cornering, and torsional case respectively. The bumping condition displayed the lowest stress level while the maximum stress was in the cornering case. Moreover, torsional stiffness of 25,234 N-m/deg was calculated during the torsional load application. It was concluded that the strength of the electric bus prototype was satisfactory to design specification and safety aspect under general driving applications. Furthermore, possible improvement of an electric bus body design was discussed regarding a structural weight optimization to increase a driving performance as well as to reduce energy consumption.

Keywords: Transient response, Electric bus prototype, Driving conditions, Torsional stiffness

1. Introduction

Due to an increasing demand for bus transport in Thailand, many buses are being constructed especially for tourism industries and public transportations. Most small or medium-sized bus structures were fabricated by the local mechanic skills with a few being supervised by qualified engineers. These buses may be subjected to various problems such as tire wear, inadequate structural durability, and excessive structural weight. Computer-Aided Engineering (CAE) was introduced to solve various engineering problems via numerical technique called Finite Element Analysis (FEA). CAE has become a necessary tool in bus body analysis for preventing any potential problems. Because of environmental issues, automotive industries and research centers have started concentrating their research on alternative energy applications such as Electric Vehicle (EV) and Fuel Cell Vehicle (FCV). An electric vehicle has become one of the solutions to reduce the usage of fossil fuel on land vehicles. In Thailand, while most buses are generally operated with an internal combustion engine (ICE), there are only few driven by an electric motor.

Fig. 1 Electric bus prototype

The bus shown in Figure 1 is an 8-metre bus prototype which could be classified as a medium-sized bus vehicle. In addition, it was powered by electricity from battery sources. A design and analysis of an electric bus structure might be

This material is reserved for educational use only, not allowed for commercial use.
Forbidden to modify the content, and cite the document when use.

Paper ID
CST 1020

The 3rd TSME International Conference on Mechanical Engineering
October 2012, Chiang Rai

significantly different from an ICE bus structure. In this study, the purpose was to investigate strength of an electric bus prototype under real driving conditions. Moreover, structural members of the body construction which tend to be less important would be identified with a view to obtaining a lightweight electric bus structure.

2. Bus structure

To construct a bus structure, there are several factors that need to be considered such as structural strength, fabrication difficulty and structural configuration. In fabrication process, a bus structure is generally divided into two sections. One is a chassis construction which is a main component built by steel sheets designing to resists an external loads either from the upper or lower structure such as reaction forces from the ground. Another part that placed on the top of the chassis is called a body structure creating to accommodate passengers and bus utilities. The body structure is constructed similar to a skeleton frame that consists of many beam elements with various cross sectional shape. For this reason, the main focus on reducing a structural weight or increasing structural stiffness could be on the body structure. In a studied electric bus structure, a significant difference from the conventional bus structure was a location and weight of the power sources. Geometry of the electric bus structure employed in this study is shown in Figure 2.

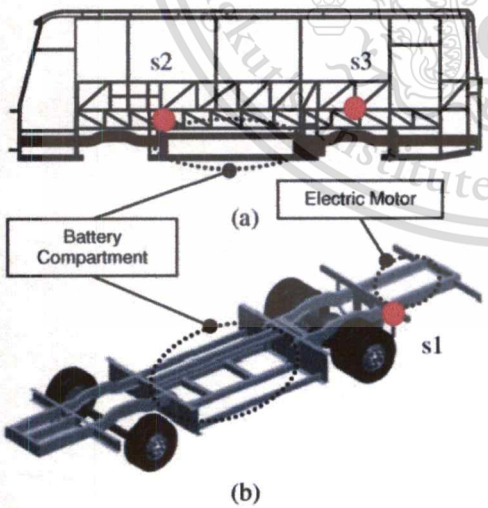

Fig. 2 Geometry of the studied electric bus: (a) Side view of the frame (b) Chassis

From Figure 2, around the center of the chassis, an empty space between front and rear wheels was reserved. This was designed for carrying battery packs which supplied current to an electric motor. Battery packs combined with high electricity voltage were necessary to be placed at the center of the chassis in order to keep a good stability. On the other hand, many structural members were observed around a waist location of the body frame above battery compartment. The s1-s3 points on the chassis and body were identified for a stress monitoring locations in this study. They were placed behind left rear wheel, at connecting joint between the chassis and body, and on the top of the right rear wheel member for s1, s2, and s3 respectively as designated in Figure 2.

3. Finite element analysis

Finite Element Analysis (FEA) is a numerical technique using partial differential equations to approximate the engineering solutions such as structural, thermal and vibration analysis. In order to take into account the effect of large moving masses, this study employed a transient mode of structural analysis to investigate strength of the bus structure under different four operating conditions.

3.1 Computational modeling

In this process, Finite Element (FE) model was generated to convert a physical geometry of the actual bus structure into an analytical model. The FE model is relatively important to obtain a precise analysis solution. Consequently, the computational modeling was separated to two types because of an appropriate computational time and accuracy. The employed model was consisted of 45,237 beam elements and 14,934 shell elements as shown in Figure 3.

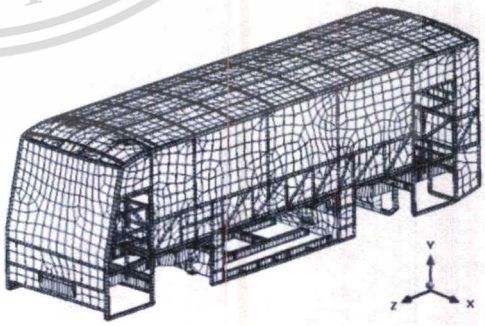

Fig. 3 FE model of the electric bus

The chassis was assigned by c-channel beams while square and rectangular tubes were assigned to the body structure. Material properties were of

This material is reserved for educational use only, not allowed for commercial use.
Forbidden to modify the content, and cite the document when use.

common steel which had a mass density, elastic modulus, yield strength, and Poisson's ratio of 7,850 kg/m^3, 210 GPa, 324 MPa, and 0.3 respectively [1].

3.2 Boundary conditions

Driving situations affecting either small or large a structural deformation could appear in two main modes [2]. Firstly, it was a bending case happened when the bus was subjected to the vertical load or displacement. Another was a torsional case, an external load attempted to deform the bus structure in rotating fashion along a longitudinal axis. In this case, a twist angle was utilized to calculate a torsional stiffness. In previous study, it was found that a large torsional deformation directly influenced the fatigue fracture of window pillar members [3]. In order to determine structural strength of the bus body operating in the different situations, several boundary conditions were considered as summarized in Table 1.

Table. 1 Driving conditions and applied loads

Driving Condition		Applied Loads
Bump		u_y = 200mm
Brake		a_z = - 0.75g
Turn		a_x = ±0.75g
Twist		u_y = 200mm (at wheel hub)

From Table 1, in a bumping situation, both front and rear axles were activated by sequential vertical forced displacement equal to double amplitude of typical speed bump height of 200 mm. A braking case was a situation where the bus was driven at constant velocity and a brake pedal was suddenly pressed. The braking deceleration of 0.75g was applied in longitudinal direction. Furthermore, a lateral loading value of 0.75g was employed to obtain both sides of a turning response. Finally, a vertical displacement of 200 mm was applied to lift one wheel upward while other three wheels were constrained to simulate a twisting behavior of the bus. In addition, distributed loads were included in the analysis comprising a battery loading of 2,000 kg, a passenger mass of 2,300 kg, and an air conditioner system of 200 kg [4].

4. Results

As mentioned in previous section, a transient dynamic analysis was employed to obtain the dynamic response of the bus structure under specified time-dependent loads and constraints. To display a solution, combined stress which was a combination between axial and bending stress was determined to distribute the calculated stress throughout the electric bus structure. Moreover, the critical location on each case was magnified for better visibility.

4.1 Bumping case

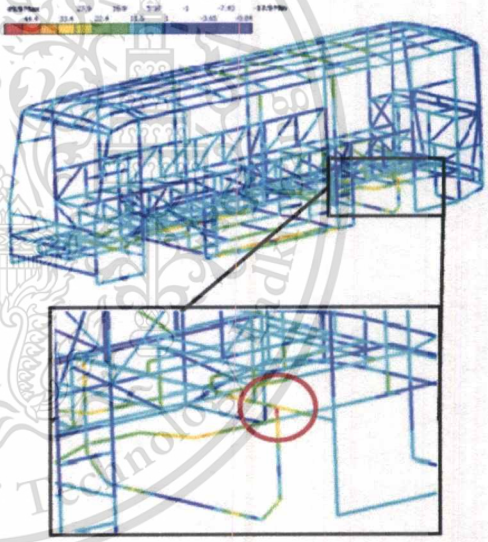

Fig. 4 Calculated stress distribution in a bumping case

Figure 4 shows a combined stress plot that was calculated by vertical displacement applying to the front and rear axles in sequence. It was found that the critical point was illustrated at location s1 that was close to an access to the rear door. The maximum stress of 57.21 MPa was exhibited for the duration of rear bump together with another significant stress observed at the lower frames carrying battery packs on both sides of the bus. Additionally, the central tubular construction was not on duty to resist the bumping condition.

This material is reserved for educational use only, not allowed for commercial use.
Forbidden to modify the content, and cite the document when use.

Paper ID
CST 1020

The 3rd TSME International Conference on Mechanical Engineering
October 2012, Chiang Rai

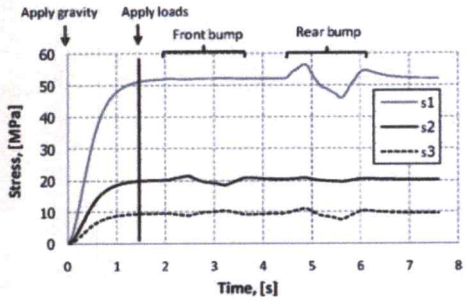

Fig. 5 Bumping responses at selected monitoring locations

Dynamic stress responses were displayed through three different monitoring locations as shown in Figure 5. Before performing a driving condition, the bus body was subjected to a gravitational acceleration of 9.81 m/s^2 as part of dynamic calculation by the software. As a result, an initial state of three monitoring points had different stress magnitudes. As can be seen in Figure 5, s1 showed 52.27 MPa followed by 19.65 MPa and 9.14 MPa at location s2 and s3 respectively. During bumping sequence, a significant stress variation was generated to be 47.5 MPa at location s1 during the rear axle climbed to the peak of the speed bump while others two locations presented minute stress level on both front and rear bumping.

4.2 Braking case

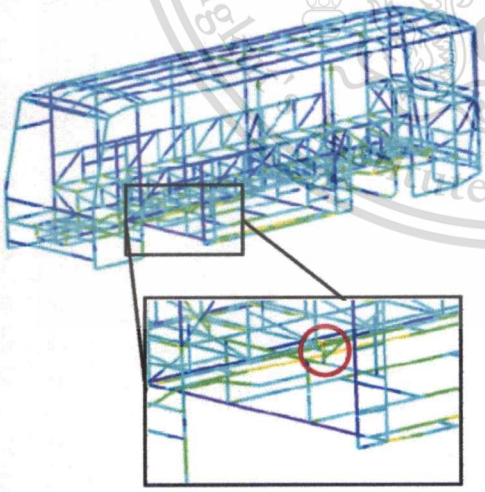

Fig. 6 Calculated stress distribution in a braking case

During a braking period, the structure was subjected to a longitudinal loading and the maximum stress of 93.41 MPa in tension was observed at location s2. This was a tubular member at the front of battery compartment located between the chassis and the body structure. In addition, tubular members around the central body construction and roof frame received little effect from the deceleration load.

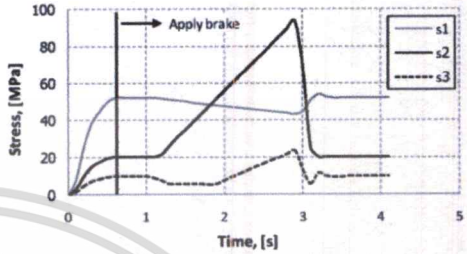

Fig. 7 Braking responses at different locations

The effect of deceleration at measurement points from braking maneuver was displayed in Figure 7. Similar to the bumping case, the stress response at s1 was the highest compared to s2 and s3 after applying only gravity to the model. The noticeable stress response was seen at location s2. The resulting stress of s2 steadily increased when a brake pedal was pressed and reached its peak at 93.41 MPa within 1.9 seconds in relation to the profile of applied deceleration. Furthermore, a dynamic stress at s3 showed two other distinct variations. It could be seen that there was a first region of small stress drop which was accompanied by a rise to the highest point of 22.35 MPa. After that, the stress dropped rapidly with small vibration response coinciding with the bus stopping completely.

4.3 Cornering case

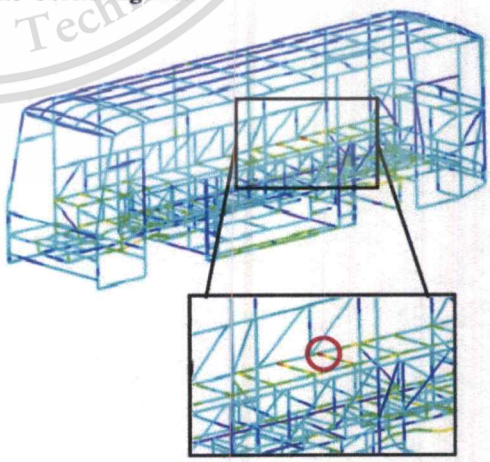

Fig. 8 Calculated stress distribution in a cornering case (Right turn)

This material is reserved for educational use only, not allowed for commercial use.
Forbidden to modify the content, and cite the document when use.

Paper ID
CST 1020

The 3rd TSME International Conference on Mechanical Engineering
October 2012, Chiang Rai

In cornering case, a beam member underneath passenger seat above the right rear wheel was estimated to be the critical point under the lateral loading. It was calculated that maximum stress of 154.64 MPa occurred during a right turning. Although both side frames were subjected to the lateral load, the roof frame was found to be under relatively small amount of stress.

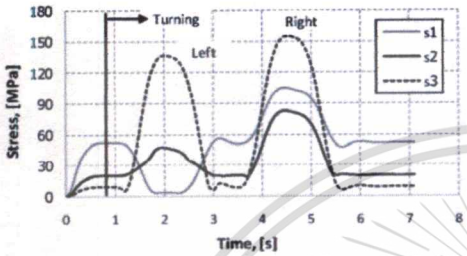

Fig. 9 Cornering responses at different locations

The cornering responses were exhibited in Figure 9. In general, there were two noticeable stress variations in the response from each monitoring location coinciding with left and right turning sequentially. However, the main focus was directed to location s3. The s3 line first climbed up smoothly to 137.23 MPa during the left turning condition followed by the second peak of the maximum stress at the right turn.

4.4 Torsional case

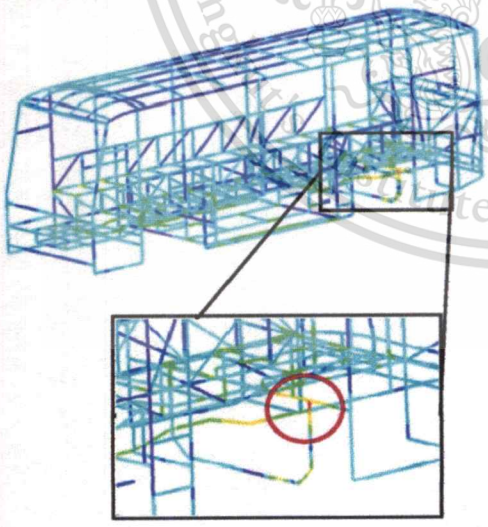

Fig. 10 Calculated stress distribution in a torsional case

In this case, the vertical displacement was used to induce a torsional load to the structure. It is important that the vehicle structure subjected to the torsional load has significant effect to the side frame of a bus structure [5]. The computed solutions showed that stress of 141.94 MPa was generated at the critical point when the left rear wheel was lifted off the ground by 200 mm. The location of maximum stress was the same as the case of rear axle bump. Consequently, a torsional stiffness of the studied bus structure was needed to assess the structural rigidity in comparison with the standard value ranging from 18,000 - 40,000 N-m/deg for a bus structure [6]. To calculate a torsional stiffness, the applied torque and twist angle were the major parameters. On the other hand, a reaction force, a distance between the wheels in the same axle, and a vertical displacement may be applicable as follows:

$$K = \frac{T}{\theta} = \frac{F_z \cdot L}{tan^{-1}\left(\frac{\Delta z}{L}\right)} \quad (1)$$

The calculation following Eq. (1) showed that a torsional stiffness could be obtained from a slope between an applied torque and twist angle as displayed in Figure 11. In this case, the corresponding torsional stiffness of the electric bus prototype was calculated to be 25,234 N-m/deg.

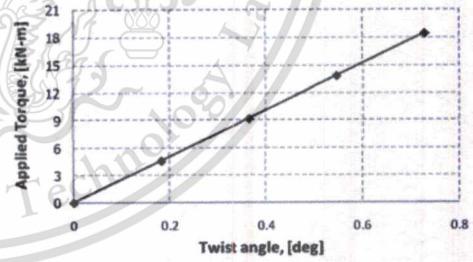

Fig. 11 Torsional stiffness

5. Discussion

In a bumping case, the structure was subjected to the vertical load. It was found that stress mainly appeared at the left rear wheel during the rear axle bump. It could be said that the members constructed around a rear door was a main reason due to lack of supporting members because of a space needed for the door frame. Besides, several areas on the body, namely the waist, the roof frame, and the construction around electric motor seemed to be diminutively affected by the bending load as shown from monitoring location s2 and s3 in Figure 5.

This material is reserved for educational use only, not allowed for commercial use.
Forbidden to modify the content, and cite the document when use.

The calculated tress distribution in a braking case was simulated by longitudinal load as shown in Figure 6. According to the load transfer of large moving mass of battery packs, the maximum stress was indicated at the joint in front of the battery compartment. It might be due to low strength by too few supporting members as well as small thickness of material used in this area. Moreover, a small stress level occurred on the roof frame and along the central body forming passenger section above the battery compartment. Additionally, significant stresses were still generated along the beams supporting battery packs in the battery compartment.

A cornering case was representing the effect of lateral load. In Figure 8, significant stress concentrations on the structure during the left and right turning were not only noticed above rear wheel positions but also on the front section of the chassis. Moreover, it was observed at the location opposite of s3, i.e. on the left side of the body structure, a similar stress response pattern to those of s3 shown in Figure 9 but in reverse order. This showed that both side of waist members were affected by a lateral loading in any direction.

Torsional loading case was studied in order to obtain a torsional rigidity of the structure during twisting action as shown in Figure 11. The vertical displacement was applied to the left rear wheel for twisting the bus structure. As a result, the torsional stiffness of the whole structure was estimated to be approximately by 71.3 % higher than the minimal requirement. Therefore, the bus structure was capable of resisting certain degree of external load which came in torsional fashion. Moreover, the safety factor in each driving condition was calculated with respect to the yield stress of steel to be 5.66, 3.46, 2.09, and 2.28 in case of a bumping, braking, cornering and torsional maneuver respectively. All analysis results illustrated that strength of the electric bus body was reasonably high enough to operate in majority of normal driving conditions.

6. Conclusions

Transient dynamic analysis was employed to determine strength of the electric bus structure in four driving situations that frequently happened during the operation. The calculated maximum stress of 57.21 MPa, 93.41 MPa, 154.64 MPa, and 141.94 MPa was presented during bumping, braking, cornering and torsional case respectively. It was clear that a speed bump with the height of 200 mm had insignificant effect to the structure while the cornering case gave the highest resulting stress in all four situations. From the simulated results, it could be concluded that overall structural strength of the electric bus prototype was satisfactory under four common driving situations and further structural optimization could be carried out. The waist beams of the body and roof frame have been observed to exhibit a common area of relatively low resulting stress from all the cases considered. These areas were generally fabricated from many square tubes in 38x38 mm with 3.2 mm thickness. Furthermore, optimum structural weight of the electric bus could be achieved by changing cross-sectional area, removing zero force members, and rearranging the alignment of the beam fabrication. These parameters will be investigated further in a future work.

7. Acknowledgements

The author would like to specially thank Automotive Laboratory, National Metal and Materials Technology Center (MTEC), Thailand for their support.

8. References

[1] Santosh B. Belure, Satish S. Kadam and S. B. Wadkar (2008). Criticality Analysis of Passenger Bus Body Structural Design Using Finite Element Method, paper presented in *National Conference on Computational Methods in Mechanical Engineering*, India.

[2] Masahiro, S. and Yukio, K. The strength of Automobile Body, 1998 (AddTech, Korea)

[3] M H Kim, MW Suh and D H Bae. (2001). Development of an Optimum Design Technique for the Bus Window Pillar Member, *IMechE*, vol. 214 Part D, pp. 11-20.

[4] D. Croccolo, M. D. Agostinis and N. Vincenzi. Structural Analysis of an Articulated Urban Bus Chassis via FEM: a Methodology Applied to a Case Study, *Journal of Mechanical Engineering*, vol.57(11), October 2011, pp. 799 – 809.

[5] Lonny L. Thompson, Srikanth R. and E. Harry Law. Design of a Winston Cup Chassis for Torsional Stiffness, SAE Technical Paper Series, paper presented in *Motorsports Engineering Conference and Exposition*, November 16-19, 1998, Michigan, U.S.A.

[6] F. Lan, J. Chen and J. Lin. (2004). Comparative Analysis for Bus side Structures and Lightweight Optimization, *IMechE*, vol.218 Part D, May 2004, pp. 1067 – 1075.

This material is reserved for educational use only, not allowed for commercial use.
Forbidden to modify the content, and cite the document when use.

BIOGRAPHY

Name: Mr. Dittapoom Shinabuth

Date of Birth: September 15, 1986

Place of Birth: Buriram, Thailand

Education:

2006 - 2009 B.Eng. in Mechanical Engineering (Outstanding Academic Performance), Faculty of Engineering, Sripatum University, Thailand

2009 - 2013 M.Eng. in Automotive Engineering (International Program), International College, King Mongkut's Institute of Technology Ladkrabang (KMITL), Thailand

Honour and Scholarship:

2008 The first prize winner of the *SolidWorks 3D Design and Skill Contest 2008*, National Competition organized by AppliCAD Co., Ltd. and King Mongkut's University of Technology North Bangkok, Thailand

2009 - 2011 TAIST-Tokyo Tech scholarship, the Master's Degree in Automotive Engineering funded by National Science and Technology Development Agency (NSTDA), Thailand

Proceedings:

1. **Shinabuth D.**, Benyajati C., Phuchamnong A., Pimsarn M., and Okuma M. 2011. *"Comparative Analysis of an Electric Bus Body Structure for Lightweight Design."* The 7th International Conference on Automotive Engineering, Bangkok, Thailand.

2. **Shinabuth D.**, Benyajati C., Phuchamnong A., Pimsarn M., and Okuma M. 2011. *"A Numerical and Experimental Measurement in a Dynamic Strain Response of an Electric Bus Body Structure."* The 2nd TSME International Conference on Mechanical Engineering, Krabi, Thailand.

3. **Shinabuth D.**, Benyajati C., Lapapong S., Pimsarn M., and Okuma M. 2012. *"Finite Element Analysis of an Electric Bus Body Structure in Real Driving Conditions."* The 3rd TSME International Conference on Mechanical Engineering, Chiang Rai, Thailand.

This material is reserved for educational use only, not allowed for commercial use.
Forbidden to modify the content, and cite the document when use.